

การพัฒนาตัวรับรู้ทางเคมีไฟฟ้าสำหรับการตรวจวัดกลูโคซามีนโดยใช้ระบบทรอปเล็ทไมโครฟลูอิดิก



บทคัดย่อและแฟ้มข้อมูลฉบับเต็มของวิทยานิพนธ์ตั้งแต่ปีการศึกษา 2554 ที่ให้บริการในคลังปัญญาจุฬาฯ (CUIR)
เป็นแฟ้มข้อมูลของนิสิตเจ้าของวิทยานิพนธ์ ที่ส่งผ่านทางบัณฑิตวิทยาลัย

The abstract and full text of theses from the academic year 2011 in Chulalongkorn University Intellectual Repository (CUIR)
are the thesis authors' files submitted through the University Graduate School.

วิทยานิพนธ์นี้เป็นส่วนหนึ่งของการศึกษาตามหลักสูตรปริญญาวิทยาศาสตรมหาบัณฑิต
สาขาวิชาเคมี ภาควิชาเคมี
คณะวิทยาศาสตร์ จุฬาลงกรณ์มหาวิทยาลัย
ปีการศึกษา 2558
ลิขสิทธิ์ของจุฬาลงกรณ์มหาวิทยาลัย

DEVELOPMENT OF ELECTROCHEMICAL SENSOR FOR DETERMINATION OF GLUCOSAMINE
USING DROPLET MICROFLUIDIC SYSTEM

Mr. Akkapol Suea-ngam



A Thesis Submitted in Partial Fulfillment of the Requirements
for the Degree of Master of Science Program in Chemistry

Department of Chemistry

Faculty of Science

Chulalongkorn University

Academic Year 2015

Copyright of Chulalongkorn University

Thesis Title DEVELOPMENT OF ELECTROCHEMICAL SENSOR
FOR DETERMINATION OF GLUCOSAMINE USING
DROPLET MICROFLUIDIC SYSTEM

By Mr. Akkapol Suea-ngam

Field of Study Chemistry

Thesis Advisor Monpichar Srisa-Art, Ph.D.

Thesis Co-Advisor Professor Orawon Chailapakul, Ph.D.
Assistant Professor Kanet Wongravee, Ph.D.

Accepted by the Faculty of Science, Chulalongkorn University in Partial
Fulfillment of the Requirements for the Master's Degree

.....Dean of the Faculty of Science
(Associate Professor Polkit Sangvanich, Ph.D.)

THESIS COMMITTEE

.....Chairman
(Associate Professor Vudhichai Parasuk, Ph.D.)

.....Thesis Advisor
(Monpichar Srisa-Art, Ph.D.)

.....Thesis Co-Advisor
(Professor Orawon Chailapakul, Ph.D.)

.....Thesis Co-Advisor
(Assistant Professor Kanet Wongravee, Ph.D.)

.....Examiner
(Assistant Professor Suchada Chuanuwatanakul, Ph.D.)

.....External Examiner
(Assistant Professor Somsak Sirichai, Ph.D.)

อัครพล เสืองาม : การพัฒนาตัวรับรู้ทางเคมีไฟฟ้าสำหรับการตรวจวัดกลูโคซามีนโดยใช้ระบบดรอปเล็ตไมโครฟลูอิดิก (DEVELOPMENT OF ELECTROCHEMICAL SENSOR FOR DETERMINATION OF GLUCOSAMINE USING DROPLET MICROFLUIDIC SYSTEM) อ.ที่ปรึกษาวิทยานิพนธ์หลัก: ดร.มนพิชา ศรีสะอาด, อ.ที่ปรึกษาวิทยานิพนธ์ร่วม: ศ. ดร.อรรณณชัยลภากุล, ผศ. ดร.คณศ วงษ์ระวี, 120 หน้า.

ตัวรับรู้ทางเคมีไฟฟ้าสำหรับการตรวจวัดกลูโคซามีนควบคู่กับระบบดรอปเล็ตไมโครฟลูอิดิกได้ถูกพัฒนาขึ้นโดยใช้ขั้วไฟฟ้าคาร์บอนเพสต์ที่ดัดแปรด้วยอนุภาคทองคำระดับนาโนเมตรและพอลิแอนิลีน วิธีการออกแบบการทดลองแบบ central composition design ซึ่งเป็นวิธีการที่มีประสิทธิภาพในการทำนายภาวะที่เหมาะสมในการทดลองได้ถูกนำมาใช้ในการหาภาวะที่เหมาะสมสำหรับตัวแปรแต่ละชนิดที่ใช้ในการดัดแปรขั้วไฟฟ้า โดยพบว่าปริมาณที่เหมาะสมสำหรับอนุภาคทองคำระดับนาโนเมตรที่ใช้ดัดแปรขั้วไฟฟ้าคือ 300 มิลลิกรัมต่อลิตร และปริมาณที่เหมาะสมของพอลิแอนิลีนคือ 3,000 มิลลิกรัมต่อลิตร และพีเอชของบัฟเฟอร์ที่เหมาะสมคือพีเอช 4 สำหรับการทดลองแบบแบทช์พบว่ามีความเป็นเส้นตรงสองช่วง โดยช่วงความเป็นเส้นตรงแรกและช่วงความเป็นเส้นตรงที่สองอยู่ที่ 0.05 – 40 มิลลิโมลาร์ และ 40 - 100 มิลลิโมลาร์ ตามลำดับ จากช่วงความเป็นเส้นตรงแรกพบว่าสามารถคำนวณขีดจำกัดการตรวจวัดและขีดจำกัดการหาปริมาณได้เท่ากับ 2.8 และ 9.4 ไมโครโมลาร์ ตามลำดับ จากนั้นจึงนำตัวรับรู้ทางไฟฟ้าที่พัฒนาขึ้นมาใช้ควบคู่กับระบบดรอปเล็ตไมโครฟลูอิดิกสำหรับการตรวจวัดกลูโคซามีน ซึ่งจะช่วยให้สามารถตรวจวัดสารจำนวนมากในเวลาอันสั้นได้ โดยพบว่าสามารถตรวจวัดสารได้อย่างต่ำ 60 ตัวอย่างต่อชั่วโมง นอกจากนี้ระบบดรอปเล็ตไมโครฟลูอิดิกสามารถป้องกันการดูดซับของสารตัวอย่างที่ขั้วไฟฟ้าได้ เนื่องจากลักษณะของดรอปเล็ตที่มีการจัดแบ่งเป็นห้องกันสารให้อยู่ภายใน ช่วงความเป็นเส้นตรงของการตรวจวัดกลูโคซามีนของระบบดรอปเล็ตคือ 0.5-5 มิลลิโมลาร์ โดยมีขีดจำกัดการตรวจวัดและขีดจำกัดการหาปริมาณ 0.45 และ 1.45 มิลลิโมลาร์ตามลำดับ และพบว่าระบบการตรวจวัดกลูโคซามีนมีความแม่นยำสูง โดยทำการวัดกลูโคซามีนจาก 50 ดรอปเล็ตภายใน 1 วัน และทำการตรวจวัด 3 ครั้งภายในเวลา 1 สัปดาห์พบว่ามีค่าเบี่ยงเบนมาตรฐานสัมพัทธ์น้อยกว่าร้อยละ 3 จากนั้นระบบดรอปเล็ตที่พัฒนาขึ้นได้ถูกนำไปใช้วิเคราะห์กลูโคซามีนในผลิตภัณฑ์อาหารเสริม โดยพบว่ามีความผิดพลาดและค่าเบี่ยงเบนมาตรฐานสัมพัทธ์ของผลการวิเคราะห์น้อยกว่าร้อยละ 3 นอกจากนี้ยังพบว่าปริมาณกลูโคซามีนที่วิเคราะห์จากระบบดรอปเล็ตมีความสอดคล้องกับปริมาณที่วิเคราะห์จากระบบคัพเปลาริโอเล็กโทรโพรซิซิส ซึ่งระบุได้ว่าระบบดรอปเล็ตที่พัฒนาขึ้นนั้นมีความเที่ยงและความแม่นยำสูงสำหรับการตรวจวัดกลูโคซามีนในผลิตภัณฑ์อาหารเสริม

ภาควิชา	เคมี	ลายมือชื่อนิสิต
สาขาวิชา	เคมี	ลายมือชื่อ อ.ที่ปรึกษาหลัก
ปีการศึกษา	2558	ลายมือชื่อ อ.ที่ปรึกษาร่วม
		ลายมือชื่อ อ.ที่ปรึกษาร่วม

5772213223 : MAJOR CHEMISTRY

KEYWORDS: DROPLET-BASED MICROFLUIDICS / GLUCOSAMINE / CARBON-PASTE ELECTRODE / CENTRAL COMPOSITE DESIGN / CHRONOAMPEROMETRY

AKKAPOL SUEA-NGAM: DEVELOPMENT OF ELECTROCHEMICAL SENSOR FOR DETERMINATION OF GLUCOSAMINE USING DROPLET MICROFLUIDIC SYSTEM. ADVISOR: MONPICCHAR SRISA-ART, Ph.D., CO-ADVISOR: PROF. ORAWON CHAILAPAKUL, Ph.D., ASST. PROF. KANET WONGRAVEE, Ph.D., 120 pp.

A droplet-based electrochemical sensor for direct measurement of D-glucosamine was developed using carbon paste electrodes (CPEs) modified with gold nanoparticles (AuNPs) and polyaniline (PANI). Central composition design (CCD) was employed as a powerful method for optimization of parameters for electrode fabrication. The optimized amounts of AuNPs and PANI were determined as 300 and 3,000 mg L⁻¹, respectively. In addition, the optimum pH of buffer was found to be pH 4. For batch measurements, two linear ranges of glucosamine were observed. The first and second linear ranges were 0.05-40 mM and 40–100 mM, respectively. Using the first linear range, limits of detection and quantitation (LOD and LOQ) were calculated as 2.8 and 9.4 μM, respectively. Coupled with a droplet microfluidic system, the analysis of glucosamine was performed in a high-throughput manner with a sample throughput of at least 60 samples h⁻¹. In addition, the adsorption of the analyte on the electrode surface was prevented due to compartmentalization in droplets. Linearity of the proposed system was found to be in the range of 0.5–5 mM with LOD and LOQ of 0.45 and 1.45 mM, respectively. High intra-day and inter-day (evaluated among 3 days) precisions for the detection of 50 droplets containing glucosamine were obtained with %RSD less than 3%. The system was successfully used to determine the amounts of glucosamine in supplementary products with error percentage and relative standard deviation less than 3%. In addition, the amounts of glucosamine measured using the developed sensors were in good agreement with those obtained from a traditional CE method. These indicate high accuracy and precision of the proposed system for determination of glucosamine in supplementary products.

Department: Chemistry

Student's Signature

Field of Study: Chemistry

Advisor's Signature

Academic Year: 2015

Co-Advisor's Signature

Co-Advisor's Signature

ACKNOWLEDGEMENTS

Firstly, I would like to express my deeply impressed to my advisor, Dr. Monpichar Srisa-Art, for her mercy, kindness, tolerance, exertion, valuable suggestions and critical reading. Moreover, I would like to express my appreciation to Assistance Professor Dr. Kanet Wongravee for the help and great advice. Also, I am very thankful to Professor Dr. Orawan Chailapakul who always encouraged and given a support to my work. In addition, I would like to thank to Dr. Poomrat Rattanarat for the help and great suggestion.

Furthermore, I specially thank to all members of Chromatography and Separation Research Unit and Electrochemistry and Optical Spectroscopy Research Unit for their useful suggestion. Also, I am thankful to all members of Microfluidic Research Group for their helpfulness. A big patience of my friends for listen to my words is much appreciated.

Finally, I am grateful to be my father's son and very thankful for the rest of the family members. Also, I would like to express all my respect to the lord Buddha and all his discipline for making me a better man.

CONTENTS

	Page
THAI ABSTRACT	iv
ENGLISH ABSTRACT	v
ACKNOWLEDGEMENTS	vi
CONTENTS	vii
LIST OF TABLES	xi
LIST OF FIGURES	xiii
LIST OF ABBREVIATIONS	xx
CHAPTER 1 INTRODUCTION	1
1.1 Glucosamine	1
1.2 Droplet-Based Microfluidic System and Electrochemical Measurements	4
1.3 Scope and Aims of This Work	8
CHAPTER 2 THEORY	9
2.1 Droplet-Based Microfluidics	9
2.1.1 Droplet Generation	9
2.1.2 Droplet Size	11
2.1.3 Mixing in Droplets	13
2.1.4 Flow Velocity	14
2.2 Microfluidic Device Fabrication	15
2.3 Detection in Microfluidics	16
2.3.1 Cyclic Voltammetry (CV)	17
2.3.2 Linear Sweep Voltammetry	19
2.3.3 Chronoamperometric Detection	21

	Page
2.4 Gold Nanoparticles.....	24
2.5 Polyaniline.....	26
2.6 Experimental Designs and Surface Response Methodology.....	28
CHAPTER 3 METHODOLOGY.....	33
3.1 Chemicals and Equipment.....	33
3.1.1 Synthesis of Gold Nanoparticles (AuNPs).....	34
3.1.2 Preparation of Polyaniline (PANI).....	35
3.2 Design and Fabrication of Devices.....	35
3.2.1 Mold Fabrication.....	35
3.2.2 PDMS Casting.....	38
3.2.3 Electrode Fabrication.....	40
3.2.4 Microfluidic Device Assembly.....	42
3.2.5 Attachment of Electric Wires.....	42
3.3 Solution Preparation.....	45
3.3.1 Preparation of AuNPs and PANI Solutions.....	45
3.3.2 Preparation of Phosphate Buffer Saline (PBS).....	46
3.3.3 Preparation of GCM Standard Solutions.....	47
3.3.4 Preparation of Sample Solutions.....	48
3.3.5 Preparation of Solutions for Capillary Electrophoresis.....	48
3.4 Experimental Design and Setup.....	49
3.4.1 Batch Measurements.....	49
3.4.1.1 Electrode Modification and Optimization.....	49
3.4.1.1.1 AuNPs Modified Electrode.....	49

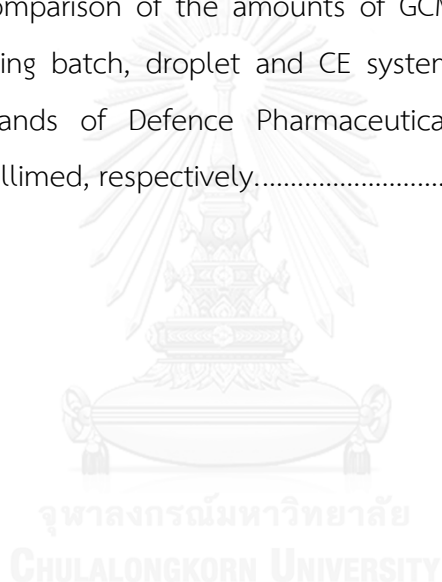
	Page
3.4.1.1.2 AuNPs and PANI Modified Electrode	49
3.4.1.1.3 Electrode Optimization.....	50
3.4.2 Droplet Measurements.....	52
3.4.2.1 Droplet Generation	52
3.4.2.2 Chronoamperometric Measurements in Droplets.....	53
3.4.2.2.1 Optimization of Flow Rate and W_f	53
3.4.2.2.2 Hydrodynamic Voltammogram	54
3.4.3 Capillary Electrophoresis (CE)	54
3.5 Analytical Performance.....	55
3.5.1 Calibration Curve	55
3.5.2 Linearity	55
3.5.3 Limit of Detection (LOD) and Limit of Quantitation (LOQ)	55
3.5.4 Precision	56
3.6 Interference Study	57
3.7 Real Samples Analysis	58
CHAPTER 4 RESULTS AND DISCUSSION	59
4.1 Electrode Optimization.....	59
4.1.1 AuNPs Modified Electrode	59
4.1.2 PANI and AuNPs Modified Electrode	61
4.1.3 CCD Calculation	63
4.2 Electrode Characterization.....	77
4.2.1 Morphological Study	77
4.2.2 Electrochemical Study	79

	Page
4.3 Method Validation for Batch Measurements	84
4.3.1 Linearity	84
4.3.2 Limit of Detection and Limit of Quantitation	87
4.3.2 Interference Study for Batch Measurements	87
4.3.3 Inter-day and Intra-day Precisions of Batch Measurements	89
4.3.3.1 Intra-day Measurements	89
4.3.3.2 Inter-day Measurements	91
4.4 Real Sample Analysis for Batch Measurements	93
4.5 Droplet-based Microfluidics	94
4.5.1 Optimization of Droplet System	97
4.5.1.1 Flow Rate	97
4.5.1.2 Applied Potential	99
4.5.2 Analytical Performance	100
4.5.3 Interference Study	102
4.5.4 Precision	104
4.5.4.1 Intra-day Measurements	104
4.5.4.2 Inter-day Measurements	105
4.5.6 Real Sample Analysis	106
CHAPTER 5 CONCLUSIONS	111
REFERENCES	113
VITA	120

LIST OF TABLES

Table 2.1	Example of the experimental design using CCD with 3 factors and each factors consisted 2 levels.	29
Table 3.1	List of chemicals and companies.	33
Table 3.2	List of equipment and companies.	34
Table 3.3	Preparations of mixed solutions between AuNPs and PANI in NMP for electrode modification.	46
Table 3.4	Preparation of GCM solutions from a stock solution of 100 mM GCM in 0.1 M PBS.	47
Table 3.5	Code values for pH and the amounts of AuNPs and PANI.	50
Table 3.6	Central composite design for optimization of pH and the amounts of AuNPs and PANI.	51
Table 3.7	Flow optimization for both water fraction and total flow rate study.	53
Table 4.1	Codes and real values of pH and the amounts of PANI and AuNPs used for CCD experiments.	64
Table 4.2	Three parameters with three levels of CCD experiments for optimization of pH and the amounts of AuNPs and PANI for determination of GCM. Electrochemical currents were obtained from CV using a scan rate of 150 mV s^{-1}	65
Table 4.3	Coefficients and p-values of each parameter obtained using regression calculation.	66
Table 4.4	Study of the effect of pH of the working solution on electrochemical current of GCM using the optimum amounts of AuNPs and PANI for electrode modification.	72

Table 4.5	Random experiments to check over-fitting of a constructed equation obtained from CCD.	75
Table 4.6	Interference study of <i>N</i> -acetyl-glucosamine added into a GCM standard solution at different ratios.	88
Table 4.7	Real sample measurements using the proposed method. All samples were prepared in 0.1 M PBS pH 4.	93
Table 4.8	Measurements of GCM in supplementary products using the droplet system.	108
Table 4.9	Comparison of the amounts of GCM in samples determined using batch, droplet and CE systems. A, B and C represent brands of Defence Pharmaceutical Factory, Glucosa, and Millimed, respectively.	110



LIST OF FIGURES

Figure 1.1	Cyclic voltammograms of 5 mM glucosamine dissolved in (a) 0.1 M NaOH and (b) 0.1 M phosphate buffer pH 7.4. Both experiments were performed using an AuNPs modified carbon-felt electrode as a working electrode. Reproduced from [8]. 3	3
Figure 1.2	(a) Laminar flow in microchannel with dispersion of sample zone. (b) A droplet-based microfluidic system with rapid mixing and no dispersion of sample zone. Reproduced from [14]. 5	5
Figure 1.3	Detection of droplets using an amperometric technique with a gold electrode. Reproduced from [17]. 6	6
Figure 1.4	The kinetic study of a catalase enzyme using an amperometric technique with valves for delivering different reaction-time droplets to the electrodes. Reproduced from [18]. 7	7
Figure 1.5	Detection of an analyte in droplets using amperometric measurements. A droplet was extended to cover all electrodes for longer time of electroanalysis. Reproduced from [15]. 8	8
Figure 2.1	Droplet generation in a T-junction microfluidic device. Reproduced from reference number [22]. 10	10
Figure 2.2	Droplet generation at different water fractions. Reproduced from reference [24]. 12	12
Figure 2.3	A model to explain the mixing of two reagents by chaotic advection in a droplet; Photographs show two layers of the modeling clay being stretched and folded, resulting in rapid mixing. Reproduced from reference number [20]. 13	13

Figure 2.4	Comparison of (a) laminar flow microfluidics and (b) droplet-based microfluidics. The droplet system exploits a winding channel to generate rapidly chaotic mixing. Reproduced from reference number [14].....	14
Figure 2.5	Fabrication of a PDMS master. (A) A design from AutoCAD is transferred to a film mask. (B) Photolithography of SU-8 onto a Si wafer. (C) A developing step to remove unpolymerized SU-8. Reproduced from reference number [28].....	15
Figure 2.6	Soft lithography for PDMS casting. (a) A PDMS master containing the designed microchannel pattern. (b) PDMS monomer is poured onto the master. (c) A PDMS plate after casting from the master.	16
Figure 2.7	(a) A potential scan of CV where V_1 to V_2 causes an oxidation reaction and V_2 to V_1 provides a reduction reaction. Both reactions are called anodic and cathodic scans, respectively. (b) A typical cyclic voltammogram; E_{pc} is cathodic peak potential, i_{pc} is cathodic peak current, E_{pa} is anodic peak potential and i_{pa} is anodic peak current. Reproduced from reference number [31].....	18
Figure 2.8	(a) Potential scans for linear sweep voltammetry. (b) Current signals obtained from varied scan rates. Reproduced from Reference [31].	20
Figure 2.9	A chronoamperogram of oxidation (0-100 ms) and reduction (101-200 ms) reactions, which demonstrates decreasing of current with time as followed the Cottrell's equation. Reproduced from reference number [36].	22
Figure 2.10	A hydrodynamic voltammogram 100 μ M dithiotheritol injection, plotted using the signal-to-noise ratio as a function of applied potential. Reproduced from reference number [37]. .	23

Figure 2.11	A mechanism of AuNPs synthesis. Reproduced from [43]. 24
Figure 2.12	Basic and redox structures of polyaniline. Reproduced from reference number [48]. 26
Figure 2.13	The interaction between PANI and AuNPs under the electric field-induced charge transfer. Reproduced from reference number [12]. 27
Figure 2.14	Generation of central composite design of two factors. 30
Figure 2.15	surface responses for effect of nitrate and calcium as the Hyoscyamine level for elicited hairy root. Reproduced from reference number [52]. 32
Figure 3.1	Fabrication of a PDMS mold on a silicon wafer using SU-8 negative photoresist. 37
Figure 3.2	Complete SU-8 masters on silicon wafers; (a) microchannel patterned and (b) electrode patterned masters. 37
Figure 3.3	A PDMS casting process for microfluidic device fabrication using SU-8 molded onto a silicon wafer as a PDMS master. 39
Figure 3.4	PDMS replicas; (a) microchannel patterned PDMS and (b) electrode patterned PDMS. A red dye in (a) and carbon paste in (b) were filled into the channels for visualization. 39
Figure 3.5	(a) Carbon paste was filled into microelectrodes on a PDMS plate using rubber as a spreader. (b) The excess carbon paste was removed using Scotch Magic Tape™. (c) A complete microchannel array on a PDMS plate after cleaning. 41
Figure 3.6	Electric wires were attached at the end of electrodes using silver paint as a conductive adhesive. 43
Figure 3.7	Complete microfluidic devices with two different designs: (a) a device containing a patterned microchannel of 500 μm width

	and 100 μm depth for the main channel and 50 μm width for a confined channel as a detection window and (b) a well-like design with a punched hole (~ 0.8 cm in diameter) as a solution container. WE, CE and RE are working, counter and reference electrode.....	44
Figure 3.8	An experimental setup of a droplet-based microfluidic device with electrochemical detection.....	52
Figure 4.1	Cyclic voltammograms of 0.1 M PBS pH 7.4 (red) and 0.1 M GCM in the same buffer (blue) using AuNPs modified CPEs with a 100 mV/s scan rate and a -0.8 to 1.3 V potential window.....	60
Figure 4.2	Cyclic voltammograms of 0.1 M PBS pH 7.4 (blue) and 0.1 M GCM (red) in 0.1 M PBS using PANI-AuNPs modified CPEs with a 100 mV/s scan rate and a -0.8 to 1.3 V potential window.....	62
Figure 4.3	Effects of the amount of AuNPs and pH on the oxidation of 100 mM GCM.....	66
Figure 4.4	Effects of the amount of PANI and pH on the oxidation of 100 mM GCM.....	67
Figure 4.5	A contour plot demonstrates the effect of the amounts of PANI and AuNPs on the oxidation current signal of 100 mM GCM.....	69
Figure 4.6	Responsive surfaces of currents as a function of the amounts of PANI and AuNPs at different pH values.....	70
Figure 4.7	A scatter plot shows the effect of pH on electrochemical signal.....	73
Figure 4.8	CVs of 100 mM GCM in 0.1 M PBS at pH 4 and 12. At pH 4, a quasi-reversible CV was obtained, while at pH 12 an irreversible CV was observed.....	74

Figure 4.9	SEM images of a PANI microfiber (a and c) and PANI with AuNPs (b and d). White spots in b and d are AuNPs on the surface of PANI microfiber.....	78
Figure 4.10	(a) CVs of 40 mM GCM in 0.1 M PBS pH 4 using scan rates from 50 to 500 mV s^{-1} . (b) Linear plots of electrochemical currents from the CVs in (a) versus square root of scan rate, which indicated the mass transfer as a diffusion controlled process.	80
Figure 4.11	(a) CVs of 100 mM GCM in 0.1 M PBS pH 4 using scan rates from 50 to 500 mV s^{-1} . (b) Plots of electrochemical currents from the CVs in (a) versus scan rate, which indicated the mass transfer as an adsorption controlled process.....	82
Figure 4.12	(a) Voltammograms of 5 to 100 mM GCM in 0.1 M PBS pH 4.0. (b) A plot of obtained electrochemical signal of standard GCM versus concentration of GCM from 0.05 to 500 mM. The experiments were performed using a scan rate of 100 mV s^{-1} and a potential window from -0.5 to 0.7 V.....	85
Figure 4.13	Schematic showing the interaction between GCM and AuNPs modified on a CPE.....	88
Figure 4.14	Intra-day measurements of 40, 60, 80 and 100 mM GCM using the optimum conditions, as shown in Figure 4.12. GCM solutions were prepared in 0.1 M PBS pH 4.0. Each concentration was measured for 10 times ($n = 10$).	90
Figure 4.15	Inter-day measurements of 40, 60, 80 and 100 mM GCM using the optimum conditions. The measurements were performed for 5 days in a month with an interval of 7 days.	91
Figure 4.16	A chronoamperogram of droplets containing 5 mM GCM in 0.1 M PBS pH 4. The experiment was performed using an applied potential of 100 mV and droplets were generated using flow	

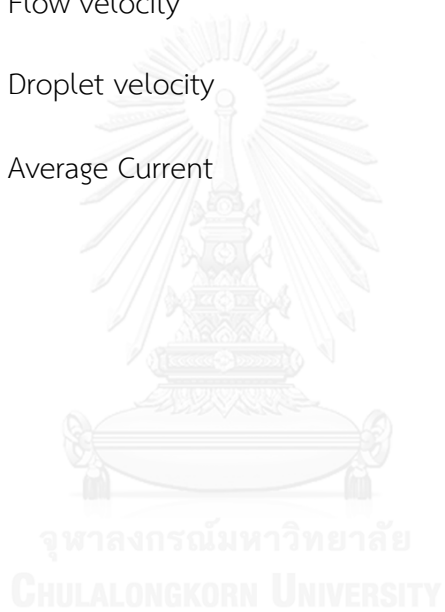
	rates of 1.4 and 0.6 $\mu\text{L min}^{-1}$ for oil and aqueous solutions, respectively.....	94
Figure 4.17	Droplet readout of 2 mM GCM. Current (Δi) was measured at the end of droplet peak. The experiment was performed using the conditions as shown in Figure 4.16.	95
Figure 4.18	Effects of W_f and total flow rate on chronoamperometric measurements of 2.5 mM GCM in droplets. Chronoamperometric measurements in droplets were performed using an applied potential of 100 mV.	98
Figure 4.19	A hydrodynamic voltammogram of 2.5 mM GCM determined using the optimized conditions; flow rates of 1.4 and 0.6 $\mu\text{L min}^{-1}$ for oil and aqueous solutions, respectively and W_f equal to 0.3.	99
Figure 4.20	(a) Chronoamperometric readout of droplets containing a concentration series of GCM from 0 to 5 mM. The measurements were carried out using a total flow rate of 2.0 $\mu\text{L min}^{-1}$ and $W_f = 0.3$ to generate droplets containing GCM. The applied potential was 100 mV vs. CPE. (b) A plot of current versus GCM concentration shows a linear range from 0.45 to 5 mM.	101
Figure 4.21	A bar chart shows a comparison between current signal obtained from 5.0 mM GCM and that from the mixtures of 5 mM GCM and <i>N</i> -acetyl-glucosamine at different ratios. Experimental conditions were the same as shown in Figure 4.20.	102
Figure 4.22	Intra-day measurements of 50 droplets containing 1.5, 2.5, and 3.5 mM GCM. Experimental conditions as shown in Figure 4.20.	104

- Figure 4.23** Inter-day measurements of 3.5 mM GCM in droplets for 3 days (n=3). All experiments were carried out using the conditions as shown in Figure 4.20. 105
- Figure 4.24** (a) A calibration curve of GCM obtained from the droplet system. (b) Chronoamperograms from the measurements of GCM in real samples (Defence Pharmaceutical Factory, Glucosa and Millimed) using the droplet system. All experiments were carried out using the conditions as shown in Figure 4.20. 107
- Figure 4.25** (a) Electropherograms of GCM standard solutions prepared in 100 mM borate buffer at a concentration series of 1 to 10 mM. (b) A calibration curve plotted between corrected areas of GCM and concentration. CE conditions: BGE as 100 mM Borate adjust to pH 9 with 0.1 M NaOH, 75 μ m ID x 60.2 cm (50 cm of the detector) uncoated fused-silica capillary; temperature 25 °C; Voltage 30 kV; UV detection at 200 nm, and 0.5 psi sample injection for 10 s. 109

LIST OF ABBREVIATIONS

A	Area
AuNPs	Gold nanoparticles
CE	Capillary electrophoresis
CPE	Carbon-paste electrode
CV	Cyclic voltammetry, Cyclic voltammogram
PANI	Polyaniline
PBS	Phosphate buffer saline
PDMS	Polydimethylsiloxane
PFD	Perfluorodecaline
S/N	Signal to noise
C_{det}	Determined concentration
$C_{labeled}$	Labeled concentration
F	Faraday's constant
F_o	Flow rate of carrier fluid
F_T	Total flow rate
F_w	Flow rate of dispersed phase
GCM	Glucosamine
γ	Surface tension
HPLC	High performance liquid chromatography
$I_{mixture}$	Current of added solution with standard solution

I_p	Peak current
I_{standard}	Current of standard solution
V	Scan rate
RSD	Relative Standard Deviation
SD	Standard Deviation
W_f	Water Fraction
V	Flow velocity
V_T	Droplet velocity
\bar{x}	Average Current



CHAPTER 1

INTRODUCTION

1.1 Glucosamine

Osteoarthritis or OA is a disease caused by the degradation of joints. This disease could occur in everyone, but particularly in the elderly, overweight people, and athletes. The main cause of OA is due to diminishing of joint fluid [1]. Glucosamine (GCM) was reported that it could help to increase joint fluid and relieve pain from the joint [2]. Therefore, the amount of glucosamine is important for healing patient from the OA. Basically, high performance liquid chromatography (HPLC) has been used as a gold standard method for determination of GCM in supplementary products [3]. To detect GCM, detectors normally used in HPLC systems include optical [4] and electrochemical [3] detectors. Nevertheless, HPLC is method that expensive, difficult to use, long analysis time and required a specialist.

For optical detection, Cheng et al. [4] reported a GCM sensor using 8-aminoquinoline and graphene. The detection method was successfully used for measurement of GCM with great sensitivity and selectivity. In addition, limit of detection of the developed method was 1 mg L^{-1} . Furthermore, Tran et al. [5] demonstrated a GCM detection system using a chemical probe which was developed from a dopamine sensor probe. This sensor provided a great selectivity for GCM detection, even though GCM was mixed with other amine and thiol compounds. However, these developed methods were required a chemical probe which was required synthesis steps. In addition, instruments for optical detection are bulky and expensive. Therefore, glucosamine detection using an optical approach is not suitable for practical use.

For electrochemical detection in HPLC, a gold plate was reported as a working electrode for carbohydrate measurements using an amperometric method [6]. Consequently, high accuracy and precision in the measurements were demonstrated [7]. Moreover, Pashkova et al. [3] reported the pharmaceutical kinetics

of GCM using an HPLC technique. This method used amperometric measurements with a gold plate electrode. All solutions were prepared in NaOH which changed gold to gold oxide. Gold oxide is an electrocatalyst for GCM oxidation [8]. A limit of detection of 20 ng mL^{-1} was found from this system. However, the traditional method using HPLC is cumbersome and uses a lot of reagents.

As GCM has been detected electrochemically using HPLC techniques, it makes a promise that electrochemical techniques could detect glucosamine with high accuracy and precision. In this work, there was an idea to develop an inexpensive and easy electrochemical sensor for determining the amount of GCM without using HPLC or other separation techniques. There have been research articles reporting electrochemical approaches for GCM oxidation.

Tominaka et al. [8] reported synthesis of glucosaminic acid from GCM using an electrochemical approach. Carbon felt was used as a working electrode which was modified with gold nanoparticles (AuNPs) which provided large surface area for enhancement of electrochemical property. The modified electrode provided great efficiency for synthesis of glucosaminic acid. Glucosaminic acid synthesis was confirmed using mass spectrometry. For the synthesis, gold oxide played a crucial role as an electrocatalyst for GCM oxidation, and alkaline solution was required to generate gold oxide. Thus, 0.1 M NaOH was used as an electrolyte solution in this report. As illustrated in Figure 1.1, cyclic voltammograms of glucosamine oxidation in NaOH and phosphate buffer were demonstrated. Using NaOH solution as an electrolyte provided a higher electrochemical peak with better synthesis efficiency of glucosaminic acid compared to phosphate buffer.

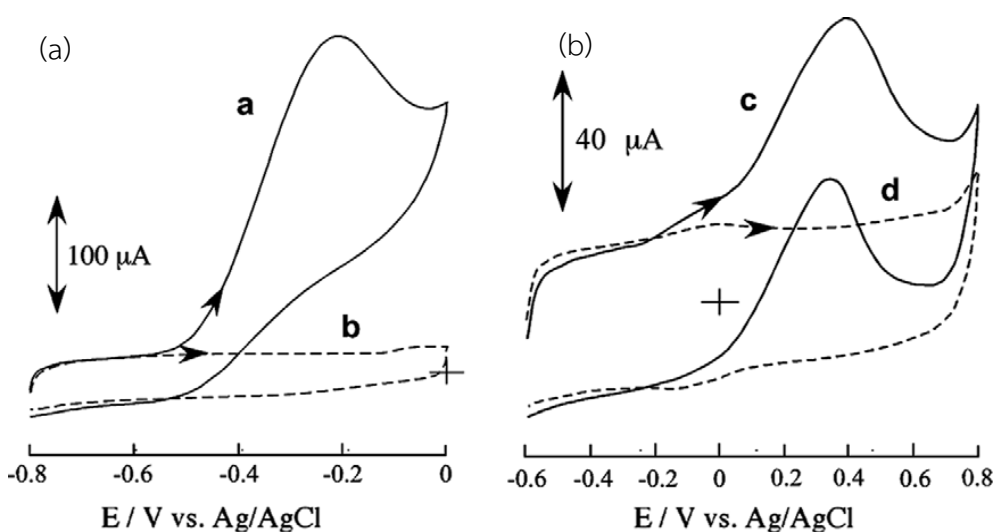


Figure 1.1 Cyclic voltammograms of 5 mM GCM dissolved in (a) 0.1 M NaOH and (b) 0.1 M phosphate buffer pH 7.4. Both experiments were performed using an AuNPs modified carbon-felt electrode as a working electrode. Reproduced from [8].

Although there have been modified electrodes using AuNPs as a modifier which provides many advantages including inexpensive and large surface area, a GCM sensor using an AuNPs modified electrode has not been reported. As mentioned above, the AuNPs modified electrode was already used for an electrochemical synthesis of glucosaminic acid from GCM. This method used small amount of gold to synthesize glucosaminic acid. However, quantitative analysis of GCM using an AuNPs modified electrode has not been report yet. In this work, an electrochemical sensor for the detection of GCM was developed. To get better sensitivity for GCM detection, a conductive polymer could be exploited. There are many kinds of conductive polymers, such as polypyrrole and polyaniline. These conductive polymers are non-toxic, easy preparation, and excellent in electron transfer [9]. Conductive polymers could increase electrochemical signal due to enhancing of surface of a working electrode [10]. As followed the Randles-Sevcik equation [11], enhancement of surface area could enhance electrochemical signal. Furthermore, the functional

groups of a conductive polymer are expected to trap AuNPs onto its surface, which could improve the sensitivity of the modified electrode [12]. Therefore, a conductive polymer was also used in this work as a modifier for enhancement of electrode surface and trapping AuNPs. In addition, this modified electrode was expected to be used in a microfluidic system for improving sample throughput and using less reagents and samples.

1.2 Droplet-Based Microfluidic System and Electrochemical Measurements

Microfluidics is a system that manipulates fluid, gas and/or liquid, in pico- to nano-liter scales in microchannels [13]. However, traditional microfluidic systems still have problems including slow mixing and dispersing in sampling zone. Droplet-based microfluidic systems, thus, have been developed to solve these problems. Droplet-based microfluidics is a system that uses multiphase fluids to generate droplets along microchannels [14]. Basically, oil and aqueous phases are used as a carrier phase and a dispersed phase, respectively. Dispersed droplets in a carrier phase act like small containers in which reactions occur within droplets and go along microchannels, as illustrated in Figure 1.2. Furthermore, the use of droplet system coupled with electrochemical detection could reduce electrode fouling during experiments due to indirect contact of droplet contents and the electrode surface [15]. It is because aqueous solution was encapsulated within droplets, which prevents droplet contents from direct contact with electrodes. This could extend electrode life time. In addition, the sizes of electrochemical instruments are much smaller than those of optical instruments. Therefore, a microfluidic system with electrochemical detection would be a good combination for on-site measurements.

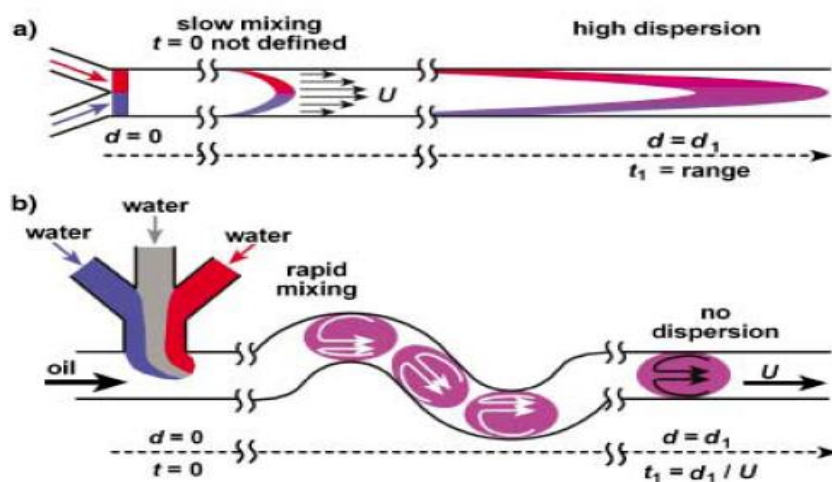


Figure 1.2 (a) Laminar flow in microchannel with dispersion of sample zone. (b) A droplet-based microfluidic system with rapid mixing and no dispersion of sample zone. Reproduced from [14].

There have been previous reports on the use of electrochemical measurements coupled with microfluidic systems. Lou et al. [16] reported gold electrodes for gauging NaCl concentrations in a droplet system. It was found that the limit of detection of this system was 0.02 mM. Moreover, this system was not only used for detection of NaCl, but also for measurements of conductivity in yeast's cell. Yeast cells were encapsulated inside the droplets for plasmid transfer using electricity (electroporation). However, a high voltage was required, which was still improper for an electroporation study in yeast cells.

Furthermore, Lui et al. [17] reported an amperometric technique with a gold electrode for monitoring oxidation reactions of N,N,N',N'-tetramethyl-1,4-phenylene diamine inside droplets, as demonstrated in Figure 1.3. It was found that microelectrodes could improve detection efficiency of N,N,N',N'-tetramethyl-1,4-phenylene diamine oxidation due to small iR drop from microelectrodes. In addition, using microelectrodes could accelerate the mass transfer process of the analyte.

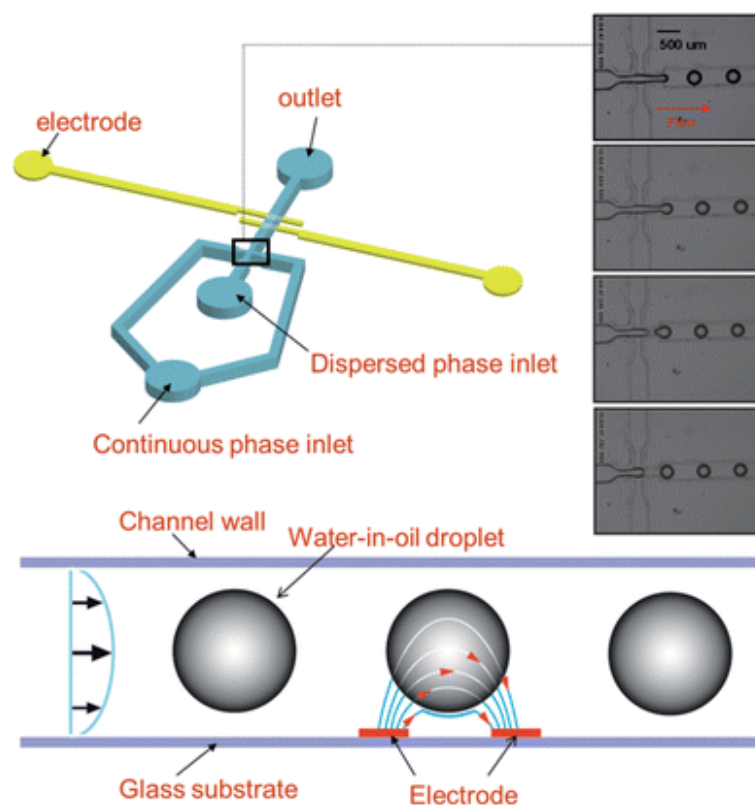


Figure 1.3 Detection of droplets using an amperometric technique with a gold electrode. Reproduced from [17].

Moreover, Han et al. [18] reported an amperometric method for detection of hydrogen peroxide (H_2O_2) in droplets. A kinetic study was performed using a catalase enzyme which was obtained from liver. As illustrated in Figure 1.4, electrodes were embedded into microchannels for monitoring the amount of H_2O_2 in each droplet. Valves were used for allowing different reaction times of each droplet to be delivered to the embedded electrodes. It was found that this electrochemical approach provided a great sensitivity of the kinetic study of catalase enzyme, which was comparable with a fluorescence method.

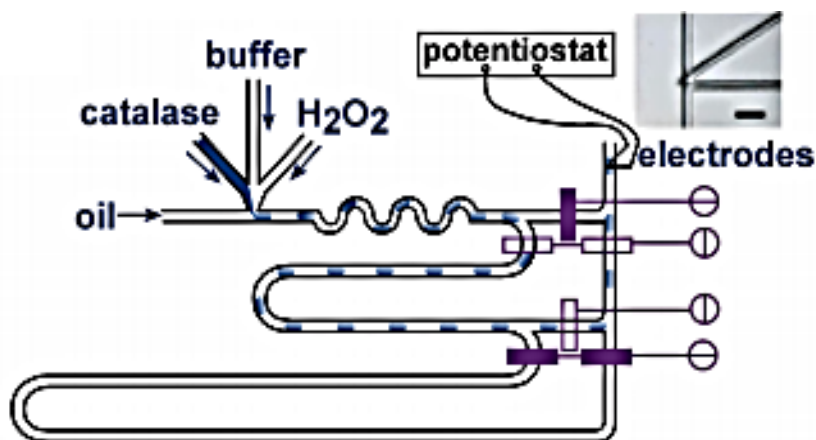


Figure 1.4 The kinetic study of a catalase enzyme using an amperometric technique with valves for delivering different reaction-time droplets to the electrodes. Reproduced from [18].

From previous reports about electrochemical detection in droplets, there has been a problem about the efficiency of droplet detection when using an electrochemical approach. Small sizes and high velocities of droplets in the system could affect electrochemical signal, resulting in low reproducibility of the method. Therefore, development and design of a system that could solve these problems were presented to improve reproducibility of electrochemical detection in droplets.

Lui and Crooks [15] reported an electrochemical method using gold micro bands for working and counter electrodes for a droplet-based system. The width of microchannel at the detection zone was reduced 10 times compared to the main channel. The confined channel was used to extend droplets to cover all electrodes, as illustrated in Figure 1.5. The confined channel provided longer analysis time, which allowed for the reaction to complete. In addition, results showed high reproducibility of electrochemical measurements of ruthenium complex in droplets.

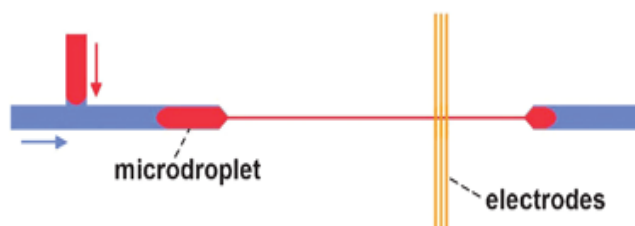


Figure 1.5 Detection of an analyte in droplets using amperometric measurements. A droplet was extended to cover all electrodes for longer time of electroanalysis. Reproduced from [15].

1.3 Scope and Aims of This Work

As mentioned from the previous reports, especially in Lui and Crooks' work, an amperometric measurement is the most proper approach for droplet detection systems because it provides the best efficiency for electrochemical measurements. In addition, an amperometric method also shows differentiation between oil and aqueous solution signals by generating droplet peaks. Thus, the aim of this work was to develop a GCM sensor coupled with droplet-based microfluidics. Carbon-paste electrodes (CPEs) were employed. CPEs not only provide high robustness, low electrode fouling and inexpensive material, but also provided the efficiency as well as gold electrodes in electrochemical methods. CPEs were modified using AuNPs and a conductive polymer, such as polyaniline and polypyrrole. The proposed sensor was expected to have high sensitivity and selectivity for determination of GCM in pharmaceutical products with high accuracy and precision. In addition, using a droplet-based system could provide high-throughput analysis, which could be used in the quality control of GCM in supplementary products.

CHAPTER 2

THEORY

2.1 Droplet-Based Microfluidics

A droplet-based or segmented flow microfluidic system has been developed for solving problems in laminar flow, including slow mixing and dispersion in sample zone in microfluidic channels. Segmented flow was originally reported by Song et al. [14]. Droplet-based microfluidic systems have been used for many applications in biological, chemical and physical fields [19]. This is because droplet microfluidic systems provide many features, such as high precision systems for monitoring reactions in real-time [20], an isolated microreactor for each micro-droplet [21] and high-throughput platforms for sample screening [22]. In addition, droplets can serve as reaction compartments with small volumes. Accordingly, small amount of samples and reagents is consumed by this microfluidic system.

2.1.1 Droplet Generation

To generate droplets in a microchannel, at least two immiscible phases are required. Generally, oil and aqueous solutions are used as well as air and aqueous solutions. To form droplets, there are two mechanisms for droplet generation, which are T-junction and hydrodynamic focusing. For T-junction configuration, oil is pumped into the microchannel while an aqueous solution flows perpendicularly to the oil flow stream. After that, the aqueous solution is then broken into droplets by oil flow, as demonstrated in Figure 2.1.

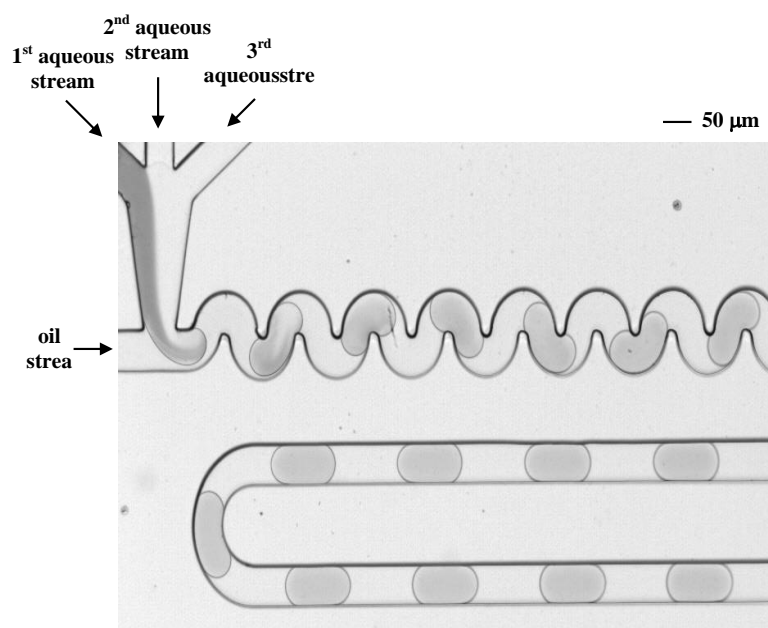


Figure 2.1 Droplet generation in a T-junction microfluidic device. Reproduced from reference [23].

For carrier phase, there are many kinds of oil used in droplet microfluidic systems, including vegetable oil [24] and perfluorodecaline (PFD) [25]. However, PFD is widely used owing to its viscosity and texture, which are similar to those of water. This makes PFD easy to manipulate. In addition, PFD is also well-known as high hydrophobic and biocompatibility.

In order to obtain clean droplet transportation along microchannels, developing of hydrophobic walls is necessary. In addition, the surface tension at the water-PDMS interface has to be higher than the surface tension at the water-PFD interface. This is to prevent the wetting of aqueous droplets on the channel walls. Therefore, the surface tension between water and PFD is necessary to be diminished to obtain clean droplet transportation. Accordingly, *1H,1H,2H,2H*-perfluoro-1-octanol as a surfactant is usually added into PFD to reduce the surface tension at the water-

PFD interface [25]. As a result, droplets move along the channel without leaving any footprints behind.

2.1.2 Droplet Size

Droplet size is determined by water fraction (W_f) which is a significant parameter indicating the fraction of water and oil phases in droplet generation. W_f is determined from flow rates of oil and aqueous solutions. To calculate W_f , an aqueous flow rate is divided by total flow [25], as shown in the equation below;

$$W_f = \frac{F_w}{F_w + F_o} \quad (2.1)$$

Where F_w ($\mu\text{L min}^{-1}$) is flow rate of an aqueous phase and F_o ($\mu\text{L min}^{-1}$) is flow rate of a carrier phase. W_f is a parameter that strongly affects the droplet size. When the W_f is higher, droplet size is larger, as seen in Figure 2.2. This is because more aqueous phase can come into droplets.

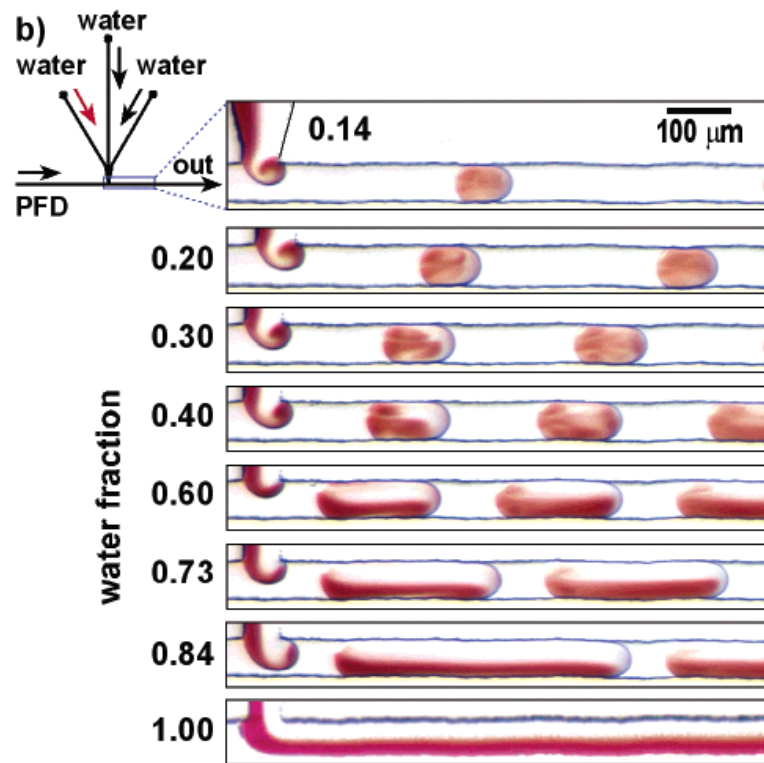


Figure 2.2 Droplet generation at different water fractions. Reproduced from reference [25].

However, if the value of W_f is too low, droplet formation may not be stable because there is a large difference between oil and aqueous flow rates. In addition, if W_f is too high, droplets could be broken and the aqueous phase would wet the channel. Furthermore, two parallel laminar flows would be observed instead of droplet formation if W_f is too high, as seen in Figure 2.2 at the W_f of 1.00. In addition, droplet size is independently of flow rate.

2.1.3 Mixing in Droplets

Mixing of solutions is very important, especially in kinetic studies. Slow mixing can cause reactions not complete before detection. Rapid mixing in droplets can be achieved using a curved channel, which is a part of the channel network. When a straight channel is replaced with a winding channel, re-orientation of droplet contents are repeated continuously. There are stretch and fold mechanisms in each droplet (Figure 2.3) [21]. When a plug is moving through a curved channel, its content is mixed chaotically, resulting in rapid mixing in droplets. However, a winding channel does not help rapid mixing in laminar flow, as shown in Figure 2.4. Therefore, a winding channel only enhances mixing in droplet systems [26, 27].

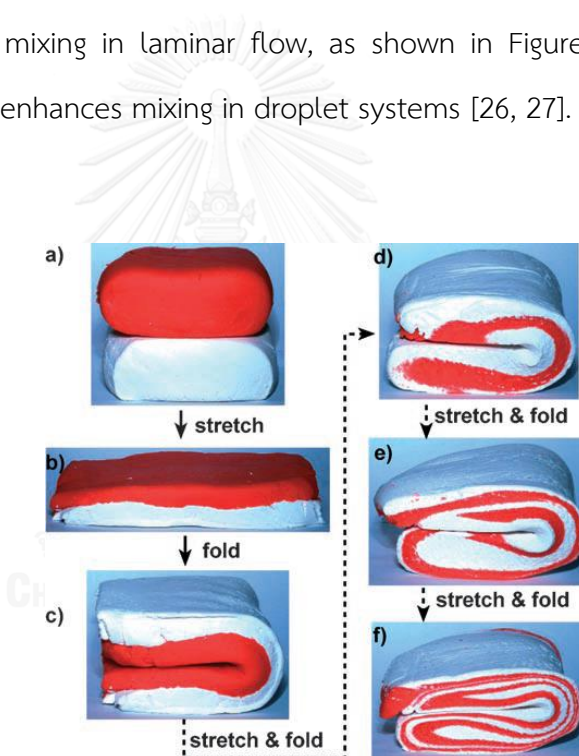


Figure 2.3 A model to explain the mixing of two reagents by chaotic advection in a droplet; photographs show two layers of the modeling clay being stretched and folded, resulting in rapid mixing. Reproduced from reference [21].

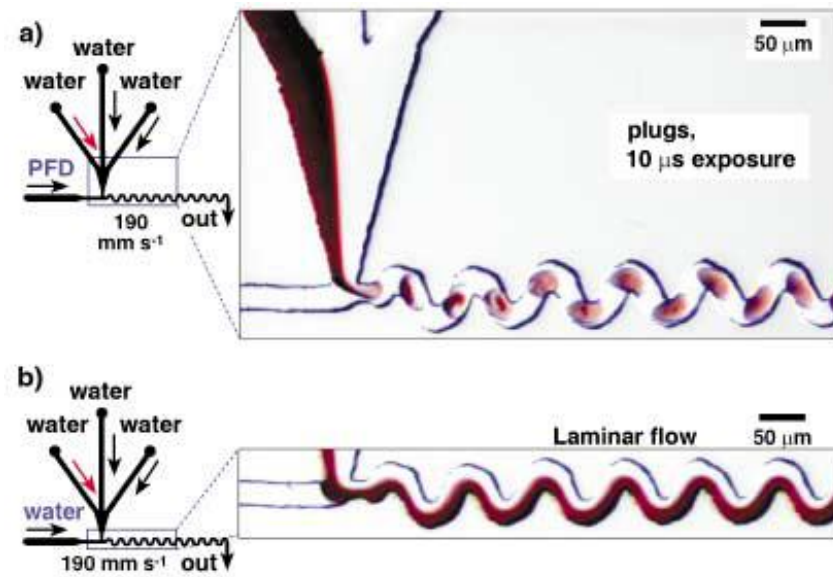


Figure 2.4 Comparison of (a) laminar flow microfluidics and (b) droplet-based microfluidics. The droplet system exploits a winding channel to generate rapidly chaotic mixing. Reproduced from reference [14].

2.1.4 Flow Velocity

Flow velocity is a parameter which is related to speed of droplets along the microchannel. Therefore, flow velocity affects analysis and reaction times.

To calculate flow velocity, Equation 2.2 is used [25];

$$V_T = (F_T A) \frac{10^6}{60} \quad (2.2)$$

where V_T (mm s^{-1}) is flow velocity, F_T ($\mu\text{L min}^{-1}$) is total flow rate in the system, which is the summation of flow rates of all inlets and A (mm^2) is droplet area in a microchannel. When flow velocity is too fast, a detector may not be able to measure the droplet contents effectively. Furthermore, too slow velocity would generate unstable droplets in the system, which may affect accuracy and precision of the measurements.

2.2 Microfluidic Device Fabrication

In order to fabricate microfluidic devices, soft lithography is generally employed[28]. First, a microchannel pattern is designed using an AutoCAD program. After that, SU-8 negative photoresist is used to fabricate a master template according to the designed pattern. Then, a monomer of polydimethylsiloxane (PDMS) mixed with a curing agent (10:1 w/w) is poured onto the master and allowed the polymer to be cured in an oven at 65 °C for 1-6 hours. A PDMS replica is then peeled from the master. Finally, the PDMS replica is bonded with another PDMS plate or glass to enclose the channels. Summary of microfluidic device fabrication is shown in Figures 2.5 and 2.6.

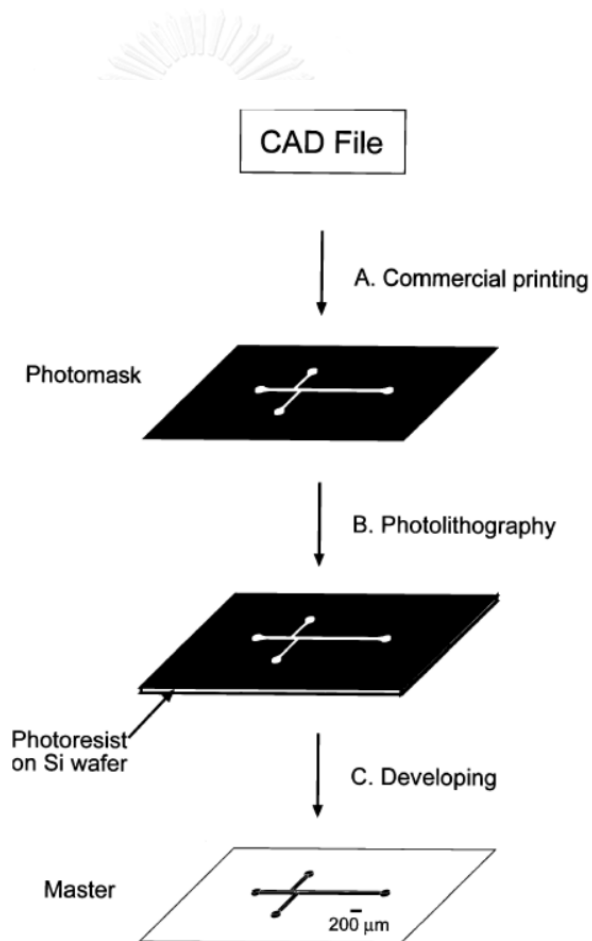


Figure 2.5 Master fabrication; (A) a design from AutoCAD (B) photograph to transfer the design onto a Si wafer (C) developing of master. Reproduced from reference [29].

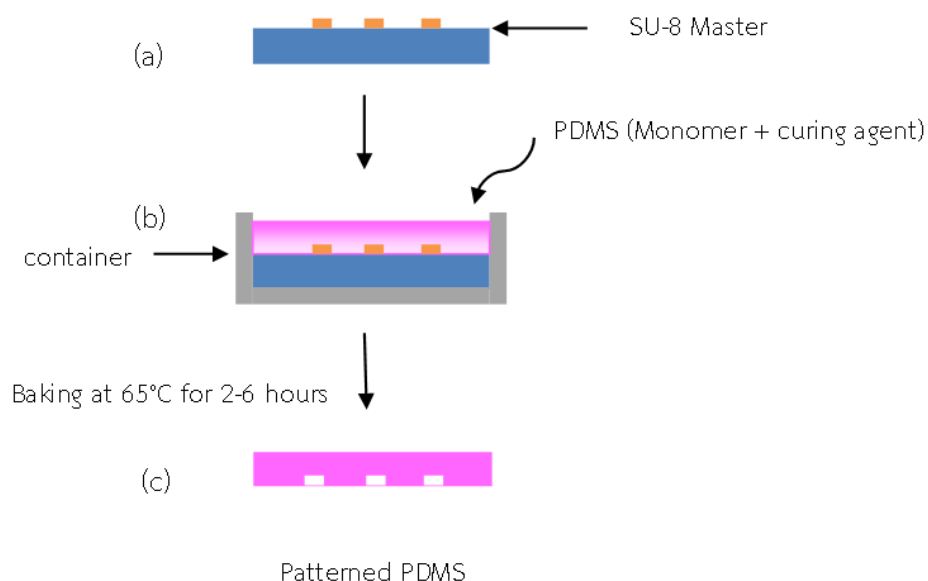


Figure 2.6 Soft lithography for PDMS casting. (a) A PDMS master containing the designed microchannel pattern. (b) PDMS monomer is poured onto the master. (c) A PDMS plate after casting from the master.

2.3 Detection in Microfluidics

Electrochemistry is one of the most useful methods for determination of electro-active species in solutions. It is not only used for qualitative analysis, but also quantitative analysis. Advantages of electrochemical detection include low limit of detection, good sensitivity, good accuracy, portability and low cost. Moreover, the size of electrochemical instruments is more suitable for microfluidic systems when compared to the size of traditional fluorescence setups. There are many techniques of electrochemical measurements, such as potentiometry, voltammetry and amperometry [30]. In this work, cyclic voltammetry, linear sweep voltammetry, and chronoamperometry were used.

2.3.1 Cyclic Voltammetry (CV)

For qualitative analysis using an electrochemical approach, cyclic voltammetry (CV) is the most powerful method to investigate the electrochemical behavior of electro-active species [31]. By combining the potential-time curve (E-t curve) and current-time curve (I-t curve), current-potential curve (I-E curve) is demonstrated. For CV, potentials of cathodic and anodic regions are scanned to measure currents and the currents are then plotted against potential to generate a cyclic voltammogram. A cyclic voltammogram shows a working potential that provides the highest current. In addition, a cyclic voltammogram shows a working potential range that can be used for measurements and may predict a suitable applied potential for amperometric measurements. Cyclic voltammograms, in this work, were generated using square wave voltammetry which gives high sensitivity and selectivity compared to other electrochemical techniques. A typical cyclic voltammogram and applied potentials are shown in Figure 2.4.

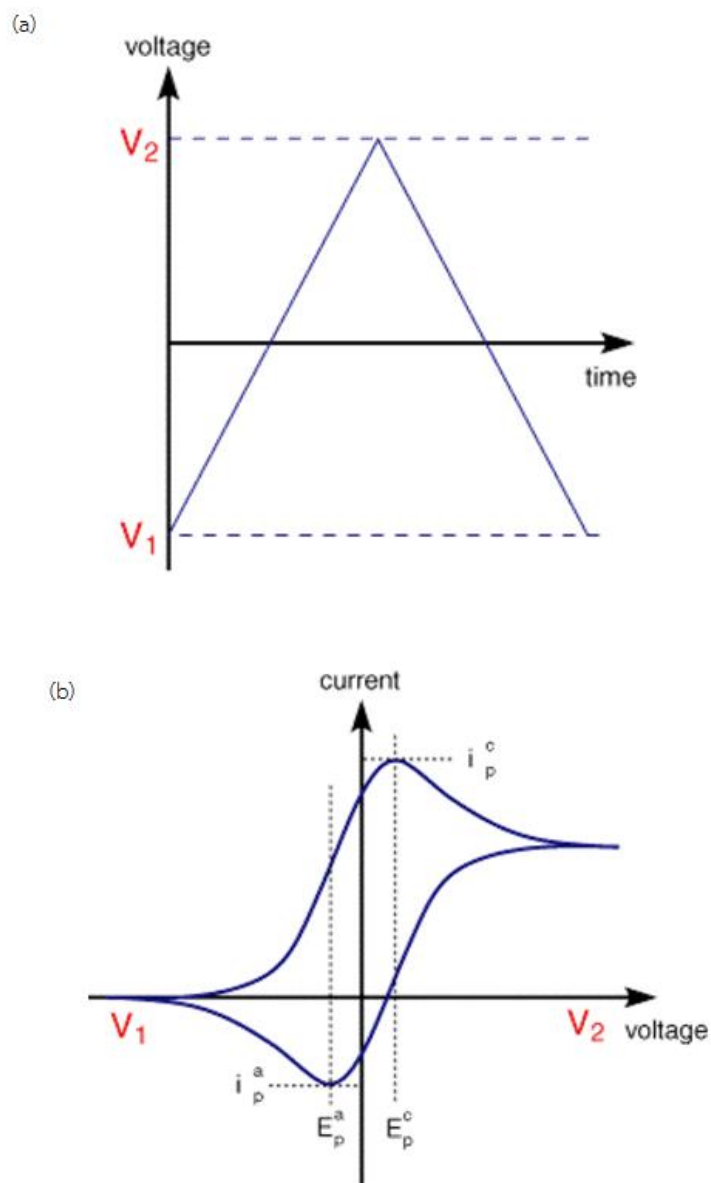


Figure 2.7 (a) A potential scan of CV where V_1 to V_2 causes an oxidation reaction and V_2 to V_1 provides a reduction reaction. Both reactions are called anodic and cathodic scans, respectively. (b) A typical cyclic voltammogram; E_{pc} is cathodic peak potential, i_{pc} is cathodic peak current, E_{pa} is anodic peak potential and i_{pa} is anodic peak current. Reproduced from reference [32].

2.3.2 Linear Sweep Voltammetry

Linear sweep voltammetry (LSV) is another useful technique which is generally used with a differential pulse [33] or square wave [34] mode. Using LSV, either cathodic or anodic reaction is determined at a time. Unlike CV, LSV is normally used for quantitative analysis in which a potential window is obtained from a cyclic voltammogram. In addition, increasing of scan rate could provide greater peak current, as followed the Randles-Sevcik equation [11];

$$i_p = 2.69 \times 10^5 A C n^{3/2} D^{1/2} \nu^{1/2} \quad (2.3)$$

where i_p is peak current (A), A is the electrode surface area (cm^2), n is the number of involved electrons, C is the concentration of analyte (mol cm^{-3}), D is the diffusion coefficient ($\text{cm}^2 \text{s}^{-1}$) and ν is scan rate (mV s^{-1}). Figure 2.8 demonstrated relationships between scan rates and peak current to obtain Randles-Sevcik relationship. Faster the scan rates result in higher the peak currents.



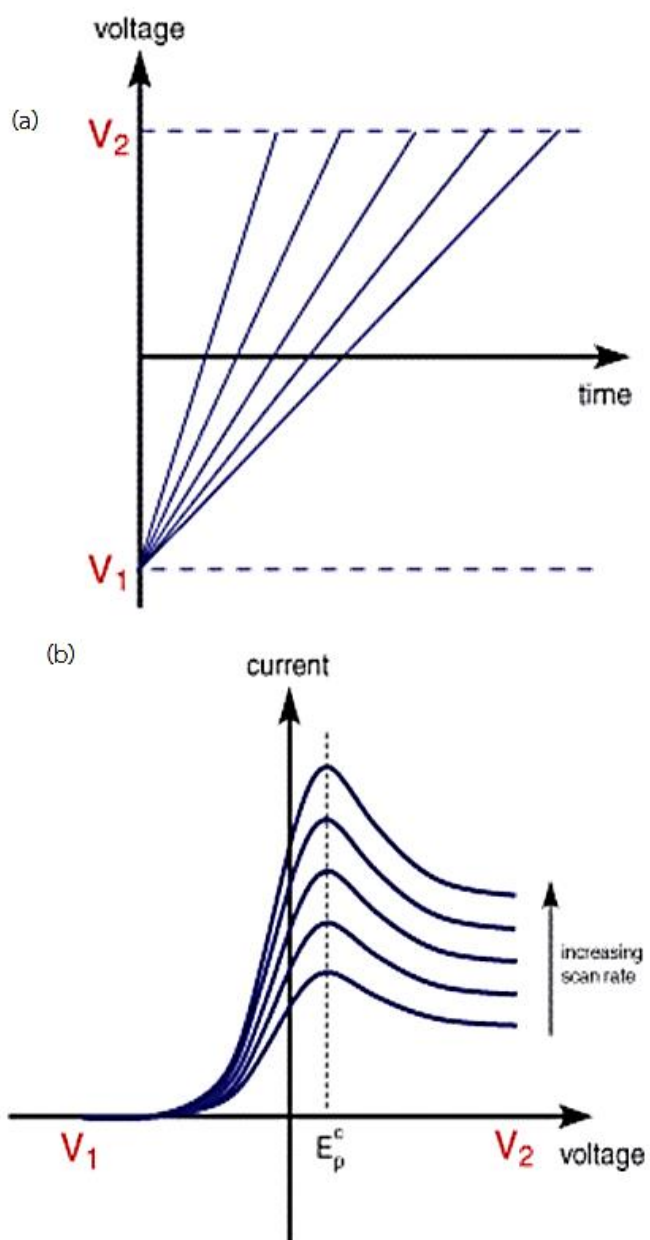


Figure 2.8 (a) Potential scans for linear sweep voltammetry. (b) Current signals obtained from varied scan rates. Reproduced from Reference [32].

2.3.3 Chronoamperometric Detection

Chronoamperometry is used to measure current with time when an applied potential is fixed [35]. Current is a result of electrochemical oxidation (positive applied potential) or reduction (negative applied potential) of electro-active compounds after applying a potential pulse across the working and auxiliary electrodes. For chronoamperogram, the initial peak current is high and then decreases exponentially with time until reaches a steady state, followed Cottrell's equation [36];

$$i = \frac{nFAC\sqrt{D}}{\sqrt{\pi t}} \quad (2.4)$$

Where i is the obtained current (A), n is the involved electron for oxidation or reduction, F is Faraday's constant which equal to $96,485 \text{ C mol}^{-1}$, A is area of electrode (cm^2). C is an initial concentration (mol cm^{-3}), D is diffusion coefficient ($\text{cm}^2 \text{ s}^{-1}$), and t is reaction time (s). A hydrodynamic voltammogram, a plot of applied potential versus signal to noise ratio of current, is normally generated to find an optimum applied potential for chronoamperometric measurements, as shown in Figure 2.9.

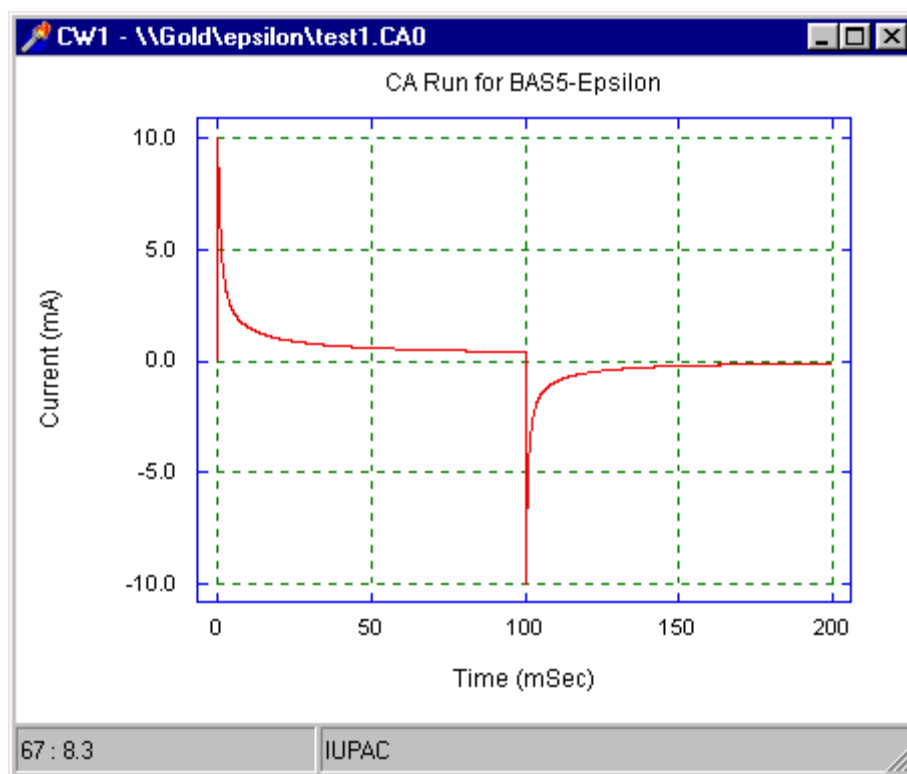


Figure 2.9 A chronoamperogram of oxidation (0-100 ms) and reduction (101-200 ms) reactions, which demonstrates decreasing of current with time as followed the Cottrell's equation. Reproduced from reference [37].

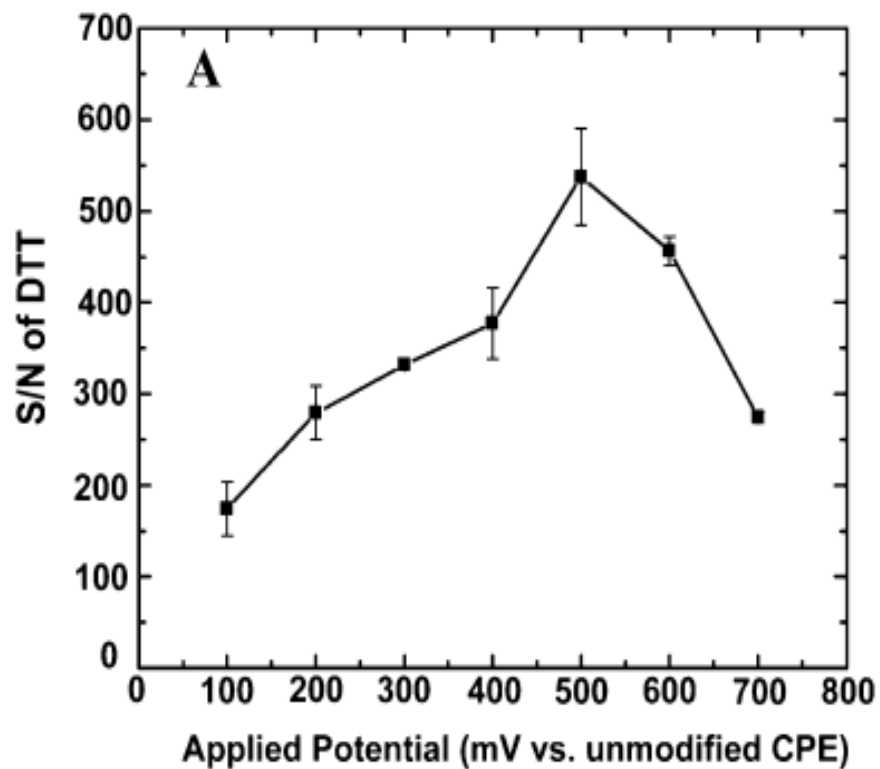


Figure 2.10 A hydrodynamic voltammogram 100 μM dithiotheritol injections plotted using the signal-to-noise ratio as a function of applied potential. Reproduced from reference [38].

2.4 Gold Nanoparticles

Almost a century metal nanoparticles have been used in electrochemical fields through electro-deposition techniques [39, 40]. By applying potential, metal ions are changed to nanoparticles onto the working electrode. One of the most useful metal nanoparticles for electrochemical approaches is gold nanoparticles (AuNPs). This is because gold metal is generally used as a working electrode in the past [41]. However, gold is a noble metal which is expensive and easy fouling. Thus, AuNPs, which are inexpensive, but still provides great electrochemical properties of gold metals, have been used and replaced gold electrodes. In addition, AuNPs have shown many outstanding advantages for electrochemical measurements, such as enhancing electrochemical signal [42] and detecting non-electroactive species [43]. In addition, enhancing of electrochemical signal is owing to large surface area of AuNPs. Furthermore, AuNPs are easily synthesized using only HAuCl_4 and sodium citrate. A synthesis mechanism of AuNPs is shown in Figure 2.11.

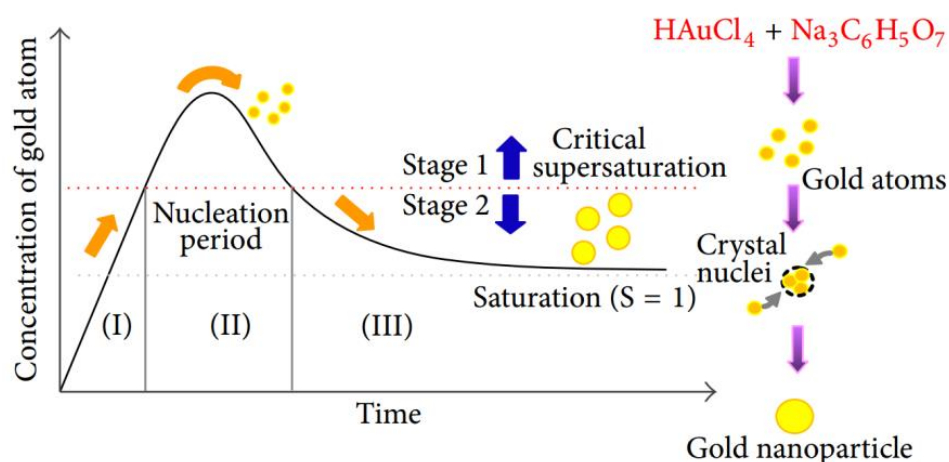


Figure 2.11 A mechanism of AuNPs synthesis. Reproduced from reference [44].

Gold plate electrodes are normally used for electrochemical detection of sugar compounds in high-performance liquid chromatography [7]. It is due to gold oxide (Au-OH) which acts as an electro-catalyst. Gold oxide can oxidize monosaccharides including glucosamine in many products [45]. However, gold plates, as mentioned above, are expensive and easy fouling. AuNPs, thus, become an alternative material for detection of sugar compounds, including glucosamine. There are many previous works reported using of AuNPs for sugar detection [46, 47].



2.5 Polyaniline

There are many kinds of conductive polymers used for electrochemical measurements, including polypyrrole, polyaniline and poly(3,4-ethylenedioxythiophene) [48]. Conductive polymers enhance electrochemical signals by increasing the working area. One of the conductive polymers widely used is polyaniline (PANI) because it is easy to prepare. In addition PANI provides many advantages including great electrochemical properties, good environmental stability and non-toxicity [9]. PANI has many forms with different colors and properties [49]. Basic and redox forms of PANI are demonstrated in Figure 2.12. Different forms of PANI provide different electrochemical properties; the green form of PANI (Emeraldine salt) provides the best electron transfer. This is because Emeraldine salt has both lone pairs of electrons and positively charged nitrogen atoms. Similar to a metal, electrons can be easily delocalized from a backbone structure of a phenyl group to a p-orbital of nitrogen atom. Thus, Emeraldine salt is the best form to be used in electrochemistry for modification of a working electrode.

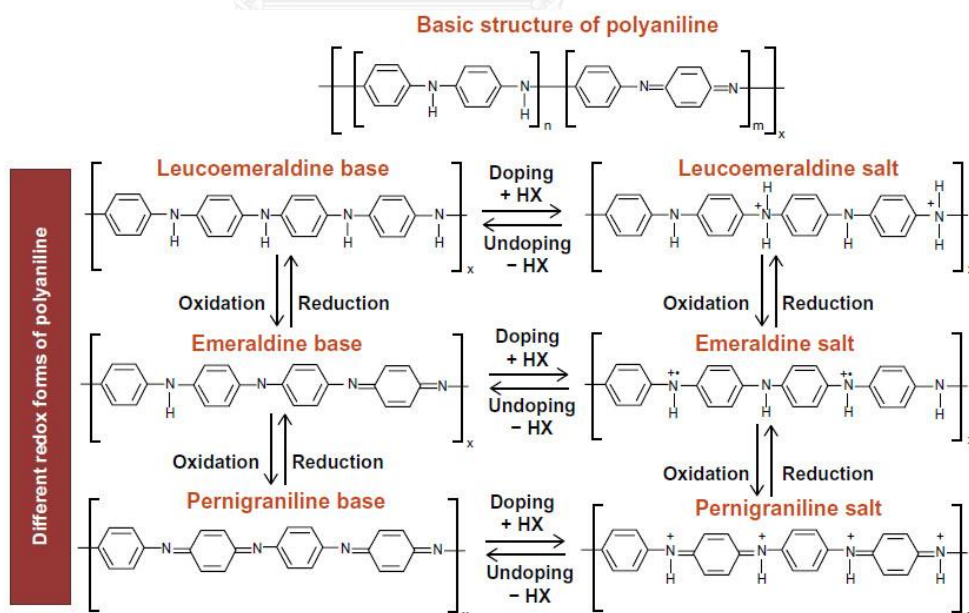


Figure 2.12 Basic and redox structures of polyaniline. Reproduced from reference [49].

In addition, PANI has known as an auto-reducer for gold metals onto its structure due to an electricfield-induced charge transfer between the PANI and AuNPs [50]. As illustrated in Figure 2.13, an electron belonging to imine may gain enough energy to move to surmount the interface between the PANI fiber and move onto the AuNPs. Accordingly, AuNPs become more negatively charged whereas PANI becomes more positively charged. Consequently, this property provides electrostatic interaction between PANI and AuNPs by mean that AuNPs could be trapped onto the PANI surface automatically. Therefore, PANI is chosen as a supporting conductive polymer for electrode modification using AuNPs.

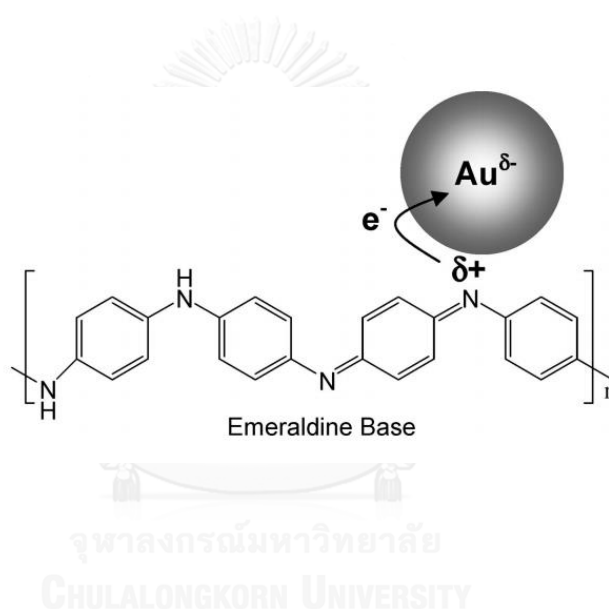


Figure 2.13 The interaction between PANI and AuNPs under the electric field-induced charge transfer. Reproduced from reference number [12].

2.6 Experimental Designs and Surface Response Methodology

The purpose of using experimental design is to deliver maximum attended information with using a minimum amount of experimentation. With a proper experimental design, a mathematical model can be calculated to represent the direct and interaction effect of the factors in the process. A central composite design (CCD) is an experimental design containing three blocks. As demonstrated in Table 2.2. The first block, experiment number 1 to 8, is a full factorial experiment which comprising of 2^3 experiments for three factors with two levels. In addition, the second block, experiment number 9 to 14, contains the star points. The third block contains replication of experiments whereas six experiments were performed. Figure 2.14 shows the graphical CCD design with a sphere corresponding to an experimental run with the experimental condition shown in a table be sided.

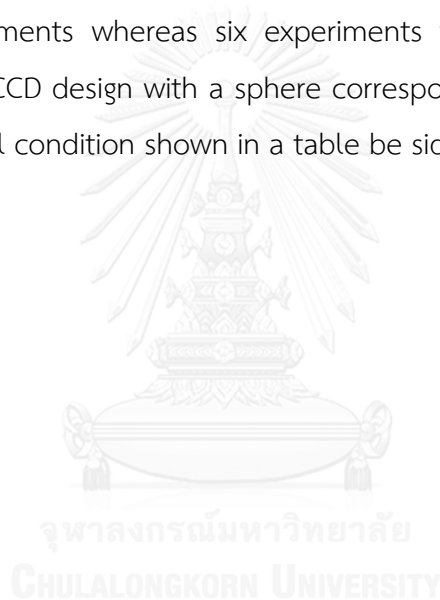


Table 2.1 Example of the experimental design using CCD with 3 factors and each factors consisted 2 levels.

Run	intercept	Factors		
		A	B	C
1	1	1	1	1
2	1	1	1	-1
3	1	1	-1	1
4	1	1	-1	-1
5	1	-1	1	1
6	1	-1	1	-1
7	1	-1	-1	1
8	1	-1	-1	-1
9	1	1.68	0	0
10	1	-1.68	0	0
11	1	0	1.68	0
12	1	0	-1.68	0
13	1	0	0	1.68
14	1	0	0	-1.68
15	1	0	0	0
16	1	0	0	0
17	1	0	0	0
18	1	0	0	0
19	1	0	0	0
20	1	0	0	0

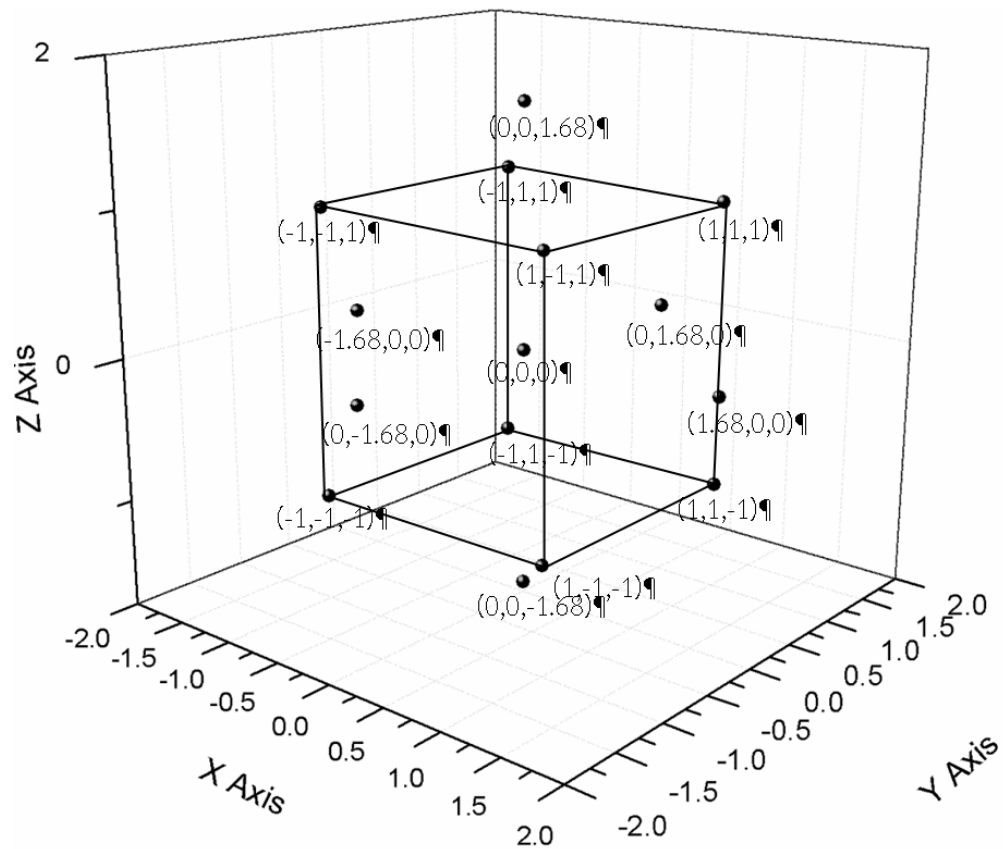


Figure 2.14 Generation of central composite design of two factors.

Varying only a single factor at a time, while the other factors are fixed at the specific conditions generally carries out for optimizing the multifactor experiments. This approach is called “One-factor at a time”. The optimized condition might be achieved in case of no interaction between factors in experiments. However, the influences of the designed factors on the response are rarely independent. There are several advantages of the approach as it is time consuming and incapable of the best optimization as the interactive effects of all primary factors are neglected. Response surface methodology (RSM) is an alternative technique to one-factor at a time approach [51]. The main advantage of RSM is to represent the interactive effects of the primary factors correlated to the response. It is very useful for developing, improving and optimizing the experimental conditions in order to obtain the most suitable responses of the process. The experimental factors X_1, X_2, \dots, X_n are

considered as the individual independent parameters with y is the responses. The regression model of these parameters with the individual, interaction and second order polynomial terms can be in order to find an appropriate approximation of the function as following equation.

$$y = b_0 + \sum b_i X_i + \sum b_{ii} X_i^2 + \sum b_{ij} X_i X_j \quad (2.5)$$

Where b_0 is the constant coefficient, b_i , b_{ii} , and b_{ij} are the regression coefficients and X_i , X_j indicate the dependent variables.

To obtain RSM of the experiment, it involves three main steps:

Step : 1 Careful design of the experiments : the statistically designed experiment using central composite design.

Step : 2 Evaluating the coefficients of the mathematical regression model : Multiple Linear Regression (MLR) technique [51, 52] was used to calculate the coefficients of each term in the regression model as following equation;

$$b = (D^T \cdot D)^{-1} \cdot D^T \cdot y \quad (2.6)$$

Where all factors are square matrices, b is coefficients ($M \times 1$), D is design matrix ($N \times M$), and y is response ($N \times 1$). In addition, M and N represent factors and samples amount, respectively.

.Step : 3 Calculate the predicted responses using the obtained regression model to produce the response surface in order to find the optimized condition.

As illustrated in Figure 2.11, a surface response can be obtained by plotting from the constructed equation which contains first order, quadratic, and interaction relationships.

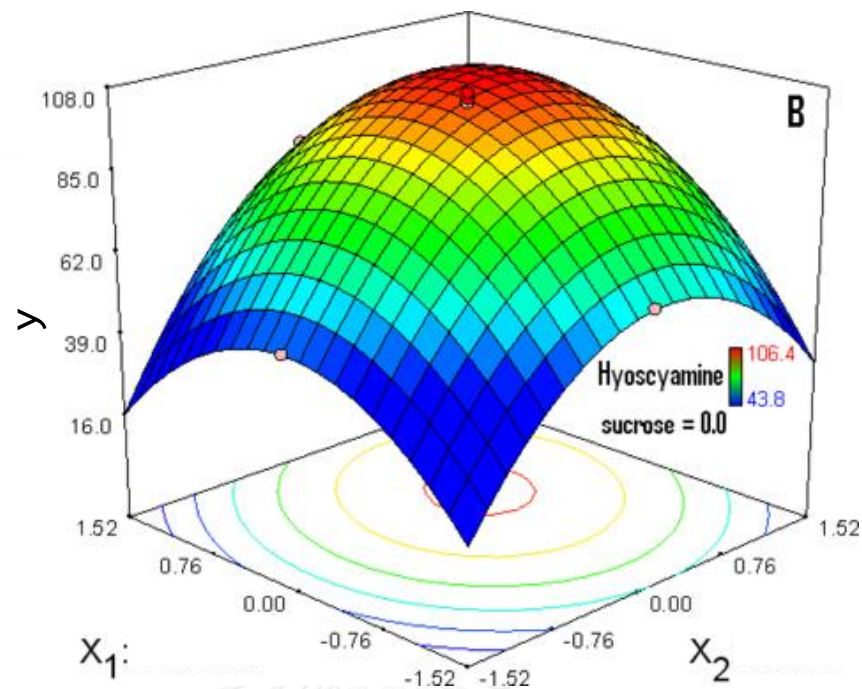


Figure 2.15 surface responses for effect of nitrate and calcium as the Hyoscyamine level for elicited hairy root. Reproduced from reference [53].

After obtaining response surface, the optimum conditions for each parameter are carried out. As response surface illustrated, the optimum condition is considered as a range for each parameter. However, first derivative of an obtained equation could use to figure out the optimum condition as an exact number.

CHAPTER 3

METHODOLOGY

3.1 Chemicals and Equipment

All chemicals were analytical grades and obtained from the companies listed in Table 3.1. In addition, all equipment used is shown in Table 3.2.

Table 3.1 List of chemicals and companies.

Chemicals	Companies
1. Noujol mineral oil	Perkin Elmer (Thailand)
2. Graphite powder ($\leq 20 \mu\text{m}$)	Sigma-Aldrich (Singapore)
3. Elastomer kit (Slygard 184)	Dow Corning (Midland, MI)
4. Silver paint	SPI supplied (Wast Chester, PA, USA)
5. Perfluorodecalin (95%)	Sigma-Aldrich (Singapore)
6. 1 <i>H</i> ,1 <i>H</i> ,2 <i>H</i> ,2 <i>H</i> -perfluoro-1-octanol	Sigma-Aldrich (Singapore)
7. Glucosamine hydrochloride	FlukaChemica CH-9471, Switzerland
8. Polyaniline	Sigma-Aldrich (Singapore)
9. 2-methyl- <i>N</i> -pyrrolidone (NMP)	Sigma-Aldrich (Singapore)
10. Defence pharmaceutical factory	Defence Pharmaceutical factory (Thailand)
11. Glucosa	Glucosa (Thailand)
12. Millimed	Millimed (Thailand)
13. Sodium chloride (NaCl)	Merck (USA)
14. Potassium chloride (KCl)	Ajax Finechem (Thailand)
15. Sodium hydrogenphosphate (Na_2HPO_4)	Merck (USA)
16. Potassium dihydrogenphosphate (KH_2PO_4)	Carlo ERBA (Thailand)
17. Deionized water (Milli-Q Gradient)	Millipore (Thailand)
18. Ethanol ($\text{CH}_3\text{CH}_2\text{OH}$)	Merck (Germany)
19. Chloroauric acid (HAuCl_4)	Sigma-Aldrich (Singapore)
20. Sodium citrate ($\text{Na}_3\text{C}_6\text{H}_5\text{O}_7$)	Sigma-Aldrich (Singapore)

Table 3.2 List of equipment and companies.

Equipment	Companies
1. Potentiostat (ED410, 410-088)	eDAQ, (Australia)
2. Syringe pump (PHD 2000)	Harvard Apparatus (USA)
3. Electric wires (AWG: 22, 100 FT.)	ALPS Industrial (Thailand)
4. Microscope (SZ-PT)	Olympus (Japan)
5. Tubing (OD: 1.09 mm, ID: 0.38 mm)	Portex (UK)
6. Syringe (1 mL)	Nipro (Thailand)
7. Safe-lock tube (1-2 mL)	Eppendorf (Thailand)
8. Micropipettes (10, 100, 1000 μ L)	Eppendorf (Thailand)

3.1.1 Synthesis of Gold Nanoparticles (AuNPs)

Gold nanoparticles (AuNPs) were synthesized using a traditional method [50]. Briefly, HAuCl_4 solution was prepared at a concentration of 1.0 mM in Milli Q water and citrate was prepared at a concentration of 38.8 mM (1% w/w). To synthesize AuNPs, 20 mL of 1.0 mM HAuCl_4 was added into a 50 mL beaker having a magnetic bar and then placed onto a stirring plate. After that, the solution was stirred and 2 mL of 1% sodium citrate was then quickly added. After allowing the reaction to occur for 10 minutes, the reaction was complete and a red wine solution was observed. This indicated that Au^{3+} was reduced to Au^0 in a nano-diameter size. The red colloid solution absorbed green light (~ 520 nm). Finally, the colloid solution of AuNPs (~ 20 nm in diameter) at concentration of 1000 ppm was successfully prepared as a stock solution.

3.1.2 Preparation of Polyaniline (PANI)

Polyaniline solution (PANI) was prepared using commercial polyaniline microfibers dissolved in NMP solution [54]. PANIs have many forms in different colors depending on pH of the solution; however, the green form (emeraldine base) provides the best electrochemical activity with a great electron transfer property. In order to prepare the green form of PANIs, 200 mg of PANIs was grinded together with 258 mg of camphor-10-sulfonic acid in 10 mL NMP solution. After that, the well-mixed solution was stirred for 5 hours to completely dissolve PANIs and sulfonic acid, which is necessary to obtain an electro-active form of PANI. Moreover, the stirred solution was sonicated for overnight before use to prevent self-aggregation of PANI microfibers in the solution.

3.2 Design and Fabrication of Devices

3.2.1 Mold Fabrication

Soft lithography, a pattern generation using a mold and soft polymer was used for device fabrication [28]. In this work, PDMS masters were fabricated into 2 patterns (an electrode array and microfluidic channels). The protocol of mold fabrication was illustrated in Figure 3.1. First, 1 mL SU-8 (3050), a negative photoresist, was dropped onto a cleaned silicon wafer. A cleaned silicon wafer was prepared by immersing a wafer into piranha solution for 1 hour, rinsed with MilliQ water and then dried using nitrogen gas. After that, the silicon wafer containing SU-8 was spun using a spin coater. For a thickness of 100 μm of SU-8 3050, two spinning steps were required. The first step was using a spin speed at 500 rpm with an acceleration rate of 100 rpm min^{-1} and hold at this speed for 10 seconds, and then the speed was increased to 1,000 rpm min^{-1} with an acceleration rate of 300 rpm and hold at this speed for 30 seconds. Furthermore, the spin-coated silicon wafer was

placed onto a hot plate at $95\text{ }^{\circ}\text{C}$ for 20 minutes to remove the solvent in SU-8 solution. Thereafter, a photomask containing microchannel and electrode patterns, which were designed using AutoCAD 2010, was placed onto the silicon wafer. To polymerize SU-8, the silicon wafer with photomask was exposed under the UV-light for 90 seconds. The UV-light initiated polymerization of SU-8 and only the exposed SU-8 was polymerized. To crosslink the SU-8 polymer, a post-baking process was performed. The exposed silicon wafer was baked onto a hotplate at $65\text{ }^{\circ}\text{C}$ for 1 minute and $90\text{ }^{\circ}\text{C}$ for 15 minutes, respectively. To develop patterns onto the silicon wafer, a developer solution containing propylene glycol monomethyl ether acetate 50% (v/v) was used. The silicon wafer was immersed into the developer for 20 minutes to remove non-polymerized SU-8, and then rinsed with isopropanol to check non-polymerized SU-8 which appeared in white. Subsequently, acetone was used to clean up and the developed patterns were then dried with nitrogen gas and baked at $90\text{ }^{\circ}\text{C}$ for 15 minutes to completely cure the SU-8 polymer, which provided a long-lasting life time. A complete PDMS master was achieved and ready to use as a mold for soft lithography of PDMS microfluidic device fabrication, as illustrated in Figure 3.2.

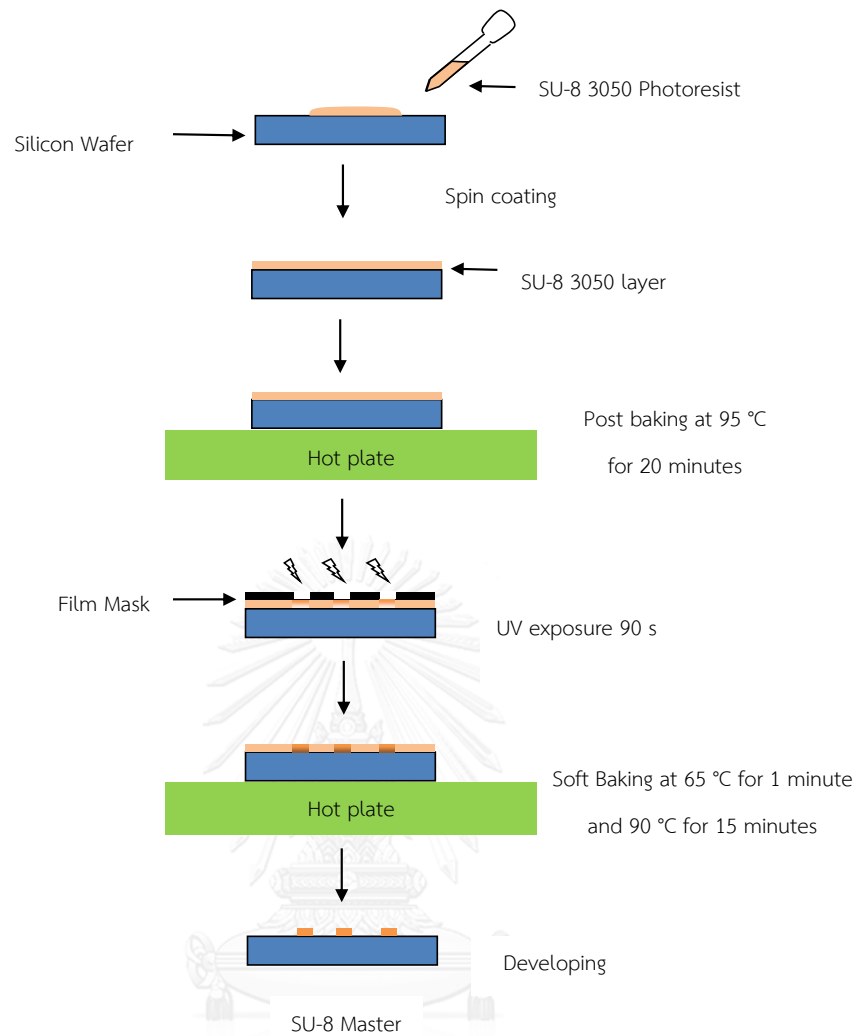


Figure 3.1 Fabrication of a PDMS mold on a silicon wafer using SU-8 negative photoresist. Adapted from reference [29].

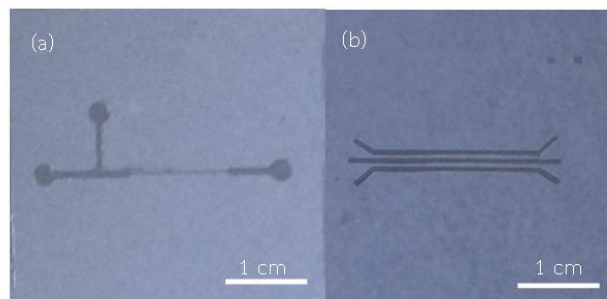


Figure 3.2 Complete SU-8 masters on silicon wafers; (a) microchannel patterned and (b) electrode patterned masters.

3.2.2 PDMS Casting

To fabricate microfluidic devices, polydimethylsiloxane (PDMS) was chosen as a material due to its elasticity and easy molding [13]. In addition, this biocompatible material provides many advantages: high reproducible fabrication in microscale patterns, optical transparency, low curing temperature, low cost, biocompatibility and easy surface modification [29]. A microfluidic device consisted of 2 parts which were well/microchannel and electrode plates. Both parts of a microfluidic device were made of PDMS using soft lithography, a traditional method for PDMS device fabrication. The PDMS molding protocol is demonstrated in Figure 3.3. The SU-8 master was used as a mold to transfer the design onto a PDMS plate. To fabricate PDMS plates, PDMS monomer was mixed together with a curing agent at a ratio of 10:1 (w/w). After well mixing, the mixture was degassed using a vacuum desiccator. Thereafter, the PDMS mixture was poured onto the SU-8 master comprising of the desired patterns and then left in an oven at 65 °C for 1 hour. After cooling, PDMS having the patterns was cut into small pieces. Finally, forceps were used for peeling a completely cured PDMS plates from the silicon master and PDMS plates were ready to use, as illustrated in Figure 3.4.

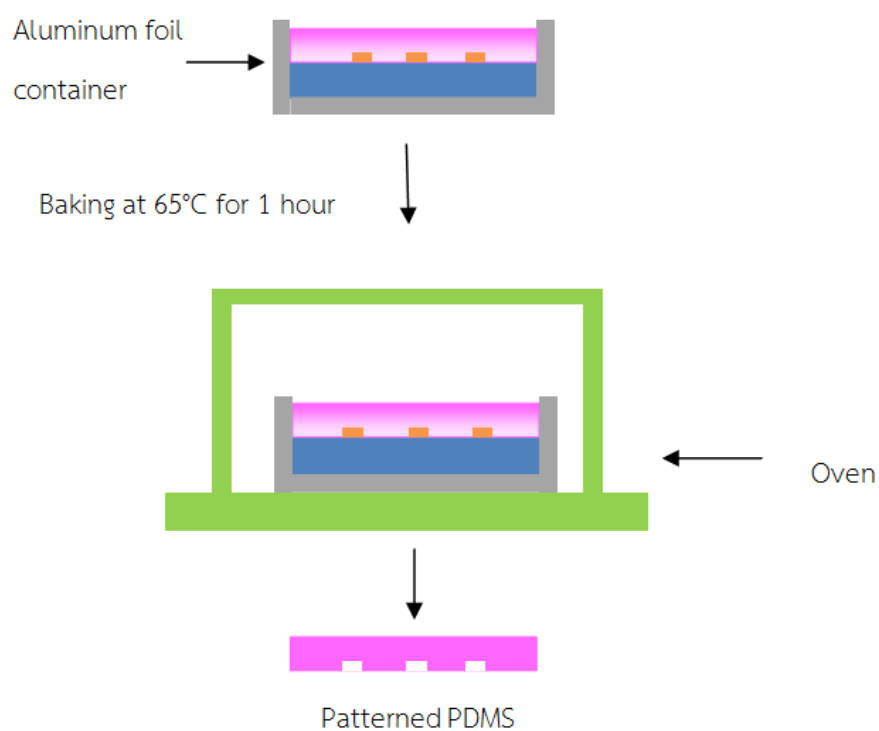


Figure 3.3 A PDMS casting process for microfluidic device fabrication using SU-8 molded onto a silicon wafer as a PDMS master.

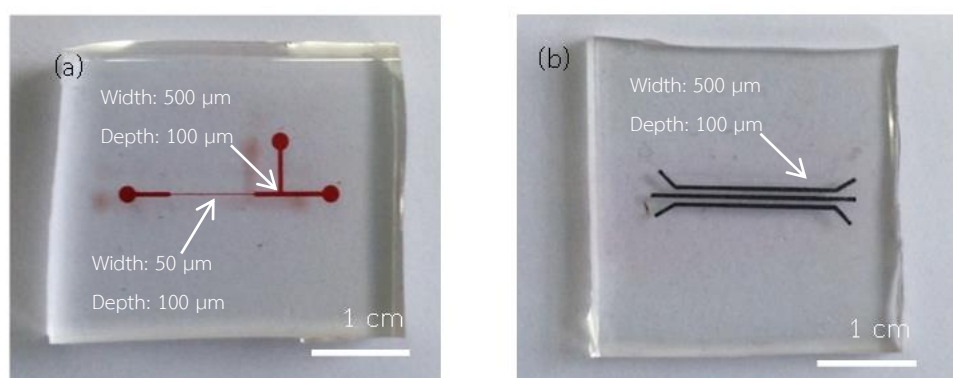


Figure 3.4 PDMS replicas; (a) microchannel patterned PDMS and (b) electrode patterned PDMS. A red dye in (a) and carbon paste in (b) were filled into the channels for visualization.

3.2.3 Electrode Fabrication

In this work, there were two electrochemical-cell platforms for batch and droplet-based microfluidic measurements. Both platforms used the same procedure to fabricate an electrode array which was carbon paste. In a manner of traditional electrochemistry, carbon paste electrodes (CPEs) generally consist of only graphite powder and mineral oil in which the mixture is easily filled into an electrode tube to be used as either a working or counter electrode. Nevertheless, using a traditional carbon paste electrode could cause a short circuit in flow-based systems because other electrodes are easily contaminated with carbon paste. Sameenoi et al. [55], therefore, developed highly robust CPEs by adding an electrochemical inactive polymer (PDMS) as a binder into a mixture of CPEs. Accordingly, graphite powder, nujol oil and PDMS were mixed at a ratio of 2:1:1 (w/w). For instance, to prepare 10 mg of carbon paste, 2.5 mg of nujol oil and 2.5 mg of PDMS were mixed in a container. After well mixing, 5 mg of graphite powder was added into the container containing liquid mixture, and then mixed until obtaining a homogeneous texture.

To fabricate CPEs, the carbon paste mixture was added into the channels of an electrode-patterned PDMS. After that, a rubber was used to embed carbon paste into the microchannels, which is illustrated in Figure 3.5 (a). As demonstrated in Figure 3.5 (b), the excess carbon paste was removed using Scotch Magic Tape™ for several times until only carbon paste left in the microchannels. Finally, CPEs were successfully fabricated and ready to be used for further steps, as shown in Figure 3.5 (c).

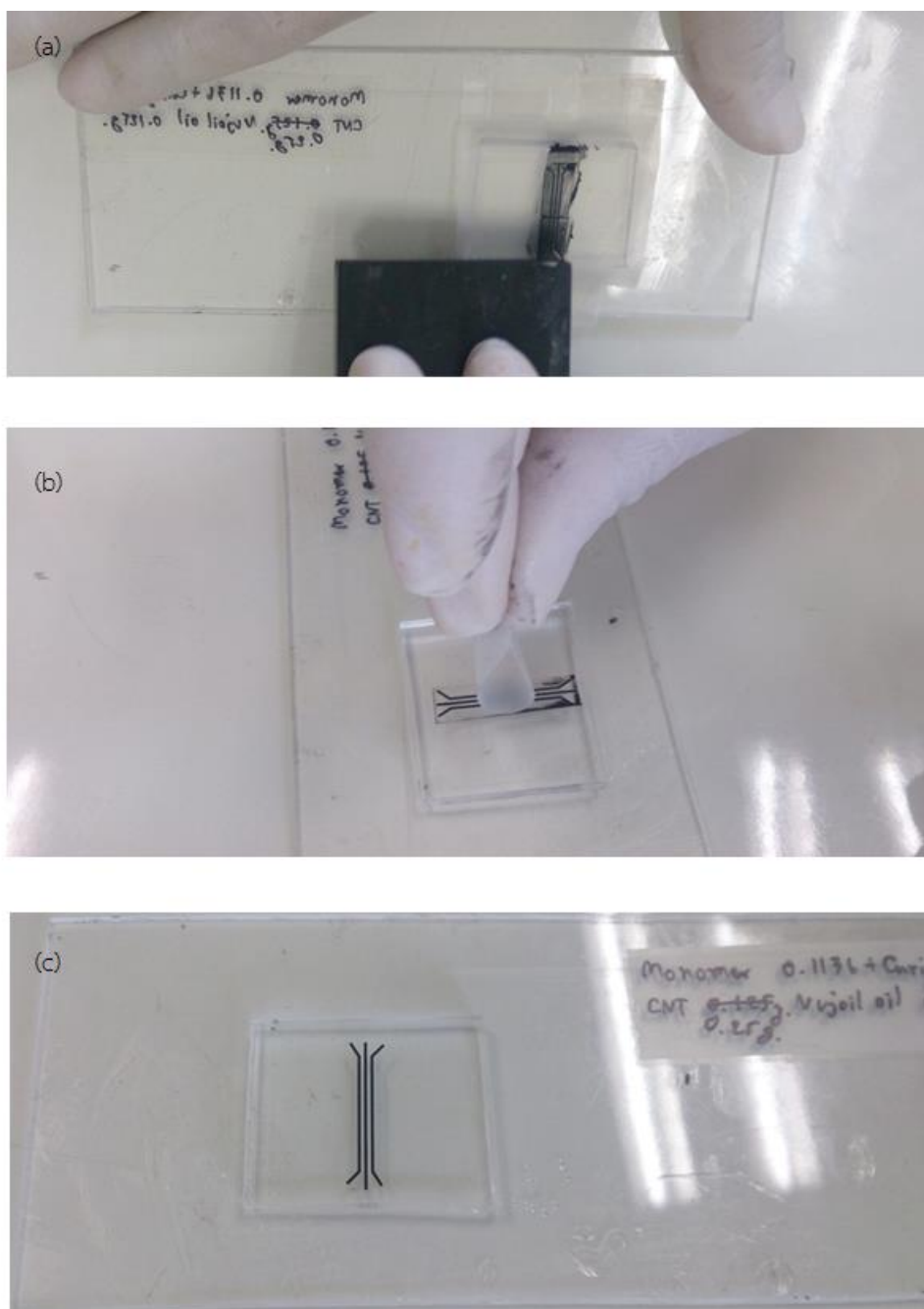


Figure 3.5 Electrode Fabrication. (a) Carbon paste was filled into microelectrodes on a PDMS plate using rubber as a spreader. (b) The excess carbon paste was removed using Scotch Magic Tape™. (c) A complete microchannel array on a PDMS plate after cleaning.

3.2.4 Microfluidic Device Assembly

To assemble a microfluidic device, oxygen plasma was employed. Due to the surface of PDMS which comprises of Si-OH and Si-CH₃, it is easily oxidized by oxygen plasma. Oxygen plasma, an electron-rich oxygen gas, can oxidize Si-OH into Si-O⁻ in which covalent bonding between Si and O provides -Si-O-Si- bonding between PDMS plates. For traditional PDMS assembly, both PDMS plates are assembled after being exposed to oxygen plasma. From the previous work [11]; however, exposing CPEs to oxygen plasma would reduce the electrochemical property of the electrodes. In addition, CPEs were comprised of nujol oil, which is an organic compound, as a dispersing agent. Using oxygen plasma could oxidize nujol oil and the absence of the organic compound in the electrode component could affect electrode properties. Therefore, to assemble microfluidic devices, only a PDMS cover plate (not electrode-patterned plate) was exposed to oxygen plasma for 30 seconds and then placed onto the other PDMS plate (an electrode-patterned plate). Thus, a complete microfluidic device was ready to be used for the next step.

3.2.5 Attachment of Electric Wires

Electric wires were attached to each electrode for connecting a microfluidic system to an electrochemical system. Electric wires were cut into ~2.5 cm length and then plastic insulator was removed ~0.3 cm from both ends of the cut wires. As illustrated in Figure 3.6, electric wires were attached to each electrode using silver paint which provided both adhesive and conductive properties.

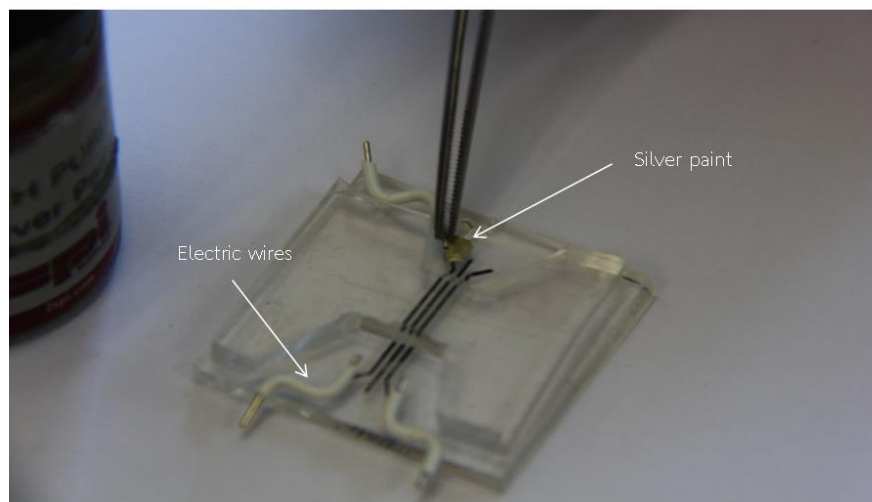


Figure 3.6 Electric wires were attached at the end of electrodes using silver paint as a conductive adhesive.

After that, epoxy glue was applied onto the connection between electric wires and electrodes for a long-lasting electrode lifetime and minimizing background noise. The epoxy glue was left for 1 hour to allow the glue to be cured. A complete microfluidic device with a patterned channel (500 μm width and 100 μm depth) is illustrated in Figure 3.7 (a). This microfluidic device was used for droplet-based microfluidic measurements. In addition, using the same protocol, a well-like microfluidic device was also fabricated and a complete device is shown in Figure 3.7 (b). This microfluidic device was used for batch measurements, including optimization of electrode modification in the CCD process.

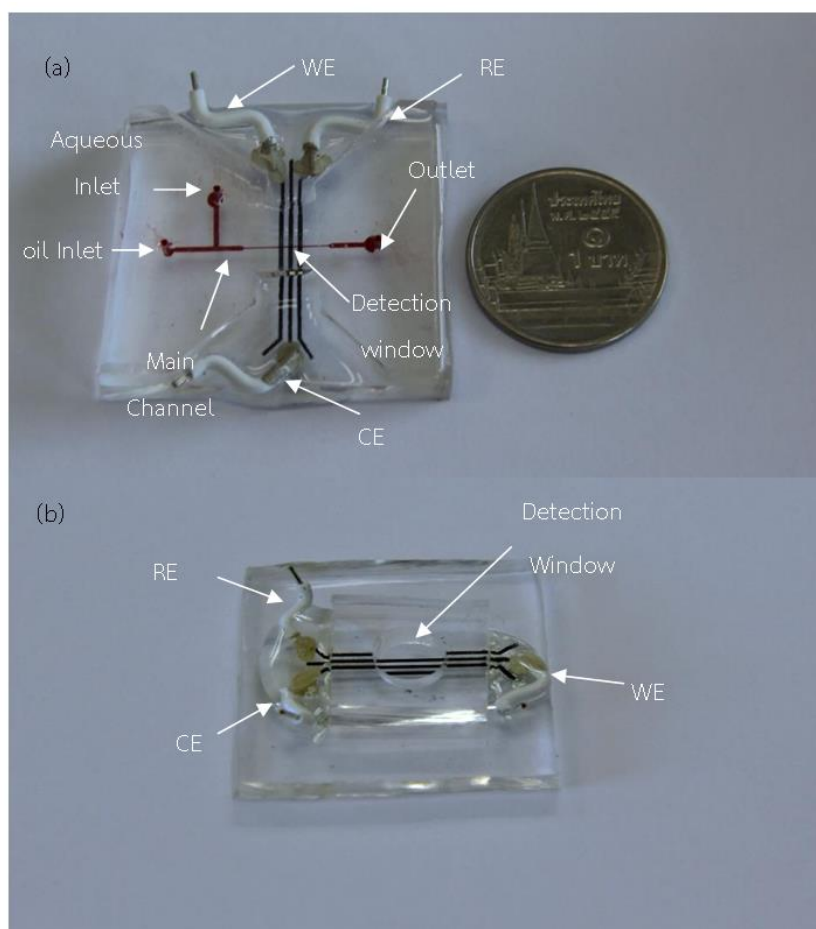


Figure 3.7 Complete microfluidic devices with two different designs: (a) a device containing a patterned microchannel of 500 μm width and 100 μm depth for the main channel and 50 μm width for a confined channel as a detection window and (b) a well-like design with a punched hole (~0.8 cm in diameter) as a solution container. WE, CE and RE are working, counter and reference electrodes.

3.3 Solution Preparation

3.3.1 Preparation of AuNPs and PANI Solutions

Solutions of AuNPs and PANI were prepared as mentioned in 3.1.1 and 3.1.2. To modify working electrode, AuNPs and the mixture of AuNPs and PANI solutions were directly applied onto the working electrode using a drop-casting technique. AuNPs in the mixture solution were prepared from a stock solution at a concentration series of 100 to 500 mg L⁻¹ in deionized water. In addition, a concentration series of PANI was also prepared in NMP at a concentration range from 1 to 5 mg mL⁻¹ from a stock solution. NMP was used as an additional solvent for the mixed solutions. The mixed solutions were prepared as demonstrated in Table 3.3 in which the total volume is 10 μ L.

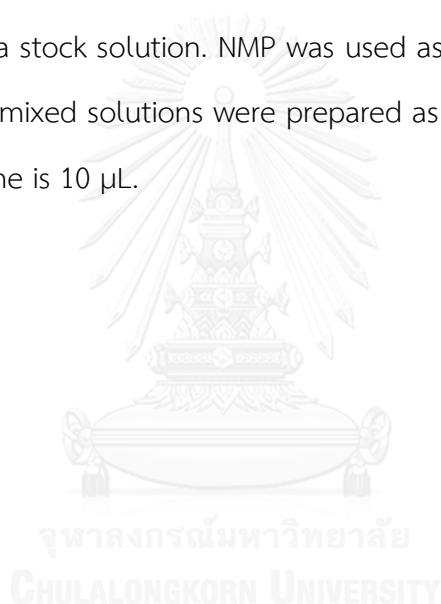


Table 3.3 Preparations of mixed solutions between AuNPs and PANI in NMP for electrode modification.

AuNPs Concentration (mg L ⁻¹)	Volume of 1000 mg L ⁻¹ AuNPs (μ L)	PANI Concentration (mg mL ⁻¹)	Volume of 10 mg mL ⁻¹ PANI (μ L)	Volume of NMP (μ L)
500	5	500	5	0
468	4.68	3	3	2.32
400	4	4	4	2
400	4	2	2	4
300	3	3	3	4
300	3	4.68	4.68	2.32
300	3	1.32	1.32	5.68
200	2	4	4	4
200	2	2	2	6
132	1.32	3	3	5.68

3.3.2 Preparation of Phosphate Buffer Saline (PBS)

In this work, phosphate buffer was chosen as an electrolyte due to the wide range of pH and easy preparation. Phosphate buffer was prepared at a concentration of 10 mM while saline solution was prepared at 0.1 M. For 250 mL of 0.1 M PBS pH 7.4, it was prepared using 0.05 g KCl, 0.36 g Na₂HPO₄ and 0.06 g KH₂PO₄, after that 2.0 g of NaCl was added into the solution. All solutions were prepared using 18.0 M Ω cm⁻¹ Milli-Q water. In addition, PBS was adjusted to a desired pH using 0.1 M phosphoric acid or NaOH.

3.3.3 Preparation of GCM Standard Solutions

GCM solutions were prepared in 0.1 M PBS pH 7.4 at a concentration of 100 mM for preliminary experiments of electrode modification using 500 mg L⁻¹ AuNPs and 5 mg mL⁻¹ PANI. For instance, a stock solution of 100 mM GCM was prepared using 2.15 g of GCM hydrochloride (MW = 215.67 g mol⁻¹) dissolved in 1 mL of 0.1 M PBS. GCM solutions with different pH values for CCD experiments were also prepared at a concentration of 100 mM. To construct a calibration curve, a concentration series of GCM was prepared in 0.1 M PBS as demonstrated in Table 3.4. In addition, at high concentrations of GCM (higher than 100 mM), solutions were prepared directly using GCM hydrochloride salt. PBS was used to adjust the final volume of 1000 μ L.

Table 3.4 Preparation of GCM solutions from a stock solution of 100 mM GCM in 0.1 M PBS.

Glucosamine (mM)	Volume of Stock Solution (μ L)	Volume of PBS (μ L)
0.05	0.5	999.5
0.1	1	999
0.5	5	995
1	10	990
2.5	25	975
5	50	950
15	150	850
25	250	750
35	350	650
40	400	600
60	600	400
80	800	200
100	1000	0

3.3.4 Preparation of Sample Solutions

For real samples, commercial GCM products (oral supplements) were obtained from a local pharmacy. Three supplementary products (Defence Pharmaceutical Factory, Glucosa, and Millimed contained 1500 mg of GCM. To prepare sample solutions, all commercial products were prepared as stock solutions at a concentration of 100 mM in 0.1 M PBS pH 4. For batch measurements, both 20 mM and 80 mM of GCM in real sample solutions were prepared because two linear ranges were obtained in this system. However, only 3.5 mM GCM solution which is a concentration in the linear range of a standard GCM was prepared for the droplet-based system. In addition, all solutions were prepared using the same criteria as shown in Table 3.4.

3.3.5 Preparation of Solutions for Capillary Electrophoresis

Borate buffer was used in this work for CE analysis and prepared at a concentration of 100 mM and then adjusted to pH 10 using 0.1 M NaOH. A concentration series (1 to 10 mM) of GCM was prepared in 100 mM borate buffer for construction of a calibration curve. The GCM solutions were left overnight to allow GCM to form complex with borate. In addition, all GCM solutions were prepared from 100 mM GCM stock solution using the same protocol as demonstrated in Table 3.4.

3.4 Experimental Design and Setup

3.4.1 Batch Measurements

For batch measurements, well-like microfluidic devices, as shown in Figure 3.7 (b) were used. These microfluidic devices used 50 μL of solution for each experiment. To obtain electrochemical data from a well-like microfluidic device, cyclic voltammetry (CV) and square-wave linear-sweep voltammetry were used. For linear sweep voltammetry, a square wave frequency of 30 Hz and a step height of 0.005 V for scanning the potentials between -1.0 and 1.3 V versus carbon pseudo-reference electrode were used. In addition, scan rates of 50 - 500 mV s^{-1} were used for electrode characterization using CV and a scan rate of 150 mV s^{-1} was employed for CCD and preliminary measurements.

3.4.1.1 Electrode Modification and Optimization

3.4.1.1.1 AuNPs Modified Electrode

In this work, AuNPs were modified onto one of the CPEs in the electrode array using the drop-casting technique. To modify electrode, 1 μL of 1000 ppm AuNPs was dropped onto the working electrode, and then casted the solution over the electrode area. To dry the solvent, the electrodes were placed into an oven at 65 $^{\circ}\text{C}$ for 1 hour. Thus, the electrodes were ready for further electrochemical measurements.

3.4.1.1.2 AuNPs and PANI Modified Electrode

To modify CPE using AuNPs and PANI, a mixture of AuNPs and PANI at various ratios as shown in Table 3.3 were modified onto a working electrode using the same technique as AuNPs modification.

3.4.1.1.3 Electrode Optimization

In this work, central composite design (CCD), a box-like design covered with a spherical shape was used as an experimental design to optimize the amounts of AuNPs and PANI for electrode modification and pH of the working solution. For CCD experiments, each parameter was coded to get rid of analytical bias from using different levels of each parameter. As demonstrated in Table 3.5, code values of each parameter are shown.

Table 3.5 Code values for pH and the amounts of AuNPs and PANI.

Factor	Code				
	-1.68	-1	0	1	1.68
pH	5.32	6	7	8	8.68
AuNPs (mg L^{-1})	132	200	300	400	468
PANI (mgmL^{-1})	1.32	2	3	4	4.68

In addition, 20 experiments were performed using the code values, as shown in Table 3.6, for construction of a surface response plot. All experiments in Table 3.6 represent each point inside a simulation sphere and box for all parameters.

Table 3.6 Central composite design for optimization of pH and the amounts of AuNPs and PANI.

Run	pH	AuNP	PANI
1	1	1	1
2	1	1	-1
3	1	-1	1
4	1	-1	-1
5	-1	1	1
6	-1	1	-1
7	-1	-1	1
8	-1	-1	-1
9	1.68	0	0
10	-1.68	0	0
11	0	1.68	0
12	0	-1.68	0
13	0	0	1.68
14	0	0	-1.68
15	0	0	0
16	0	0	0
17	0	0	0
18	0	0	0
19	0	0	0
20	0	0	0

For each experiment, square wave cyclic voltammetry was used to obtain electrochemical peaks of GCM. Peak currents from CVs were used for calculation in CCD process which provided the equation for prediction of the optimum values.

3.4.2 Droplet Measurements

3.4.2.1 Droplet Generation

For droplet generation, a T-junction microchannel was employed to generate droplets, as illustrated in Figure 3.8. There were two immiscible phases including oil and aqueous solutions. For oil solution or a carrier phase, perfluorodecalin was mixed with 1*H*, 1*H*, 2*H*, 2*H*-perfluoro-1-octanol at a ratio of 10:2 (v/v). 1*H*, 1*H*, 2*H*, 2*H*-perfluoro-1-octanol was used as a surfactant to stabilize aqueous droplets inside the microchannel. To generate droplets, both oil and aqueous solutions were filled into 1 mL of plastic syringes which were connected to tubing, and then placed onto syringe pumps. After that, oil was pumped into the microfluidic channel for 10 minutes for generation of hydrophobicity onto the PDMS channel walls. Subsequently, an aqueous solution was delivered into the microchannel perpendicularly to the oil flow. When the aqueous solution came into the T-junction, it was then broken by the oil stream into droplets which traveled along the microchannel. Droplet generation was observed under a microscope for visualization.

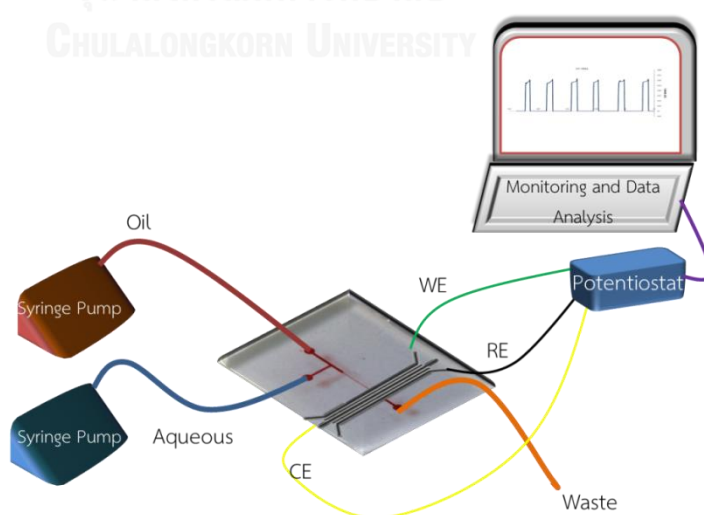


Figure 3.8 An experimental setup of a droplet-based microfluidic device with electrochemical detection.

3.4.2.2 Chronoamperometric Measurements in Droplets

3.4.2.2.1 Optimization of Flow Rate and W_f

To study effect of total flow rate on electrochemical measurements in droplets, water fraction (W_f) was fixed at 0.3, 0.4, and 0.5, respectively, to maintain droplet size. For each fixed W_f , total flow rate was varied from 1.0 to 3.0 $\mu\text{L min}^{-1}$. To study effect of W_f , total flow rate was kept constant 1.0, 1.5, 2.0, 2.5 and 3.0 $\mu\text{L min}^{-1}$, and for each fixed total flow rate, W_f was varied from 0.3 to 0.5. All experimental conditions are demonstrated in Table 3.7.

Table 3.7 Flow optimization for both water fraction and total flow rate study

Water Fraction	Aqueous Flow ($\mu\text{L min}^{-1}$)	Oil Flow ($\mu\text{L min}^{-1}$)	Total Flow ($\mu\text{L min}^{-1}$)
0.5	0.50	0.50	1.00
0.5	0.75	0.75	1.50
0.5	1.00	1.00	2.00
0.5	1.25	1.25	2.50
0.5	1.50	1.50	3.00
0.4	0.40	0.60	1.00
0.4	0.60	0.90	1.50
0.4	0.80	1.20	2.00
0.4	1.00	1.50	2.50
0.4	1.20	1.80	3.00
0.3	0.30	0.70	1.00
0.3	0.45	1.05	1.50
0.3	0.60	1.40	2.00
0.3	0.75	1.75	2.50
0.3	0.90	2.10	3.00

3.4.2.2.2 Hydrodynamic Voltammogram

From CV measurements, an applied potential range of 0 to 500 mV was employed. To perform hydrodynamic measurements, 0.1 M PBS pH 4 was pumped into the microchannel to generate droplets. After that, 0, 50, 100, 150, 200, 250, 300, 350, 400, 450 and 500 mV of potential were applied, respectively, to investigate background current for each potential. Subsequently, an aqueous solution containing 3 mM GCM was delivered into the microchannel instead of PBS for droplet generation. To construct a hydrodynamic voltammogram, current signals of analytes from each potential were divided by background currents (S/B) from the same potential. Furthermore, S/B values from each potential were plotted versus applied potential to point out the potential that provides the highest S/B. Therefore, the optimum potential was used as an applied potential of the droplet system.

3.4.3 Capillary Electrophoresis (CE)

For capillary electrophoresis, a separation method for validation of the proposed droplet system, CE experiments were setup using the guideline from previous work [56]. All CE separations were performed on a P/ACE MDQ capillary electrophoresis system (Beckman Coulter). An uncoated fused-silica capillary was 60.2 cm in length (50 cm to the detector), 75 μm ID, thermostatted at 25 °C. A separation voltage was set at 30 kV, and UV detection was performed at 200 nm using a photo diode array UV detector. A sample solution was injected using 0.5 psi pressure for 10 s. Prior to analysis each day, the capillary was rinsed with 0.1 M NaOH for 15 min and then with water for 15 min. Each experiment was run in duplicate.

From electropherograms, peak areas were measured and divided by migration time. The corrected peak areas were plotted versus concentration (1 to 10 mM GCM) for construction of a calibration curve for quantitative CE analysis.

3.5 Analytical Performance

3.5.1 Calibration Curve

For batch and droplet microfluidic measurements, calibration curves were constructed using concentration of GCM plotted versus obtained electrochemical signals. For batch measurement, GCM concentrations of 0.05 to 500 mM were prepared in 0.1 M PBS pH 4. The electrochemical currents for batch measurement were obtained from LSV and then plotted versus concentration. For droplet system, 0.5 to 30 mM of GCM prepared using same condition as batch measurements, concentrations were plotted versus electrochemical signal which obtained from chronoamperograms.

3.5.2 Linearity

In this work, linearity was investigated from the calibration curves. For batch measurements, a concentration series from 0.05 to 500 mM of GCM was used to construct a calibration curve. After that, the linear range was chosen from the calibration curve to obtain linearity of the system. For droplet system, a concentration series from 0.5 to 30 mM of GCM was employed for construction of a calibration curve. In addition, a linearity of the system was obtained from the linear range of the calibration curve. Furthermore, the correlation coefficient (R^2) was used to determine the linearity.

3.5.3 Limit of Detection (LOD) and Limit of Quantitation (LOQ)

To calculate LOD and LOQ, 3 and 10 times of the signal to noise ratio (S/N) were used, respectively. After that, LOD and LOQ were rechecked using prepared GCM solutions at the same concentrations as calculated LOD and LOQ

3.5.4 Precision

Intra-day precision was determined in one day using 4 concentrations of GCM (40, 60, 80 and 100 mM) for batch measurements. For each concentration, 10 measurements were performed using SWLSV with the optimum conditions. For droplet measurements, 0.5, 2.5 and 3.5 mM of GCM solutions were measured to determine intra-day precision. For each concentration, 50 droplets were measured for currents. %RSD was used to figure out the method precision. %RSD was calculated using the equation below;

$$\%RSD = \frac{SD}{\bar{x}} \times 100 \quad (3.1)$$

where SD is standard deviation and \bar{x} is averaged current.

For inter-day measurements of the batch system, 4 concentrations were measured using the optimized conditions. In this work, the inter-day experiments were carried out for 5 days in the month. Furthermore, GCM solution was prepared at a concentration of 3.5 mM to determine intra-day precision from 5 days in a week of the droplet-based system. Ten droplets for each day were measured and averaged for current. From averaged currents from each day, %RSD was calculated to determine inter-day precision. In addition, student t-test was used for comparing obtained data from each day. Using a 95% confidence interval for comparison of the data, if the t-value is higher than t-critical, it indicates that there is a significant difference among data obtained from different days.

3.6 Interference Study

For interference study, *N*-acetyl-glucosamine was used for this study because it is also a product from the synthesis of GCM and has an amino group as well as GCM on its structure. For batch measurements, *N*-acetyl-glucosamine was added into 5 mM glucosamine solution at ratios of 1:10, 2:10, 3:10, and 4:10 (w/w). For droplet system, *N*-acetyl-glucosamine was added into 5 mM glucosamine solution at ratios of 1:10, 2:10, 3:10, 4:10 and 5:10 (w/w). After that, obtained currents of the mixtures were compared to current of 5 mM GCM to calculate %difference. Student t-test was then used to figure out the statistical difference between the currents of the mixtures and the current of 0.5 mM GCM. In addition, %difference was calculated using an equation as shown below;

$$\% \text{Different} = \frac{(I_{\text{standard}} - I_{\text{mixture}})}{I_{\text{standard}}} \times 100 \quad (3.2)$$

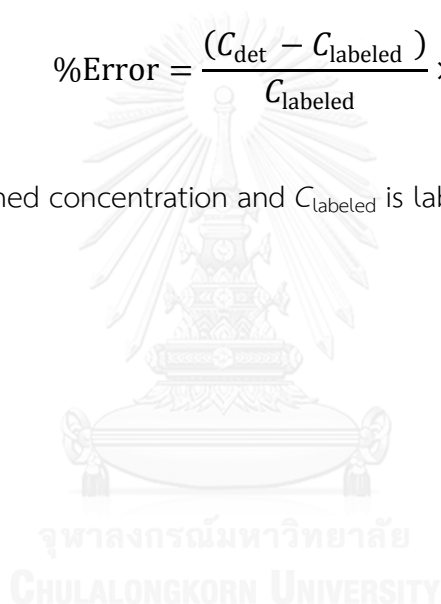
Where I_{standard} is current of standard GCM and I_{added} is current of *N*-acetyl-glucosamine added into mixture solution.

3.7 Real Samples Analysis

For batch measurements, real sample was prepared at a concentration of 20 mM in 0.1 M PBS pH 4.0. All real samples were detected electrochemically using linear sweep voltammetry. Real samples for droplet-system were prepared at a concentration of 3.5 mM. In addition, the droplet contents were measured for currents using an applied potential of 100 mV. The obtained currents were converted to concentrations using an equation of a linear calibration curve. After that, the calculated amounts were statistically compared with labeled amounts using t-test and percentage error which were calculated using the equation below;

$$\%Error = \frac{(C_{det} - C_{labeled})}{C_{labeled}} \times 100 \quad (3.3.)$$

where C_{det} is determined concentration and $C_{labeled}$ is labeled concentration.



CHAPTER 4

RESULTS AND DISCUSSION

4.1 Electrode Optimization

In this work, there are two types of microfluidic devices: well-like and microchannel patterned devices. To make a well-like microfluidic device, a PDMS plate having a punched hole (~0.8 cm in diameter) was assembled with an electrode-patterned PDMS, as demonstrated in Figure 3.7 (b). In addition, this device was used for optimization and characterization of electrodes in the CCD process. For microchannel patterned devices, they were used for droplet-based microfluidic experiments.

4.1.1 AuNPs Modified Electrode

After PDMS casting, CPEs were embedded into an array of microfluidic channels using a screen-printed technique as working, counter and reference electrodes. As considered the performance of CPEs, GCM cannot be detected using bare CPEs which contained only graphite, nujol oil and PDMS

In this work, AuNPs were used to modify CPEs for GCM detection. AuNPs provided not only high surface area, but also great electron transfer ability as well as gold plate electrodes. Cyclic voltammetry was used to determine electrode performance using a well-like microfluidic device. As shown in Figure 4.1, cyclic voltammograms (CVs) show that using AuNPs as an electrode modifier, the background current of 0.1 M PBS pH 7.4 showed an oxidation peak of gold.

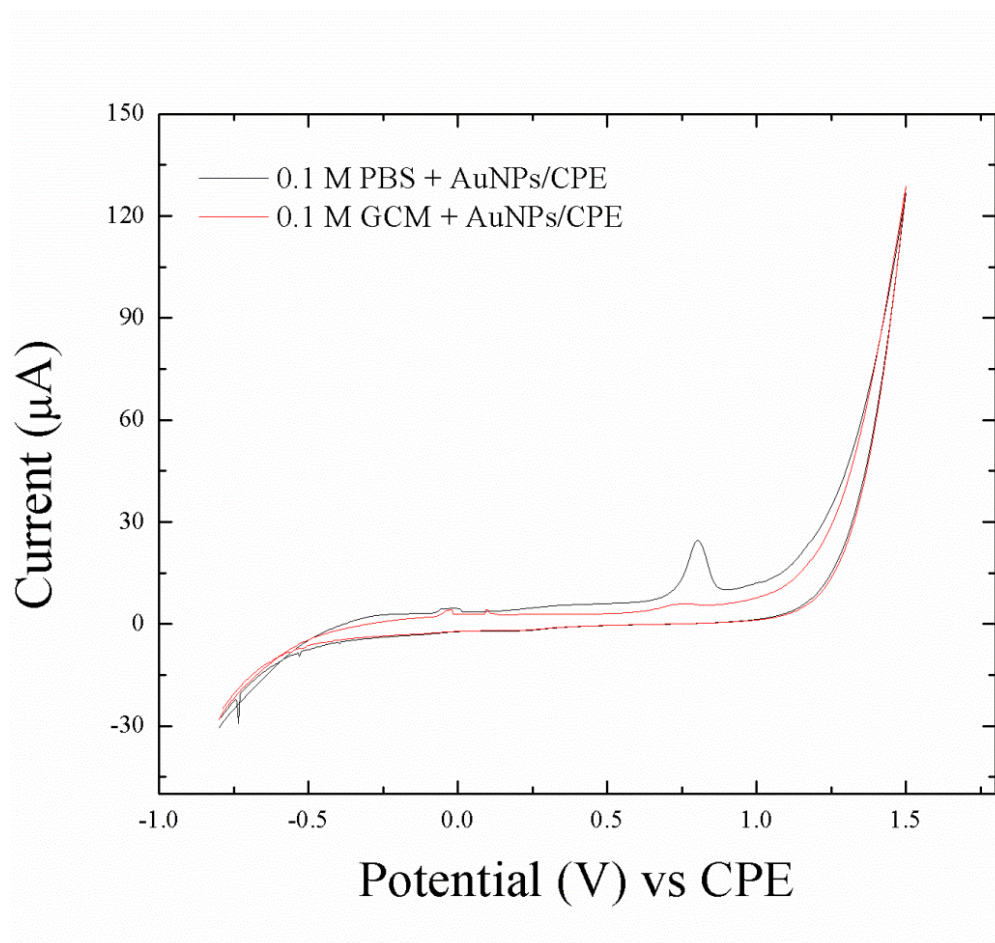


Figure 4.1 Cyclic voltammograms of 0.1 M PBS pH 7.4 (red) and 0.1 M GCM in the same buffer (blue) using AuNPs modified CPEs with a 100 mV s⁻¹ scan rate and a -0.8 to 1.3 V potential window.

After adding 0.1 M GCM solution onto the electrode surface, the gold oxidation peak disappeared. It should be noted that the amino group (-NH₂) of GCM has high potential to be trapped onto the AuNPs surface [12]; therefore, the gold signal was reduced as observed in Figure 4.1. The alkyl structure of GCM could obstruct electron transfer of gold oxidation. In addition, alkyl chains are normally not easy to be either oxidized or reduced at low potentials as used in this work. The results indicated that using only AuNPs as a modifier cannot detect GCM. Therefore, an additional modifier which is a conductive material could be employed for the GCM sensor in this work.

4.1.2 PANI and AuNPs Modified Electrode

There are many conductive polymers, such as polypyrrole, polyaniline and polyacetylene, used in electrochemical fields. These materials provide great electron transfer behaviors and enhance the working area of electrode surface.

Polyaniline (PANI) is a conductive polymer comprising of benzene rings together with an amino group in its structure. This structure provides great electron transfer due to its excellent electrochemical properties, good environmental stability and non-toxicity, which is attractive to be used in electrode modification [9]. Moreover, the amino group of PANI can be easily attached to the surface of AuNPs through the electrostatic force [12].

As illustrated in Figure 4.2, when using 5 mg mL⁻¹ PANI and 0.5 mg mL⁻¹ AuNPs to modify CPEs, electrochemical peak current of 0.1 M GCM was observed at 0.5 V.

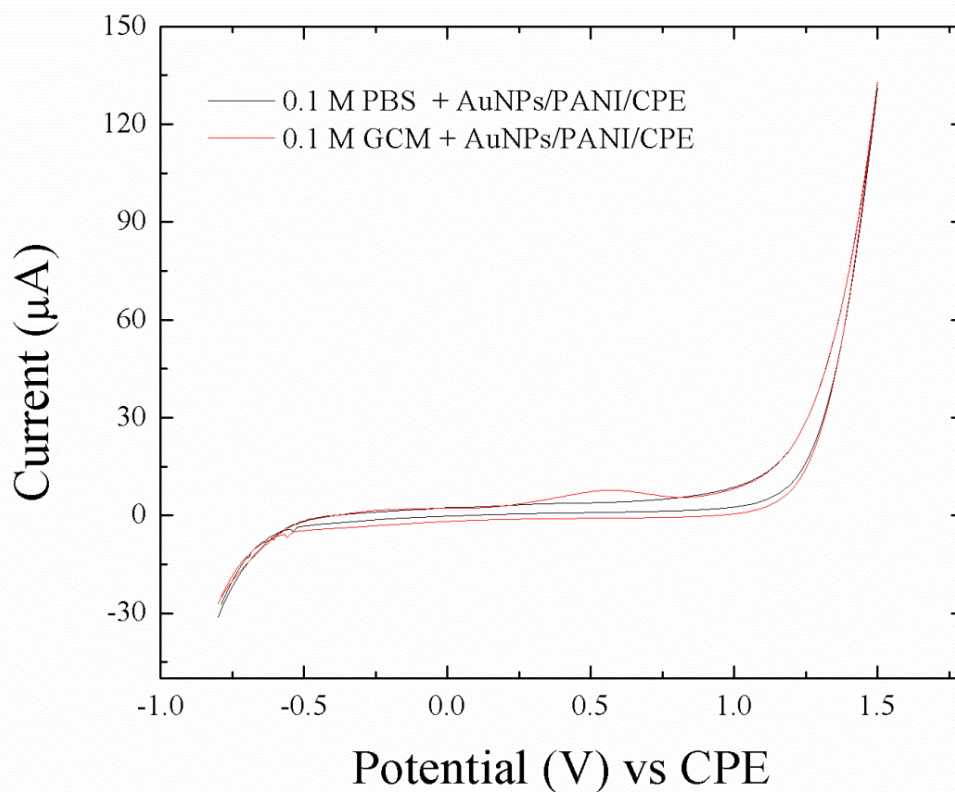


Figure 4.2 Cyclic voltammograms of 0.1 M PBS pH 7.4 (blue) and 0.1 M GCM (red) in 0.1 M PBS using PANI-AuNPs modified CPEs with a 100 mV s^{-1} scan rate and a -0.8 to 1.3 V potential window.

The CVs in Figure 4.2 clearly show that using PANI and AuNPs as electrode modifiers was able to detect GCM. This indicated that PANI and AuNPs have electrocatalytic properties for oxidizing GCM at low applied potentials. In addition, the oxidation current could refer to the oxidation of GCM to glucosaminic acid [8]. Even though GCM was detected using PANI-AuNPs modified CPEs, the sensitivity of the modified CPEs was relatively low. Therefore, optimization of the amounts of PANI and AuNPs was considered to obtain the best condition for GCM detection.

Although AuNPs together with PANI showed a good property for detecting GCM in PBS pH 7.4, the suitable pH of both materials is opposite to each other. On one hand, AuNPs were known as a great catalyst for sugar oxidation at high pH values. On the other hand, PANI was known as a changeable form polymer in different pH values. The most suitable pH is at pH 4 because it is a conductive form which is a green form of material. Therefore, pH was another factor to be optimized.

4.1.3 CCD Calculation

One of the best ways for optimization of parameters for experiments is central composite design (CCD). CCD is the state-of-the-art of experimental design in which a box-like experiment is simulated to figure out the optimum point using an obtained equation. There are many conditions for construction of CCD, but in this work, 3 parameters with 3 levels were investigated for optimization of pH of the working solution and the amounts of PANI and AUNPs for electrode modification. To construct a box-like experiment with a spherical shape, 20 experiments were performed using CV with a 100 mV/s scan rate and a -0.8 to 1.3 V potential window. Furthermore, using real numbers for each parameter as filled values into CCD may be considered as a bias. Thus, codes which are representative of real values were used. The representative amounts of real values and codes are presented in Table 4.1.

Table 4.1 Codes and real values of pH and the amounts of PANI and AuNPs used for CCD experiments.

Factors	Code				
	-1.68	-1	0	1	1.68
pH	5.32	6	7	8	8.68
AuNPs (mg L ⁻¹)	132	200	300	400	468
PANI (mg mL ⁻¹)	1.32	2	3	4	4.68

CPEs were fabricated according to each code and electrochemical experiments were then performed using CV to observe currents. Table 4.2 shows 20 experiments performed and all results from CV were included. In addition, 1.68 and -1.68 values were also used to generate a spherical shape of a box-like experimental design. The repeated-codes (run 15 to 20) were also performed to obtain more precise results.

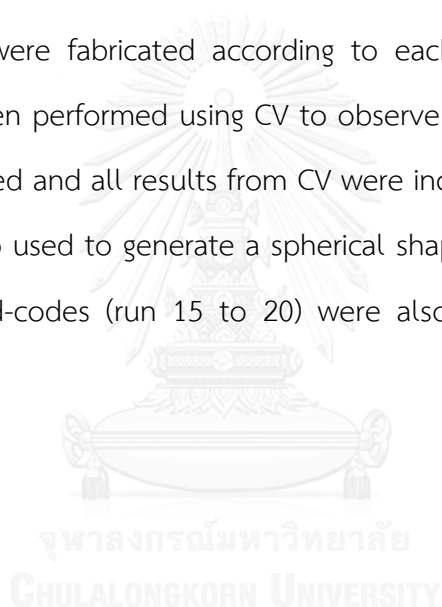


Table 4.2 Three parameters with three levels of CCD experiments for optimization of pH and the amounts of AuNPs and PANI for determination of GCM. Electrochemical currents were obtained from CV using a scan rate of 150 mV s^{-1}

Run	Factor										Current(μA)
	intercept	A	B	C	A ²	B ²	C ²	AB	AC	BC	
	pH	AuNPs	PANI	pH ²	AuNPs ²	PANI ²	pH*AuNPs	pH*PANI	AuNPs*PANI		
1	1	1	1	1	1	1	1	1	1	1	21.73
2	1	1	1	-1	1	1	1	1	-1	-1	5.41
3	1	1	-1	1	1	1	1	-1	1	-1	3.91
4	1	1	-1	-1	1	1	1	-1	-1	1	9.34
5	1	-1	1	1	1	1	1	-1	-1	1	2.7
6	1	-1	1	-1	1	1	1	-1	1	-1	24.03
7	1	-1	-1	1	1	1	1	1	-1	-1	17.52
8	1	-1	-1	-1	1	1	1	1	1	1	8.42
9	1	1.68	0	0	2.8224	0	0	0	0	0	23.42
10	1	-1.68	0	0	2.8224	0	0	0	0	0	30.39
11	1	0	1.68	0	0	2.8224	0	0	0	0	0.33
12	1	0	-1.68	0	0	2.8224	0	0	0	0	0
13	1	0	0	1.68	0	0	2.8224	0	0	0	0.06
14	1	0	0	-1.68	0	0	2.8224	0	0	0	10.79
15	1	0	0	0	0	0	0	0	0	0	13.72
16	1	0	0	0	0	0	0	0	0	0	13.51
17	1	0	0	0	0	0	0	0	0	0	13.49
18	1	0	0	0	0	0	0	0	0	0	13.61
19	1	0	0	0	0	0	0	0	0	0	13.72
20	1	0	0	0	0	0	0	0	0	0	13.68

From experimental data, all parameters were considered as quadratic terms to obtain more accurate results. In addition, the relationships between two parameters were also observed to examine the effect of each interaction. Subsequently, linear regression was employed to obtain a coefficient for each term, as shown in Table 4.3. These coefficients were used for construction of an equation which responded as 3D surface plots to figure out the optimum points for each parameter. Moreover, p-values were calculated to determine the significance of each parameter.

Table 4.3 Coefficients and p-values of each parameter obtained using regression calculation.

	intercept	pH	AuNPs	PANI	pH ²	AuNPs ²	PANI ²	pH*AuNPs	pH*PANI	AuNPs*PANI
Coefficient	13.59	-1.76	1.12	-1.42	4.91	-4.56	-2.70	1.64	2.89	-1.09
p-value (ANOVA test)	0.00	0.32	0.52	0.42	0.01	0.02	0.13	0.47	0.21	0.63

Figure 4.3 shows the relationship between the amount of AuNPs and pH of the working solution. Red and blue colors represent the highest and lowest experimental currents, respectively. In addition, the numbers demonstrated in the graph represent predicted currents from the CCD calculation.

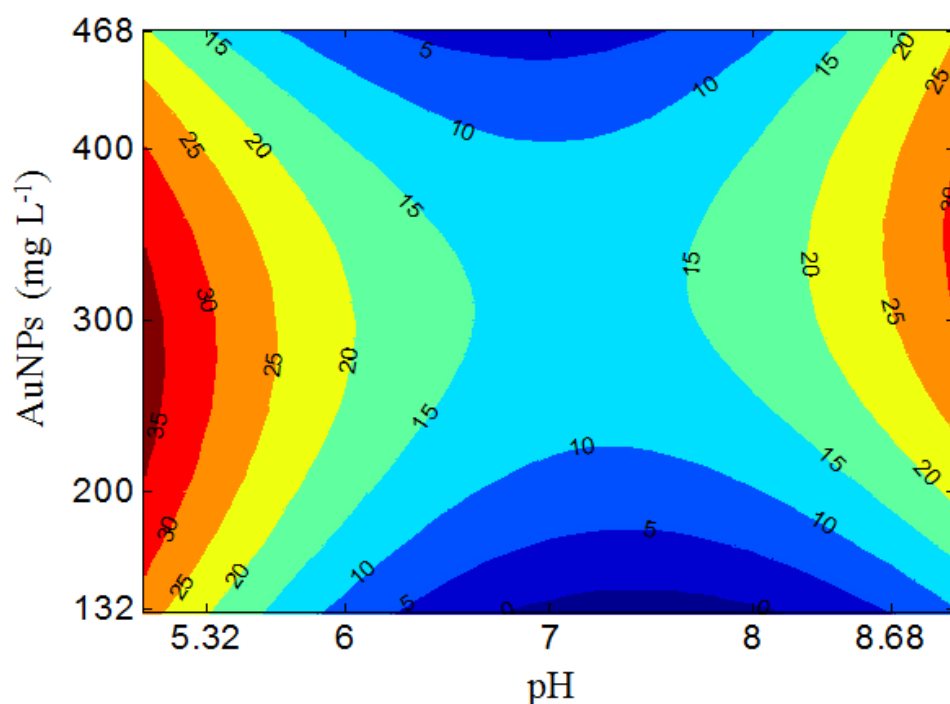


Figure 4.3 Effects of the amount of AuNPs and pH on the oxidation of 100 mM GCM.

Results demonstrated that the red contour areas (high current) were on the left and right sides of the figure, which corresponded to pH values of lower than 5.32 and higher than 8.68. Results showed that the optimum amount of AuNPs was in the range of 0.2 to 0.4 mg mL⁻¹ (dark red) and the optimum pH could be lower than pH 5 or higher than pH 9. In addition, the relationship between the amount of PANI and pH was also considered.

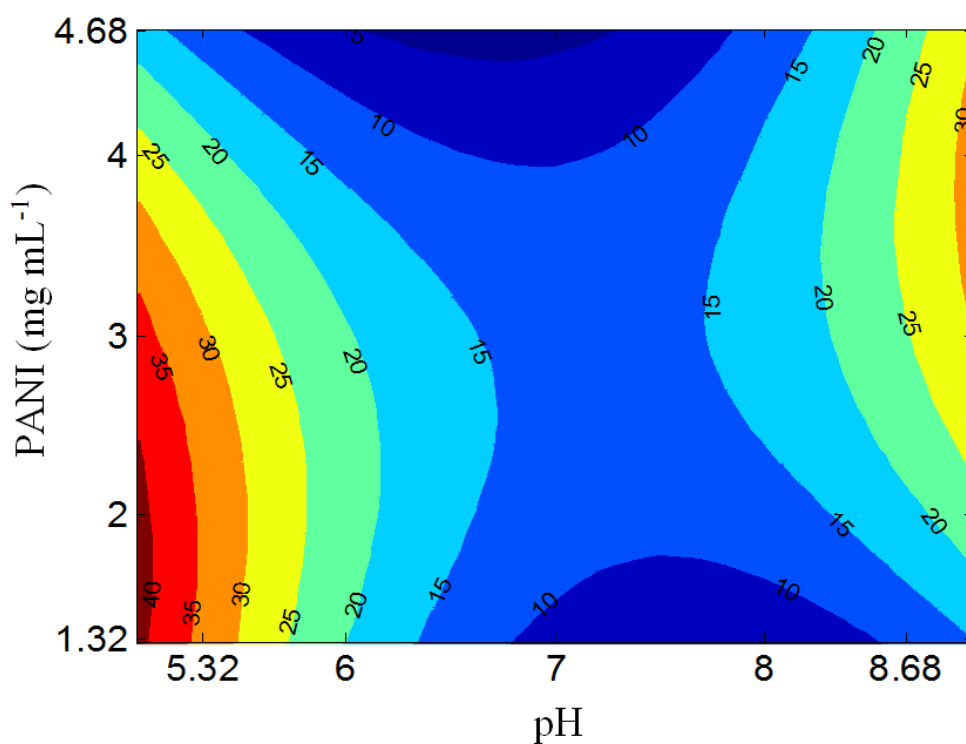


Figure 4.4 Effects of the amount of PANI and pH on the oxidation of 100 mM GCM.

Results from Figure 4.4 demonstrated a contour plot showing the relationship between the amount of PANI and pH. High current signals were obtained when using higher pH values than 9 or lower pH values than 5. In addition, results from both Figures 4.3 and 4.4 indicate that high currents were observed from either lower pHs than 5 or higher pHs than 9. However, from Figures 4.3 and 4.4, there were slight differences between the amounts of AuNPs and PANI at low and high pH values. At low pH values in Figure 4.4, the optimum amount of PANI was lower than 3 mg mL^{-1} , while the optimum amount of PANI amount at high pH values was higher than 3 mg mL^{-1} . Therefore, it is not clear to consider the amounts of both PANI and AuNPs from both Figures 4.3 and 4.4.

To determine the optimum amounts of AuNPs and PANI used in this work, Figure 4.5 was constructed to observe the relationship between the amounts of AuNPs and PANI. As seen from Figure 4.5, the optimum amount of PANI was considered to be in the range of 1.32 to 4.68 mg mL^{-1} while the amount of AuNPs was in the range of 0.132 to 0.468 mg mL^{-1} .

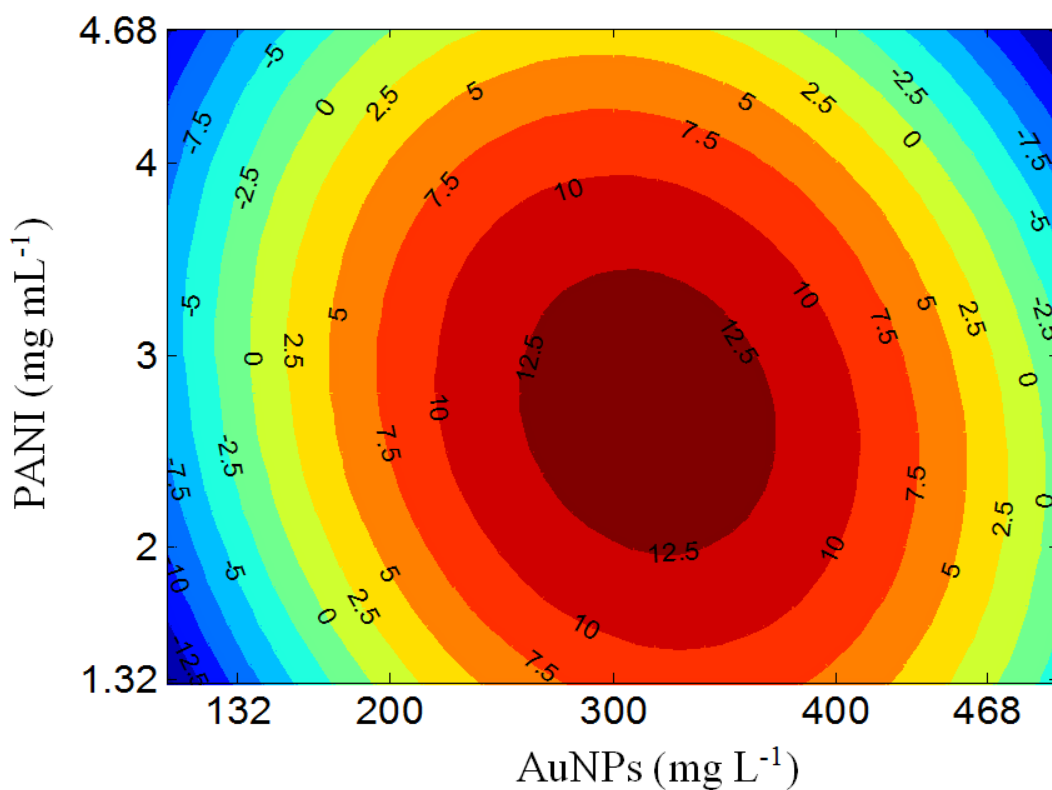


Figure 4.5 A contour plot demonstrates the effect of the amounts of PANI and AuNPs on the oxidation current signal of 100 mM GCM.

From Figure 4.5, a red area is located at the middle of the figure, which indicates optimum values for both parameters. The optimum amount of PANI was considered to be in the range of 2 to 3.25 mg mL⁻¹ while the amount of AuNPs was determined to be in the range of 0.250 to 0.350 mg mL⁻¹.

Figure 4.6 shows responsive surface plots from CCD experiments. Current responses were plotted as a function of the amounts of PANI and AuNPs used for electrode modification.

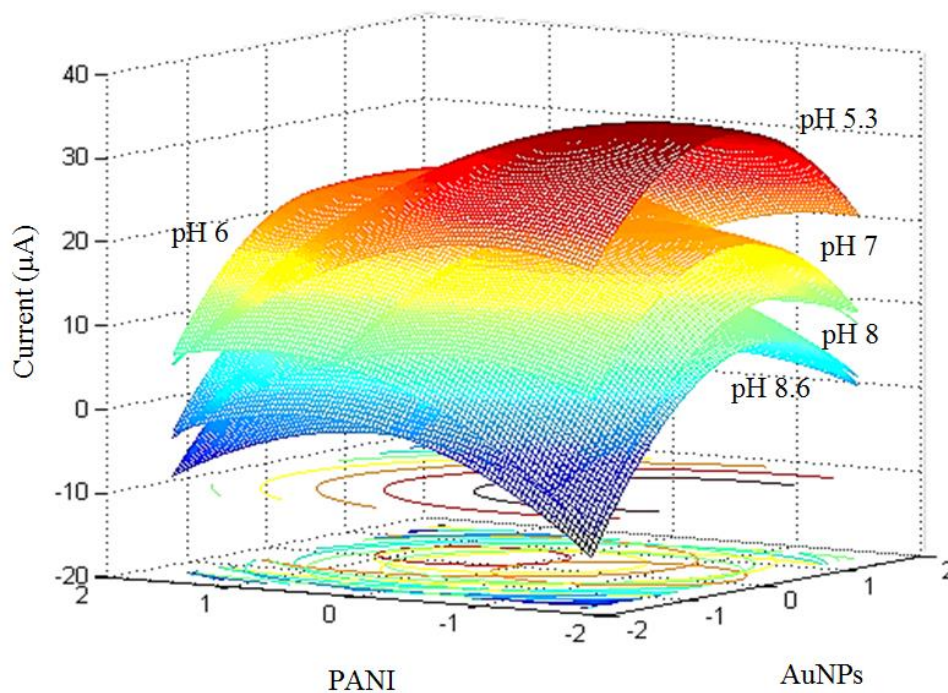


Figure 4.6 Responsive surfaces of currents as a function of the amounts of PANI and AuNPs at different pH values.

The surface plots show that increase in pH (up to pH 7) decreased electrochemical signal. After pH 7, electrochemical signal increased with pH. Enhancement of electrochemical signal at high pH was because at high pH, gold oxide occurred at the surface of AuNPs, which acted as an electrocatalyst for GCM oxidation. The plots also show that the amounts of PANI and AuNPs were independent of pH. It is because the amounts of AuNPs and PANI provided the optimum current as illustrated in Figure 4.5 which the pH is not relevant to the using amount of AuNPs and PANI. Consequently, the illustrated response surface for each pH (as shown in Figure 4.6) showed that pH was independent of the amounts of AuNPs and PANI.

Using the multiple linear regressions, a regression model was calculated from the responsive surface plots, as shown in the equation below:

$$y = 13.59 - 1.76(\text{pH}) + 1.12(\text{AuNPs}) - 1.42(\text{PANI}) + 4.91(\text{pH})^2 - 4.56(\text{AuNPs})^2 - 2.70(\text{PANI})^2 + 1.64(\text{pH} \times \text{AuNPs}) + 2.89(\text{pH} \times \text{PANI}) - 1.09(\text{AuNPs} \times \text{PANI}) \quad (4.1)$$

Each coefficient in Equation (4.1) was obtained from Table 4.3, which indicated the significance of the parameters in terms of either an isolated term or a related term. The optimized values of the parameters were figured out using the first derivative method from the constructed equation. It was found that the optimized amounts of AuNPs and PANI were found to be 0.300 mg mL^{-1} and 3 mg mL^{-1} , respectively. However, the optimized pH was still unclear. Therefore, a wider pH range was studied using the optimum amounts of PANI and AuNPs for electrode modification.

To study effect of pH on detection of GCM using the optimum amounts of PANI and AuNPs, pH 4 and pH 11 were chosen as the lowest and the highest pH values. The criteria for choosing the pH range was regarded to the chemical properties of both materials. On one hand, gold is known as an electrochemical catalyst for sugar oxidation at high pH values in which gold oxide is formed as a catalytic form for GCM oxidation [8]. On the other hand, PANI is known as a great conducting polymer in which a green form at pH 4 provides the best electron-transfer process. From Table 4.4, a series of experiments for studying the effect of pH was performed using CV.

Table 4.4 Study of the effect of pH of the working solution on electrochemical current of GCM using the optimum amounts of AuNPs and PANI for electrode modification.

Run	pH		Current (μ A)	SD
	Code	Real		
1	-3	4	52.3	4.112
2	-2.5	4.5	45.12	3.221
3	-2	5	35.69	2.323
4	-1.5	5.5	27.61	2.221
5	-1	6	19.5	1.235
6	-0.5	6.5	16.85	2.001
7	0	7	13.92	2.112
8	0.5	7.5	13.79	1.232
9	1	8	16.89	2.221
10	1.5	8.5	22.38	1.009
11	2	9	27.79	2.3565
12	2.5	9.5	34.26	3.225
13	3	10	39.16	4.112
14	3.5	10.5	37.55	3.232
15	4	11	39.78	3.221

CHULALONGKORN UNIVERSITY

A scatter plot between current and pH was constructed using data from Table 4.4, as shown in Figure 4.7, for consideration of the effect of pH on GCM detection.

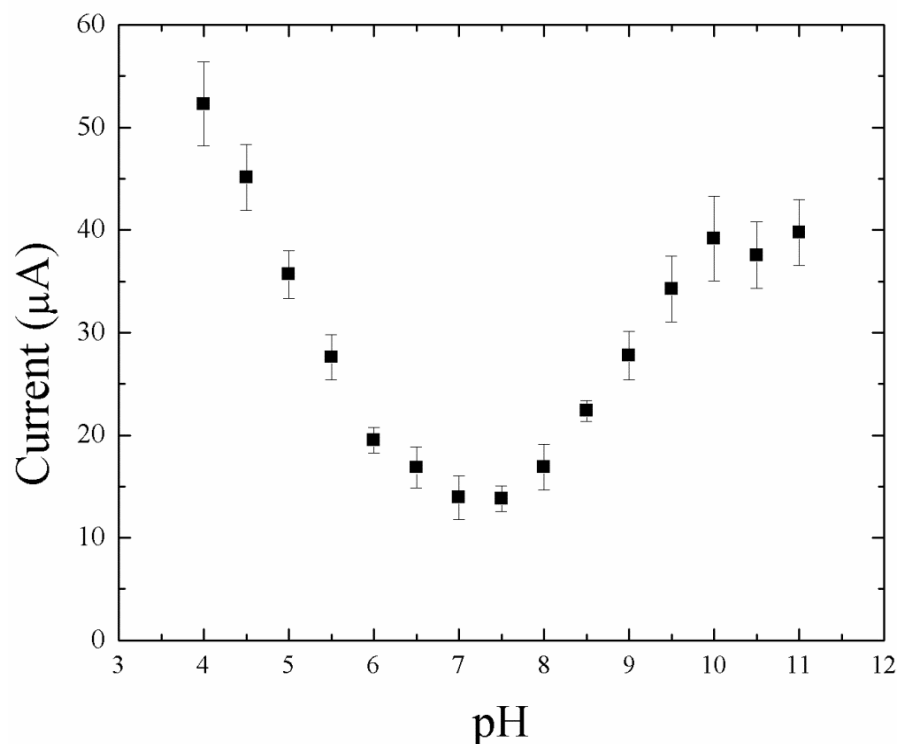


Figure 4.7 A scatter plot shows the effect of pH on electrochemical signal of GCM.

Figure 4.7 shows the lowest current at pH 7. In contrary, the higher currents were found at both low and high pH values. This result indicated that both low and high pH values provided great electron transfer for GCM oxidation. As mentioned previously, high pH is a good electron transfer condition for AuNPs, while low pH is good for PANI. Therefore, pH 4 and 12 were chosen for further optimization of pH. From Figure 4.8, quasi-reversible and irreversible cyclic voltammograms (CVs) of GCM were obtained at pH 4 and pH 12, respectively.

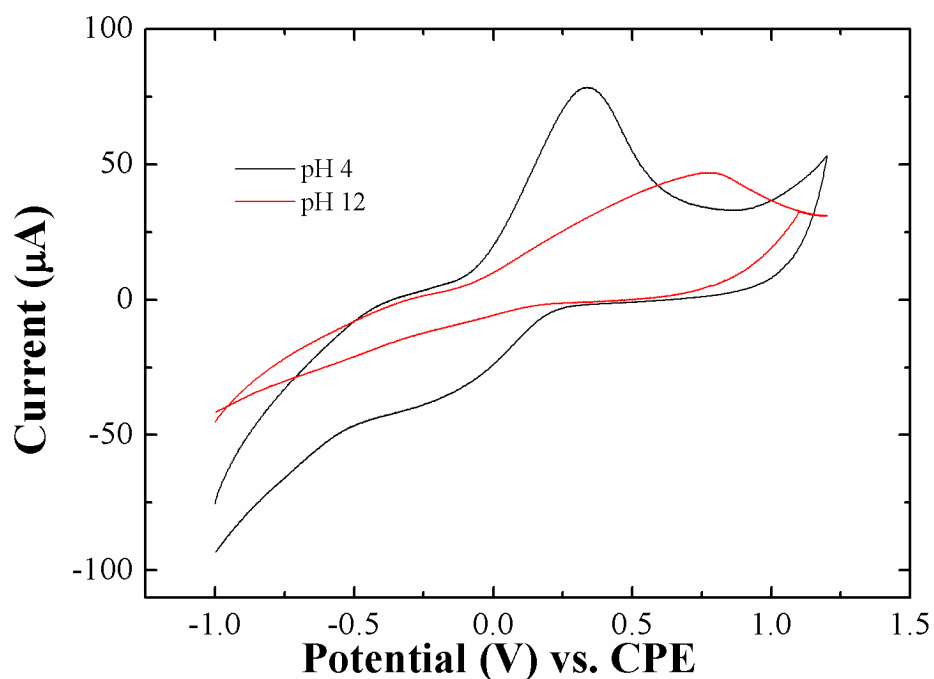



Figure 4.8 CVs of 100 mM GCM in 0.1 M PBS at pH 4 and 12. At pH 4, a quasi-reversible CV was obtained, while at pH 12 an irreversible CV was observed.

As shown in Figure 4.8, both irreversible and quasi-reversible forms were obtained from different pH values. For irreversible CV, only an oxidative peak was obtained, indicating that the kinetic process was relatively low compared to a quasi-reversible CV. For quasi-reversible CV, a major oxidation peak with a minor reduction peak was observed, indicating a better electron-transfer process, even though the electron transfer rate was lower than that of a reversible CV. However, a quasi-reversible CV is usually preferred to an irreversible CV. This means that better electron transfer was obtained, indicating that this process depended on thermodynamic control more than kinetic control. Furthermore, the quasi-reversible CV was also well-defined with a symmetric peak which was utilized for further quantitative analysis.

In conclusion, the optimized conditions (using CCD as an experimental design) for GCM detection in this work, were 0.300 mg mL^{-1} AuNPs and 3 mg mL^{-1} PANI for modification of CPEs and 0.1 M PBS at pH 4 as a working solution. Although CCD provided a utilized equation with a surface response, this obtained equation may be over-fitted to the series of the experiments used for construction of the equation only. Therefore, over-fitting of the equation was checked using random experiments as shown in Table 4.5.

Table 4.5 Random experiments to check over-fitting of a constructed equation obtained from CCD.



pH	Code		Current (μA)	
	Au	PANI	Predicted	Experimental
0.5	0.5	0.5	12.83	13.53
0.5	0	0.5	13.28	13.39
0.75	0.5	0.25	14.95	14.02
-1	0.5	0.5	15.76	16.57
0	0.5	0.5	11.35	12.71
1	0.5	0.5	16.77	16.45
-1	-0.5	-0.5	20.59	20.25
0	-0.5	-0.5	11.65	12.89
-2	0	0	36.75	35.69
1	-0.5	-0.5	12.54	12.93

As seen from Table 4.5, both predicted and experimental currents were compared using student's t-test. A series of 10 runs ($n=10$) with one-tail t-test was performed using $\alpha = 0.05$ which corresponded to a 95% confidence interval. Results provided t-value equal to 0.73 which was lower than the t-critical value (1.83). This result indicated insignificant difference between predicted and experimental currents. Therefore, the constructed equation was not an over-fitted equation, which could be used for prediction of current for GCM detection when using different amounts of AuNPs and PANI for electrode modification at different pH values of PBS as a working solution.



4.2 Electrode Characterization

PANI and AuNPs were used as electrode modifiers in this work to fabricate an electrochemical sensor for GCM detection. Physical mixing of PANI and AuNPs was performed using a vortex. Characterization of the working electrode was important for explaining the reaction which occurred at the electrode surface. In this work, both morphology and electrochemical characterizations were performed.

4.2.1 Morphological Study

To perform morphology characterization of the modifier materials, scanning electron microscope (SEM) was used and results were shown in Figure 4.9. Results show that, AuNPs self-assembled on the surface of PANI microfiber. The interaction occurred through the $-NH$ functional group of PANI and the gold surface [12]. The PANI microfiber was well-known as an AuNPs auto-reducer; therefore, AuNPs can be attached onto a PANI microfiber even using only physical mixing or an applied potential.

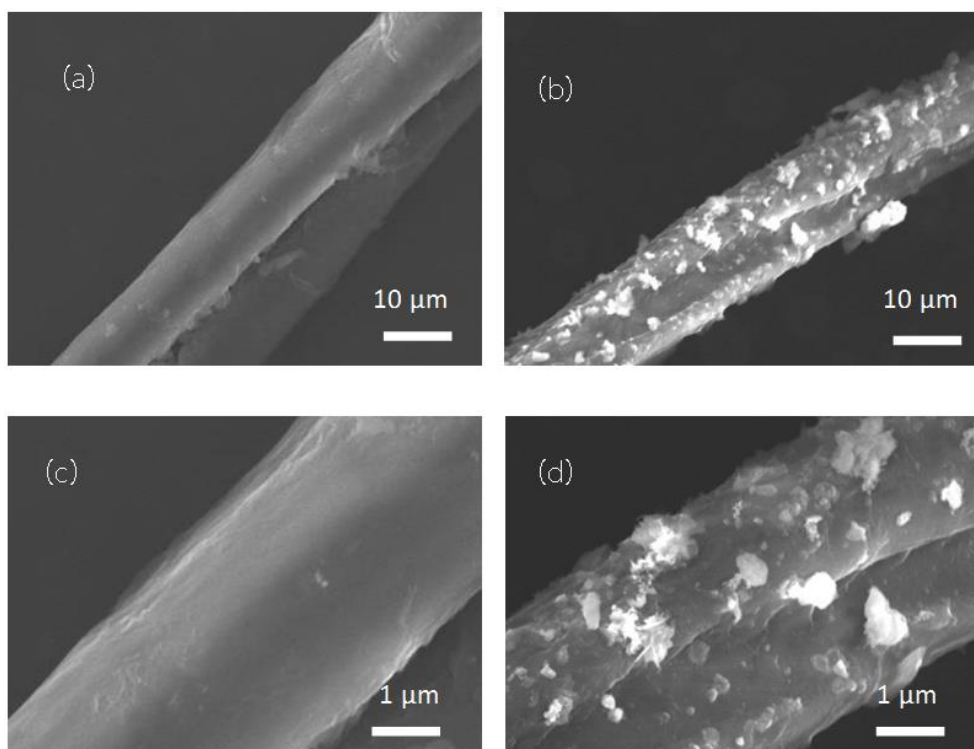


Figure 4.9 SEM images of a PANI microfiber (a and c) and PANI with AuNPs (b and d). White spots in b and d are AuNPs on the surface of PANI microfiber.

In addition, a self-assembly of AuNPs onto the polyaniline was due to the electrostatic force [12]. Different sizes of AuNPs were observed onto the PANI microfiber, as illustrated in Figures 4.9 b) and d). This phenomenon was explained using the aggregation nature of metal nanoparticles, which spontaneously occurs when metal nanoparticles either lose their stabilized states or are close enough to aggregate [57]. In this case, self-assembly would occur due to a confined environment because AuNPs were trapped onto the PANI microfiber surface. Each Au nanoparticle was very close to each other on the PANI surface, in which the equilibrium process was driven through a minimization of the Gibbs free energy at the surface interaction [58].

4.2.2 Electrochemical Study

One of the most important electrochemical studies is mass transfer. A mass transfer process of an analyte occurs between bulk solution and at electrode surface. This phenomenon is a well-known process that points out that current is obtained from either faradaic or non-faradaic process. For Faradaic current, diffusion plays a crucial role as well as flux transportation from bulk solution to the surface of working electrode. On the other hand, others phenomena, including adsorption process, occurring at the working electrode surface are considered as non-faradaic current. To figure out the mass transfer process, CV is used together with the Randles-Sevcik equation (Equation 2.3).

To study the mass transfer behavior of the modified CPE in this work, CV measurements of 40 mM GCM in 0.1 M PBS pH 4 were performed using a potential window from -1.00 to 1.30 V at scan rates ranging from 50 to 500 mV s⁻¹. Peak currents obtained from CVs were plotted versus scan rate and square root of scan rate to determine whether the mass transfer is an adsorption or diffusion-controlled process. CVs of these experiments are shown in Figure 4.10 (a), In addition, plots between peak current (i_p) and square root of scan rate was constructed, as illustrated in Figure 4.10 (b).

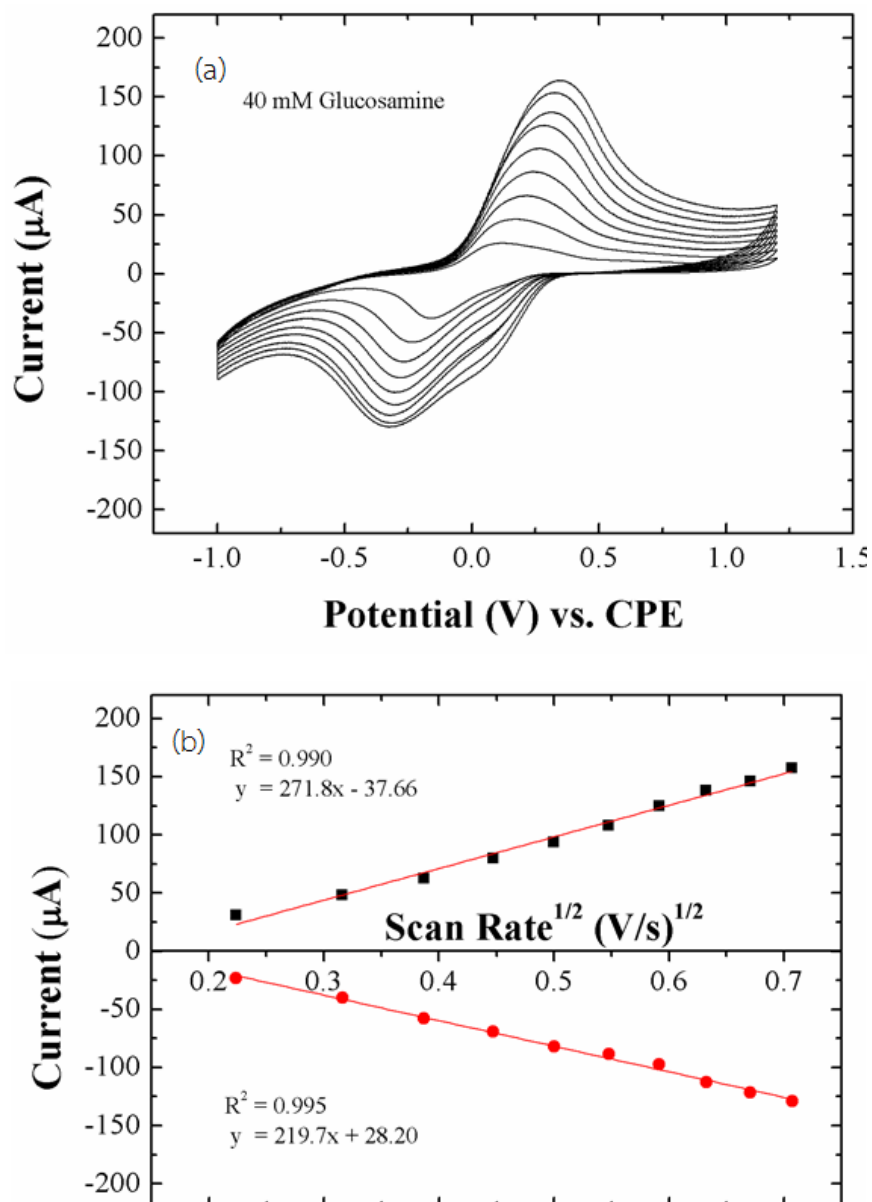


Figure 4.10 (a) CVs of 40 mM GCM in 0.1 M PBS pH 4 using scan rates from 50 to 500 mV s^{-1} . (b) Linear plots of electrochemical currents from the CVs in (a) versus square root of scan rate, which indicated the mass transfer as a diffusion controlled process.

Figure 4.10 (a) illustrated CVs when faster scan rates were used, the greater peak heights were observed, corresponding to the Randles-Sevcik equation. Oxidation and reduction peaks were measured and plotted as shown in Figure 4.10 (b) to figure out the Randles-Sevcik relationship. In addition, the Randles-Sevcik plots were used to prove mass transfer process to be whether a diffusion- or adsorption-controlled process. Figure 4.10 (b) shows a linear relationship between peak current and square root of scan rate with $R^2 = 0.990$ and 0.995 for oxidation and reduction currents, respectively. This relationship for both electrochemical processes indicated a mass transfer behavior as a diffusion-controlled process at 40 mM and lower concentrations of GCM. However, slight peak shift, which was observed at a 50 mV s^{-1} scan rate for the reduction peak, was due to minor effect of an adsorption-controlled process. In addition, a high concentration of GCM at 100 mM in 0.1 M PBS pH 4 was also used to observe the mass transfer using cyclic voltammetry with the same scan rates and applied potentials used for 40 mM GCM. CVs of 100 mM GCM are shown in Figure 4.11 (a). After that peak height for both oxidation and reduction were plotted versus scan rate, which is illustrated in Figure 4.11 (b).

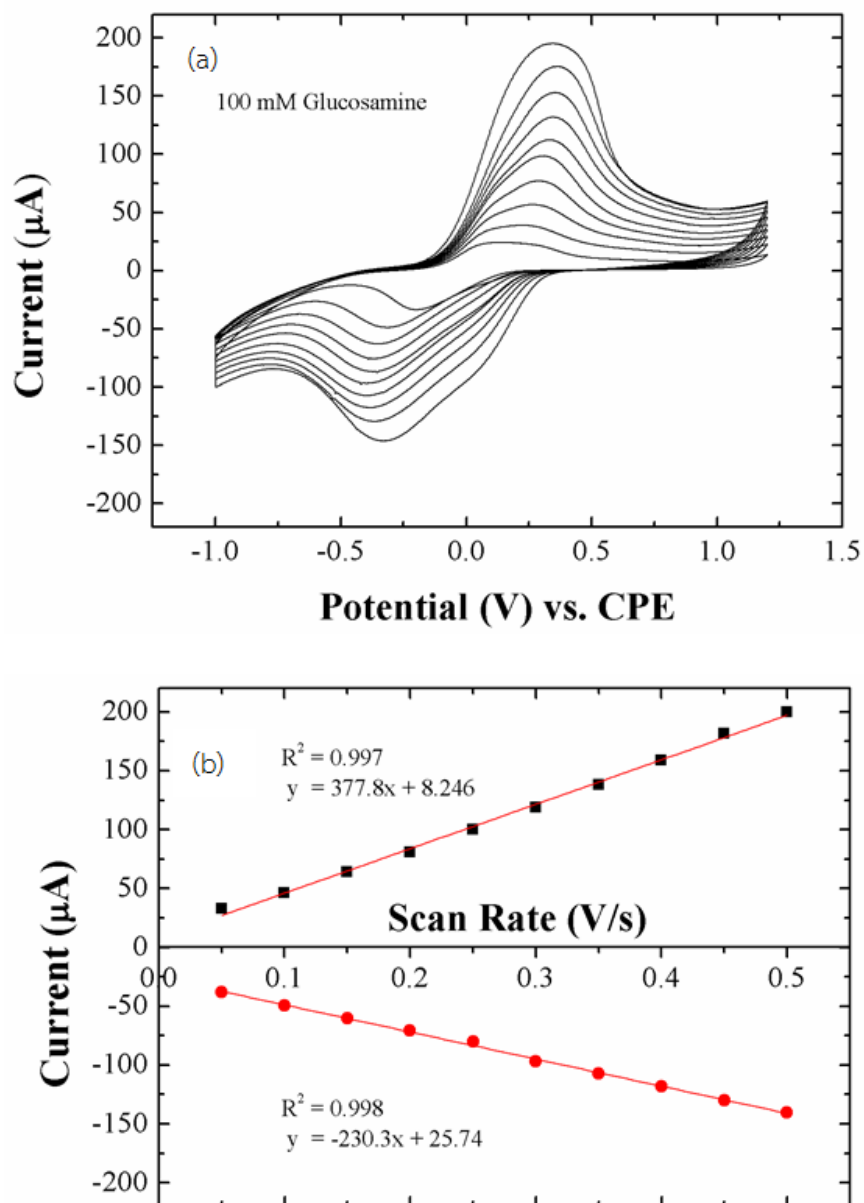
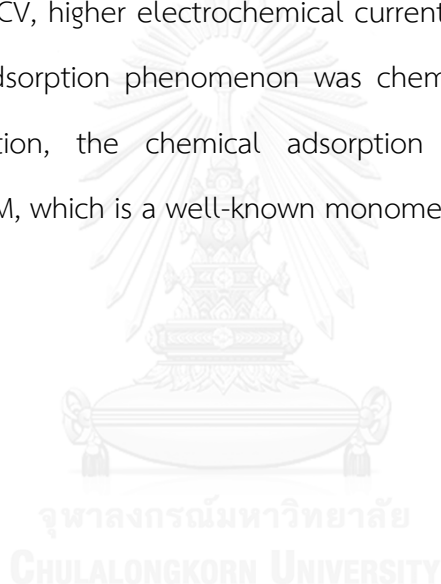


Figure 4.11 (a) CVs of 100 mM GCM in 0.1 M PBS pH 4 using scan rates from 50 to 500 mV s^{-1} . (b) Plots of electrochemical currents from the CVs in (a) versus scan rate, which indicated the mass transfer as an adsorption controlled process.

Results demonstrated that a linear relationship in Figure 4.11 (b) was not a diffusion-controlled process, but an adsorption-controlled process. In addition, the adsorption-controlled process occurring at the working electrode surface includes physical and chemical adsorptions. In this work, when a high concentration of GCM was applied onto the modified working electrode surface for 1 hour, then rinsed with MilliQ water and then performed CV, low current was observed. It was owing to the $-NH$ group of GCM which could be trapped onto the surface of AuNPs. However, when a high concentration of GCM was applied onto the working electrode and then performed CV, higher electrochemical current was observed. These results indicated that the adsorption phenomenon was chemical adsorption, not physical adsorption. In addition, the chemical adsorption would occur due to the polymerization of GCM, which is a well-known monomer of chitosan and chitin.



4.3 Method Validation for Batch Measurements

4.3.1 Linearity

To validate electroanalytical performance, a calibration curve was studied using a standard GCM concentration series from 0.05 to 500 mM using LSV (square wave mode) with a potential window from -0.50 to 0.7 V and a scan rate of 100 mV s^{-1} . LSVs of 5 to 100 mM standard GCM are shown in Figure 4.12 (a). Peak heights were measured and subtracted from the background current to obtain current signal for each concentration.



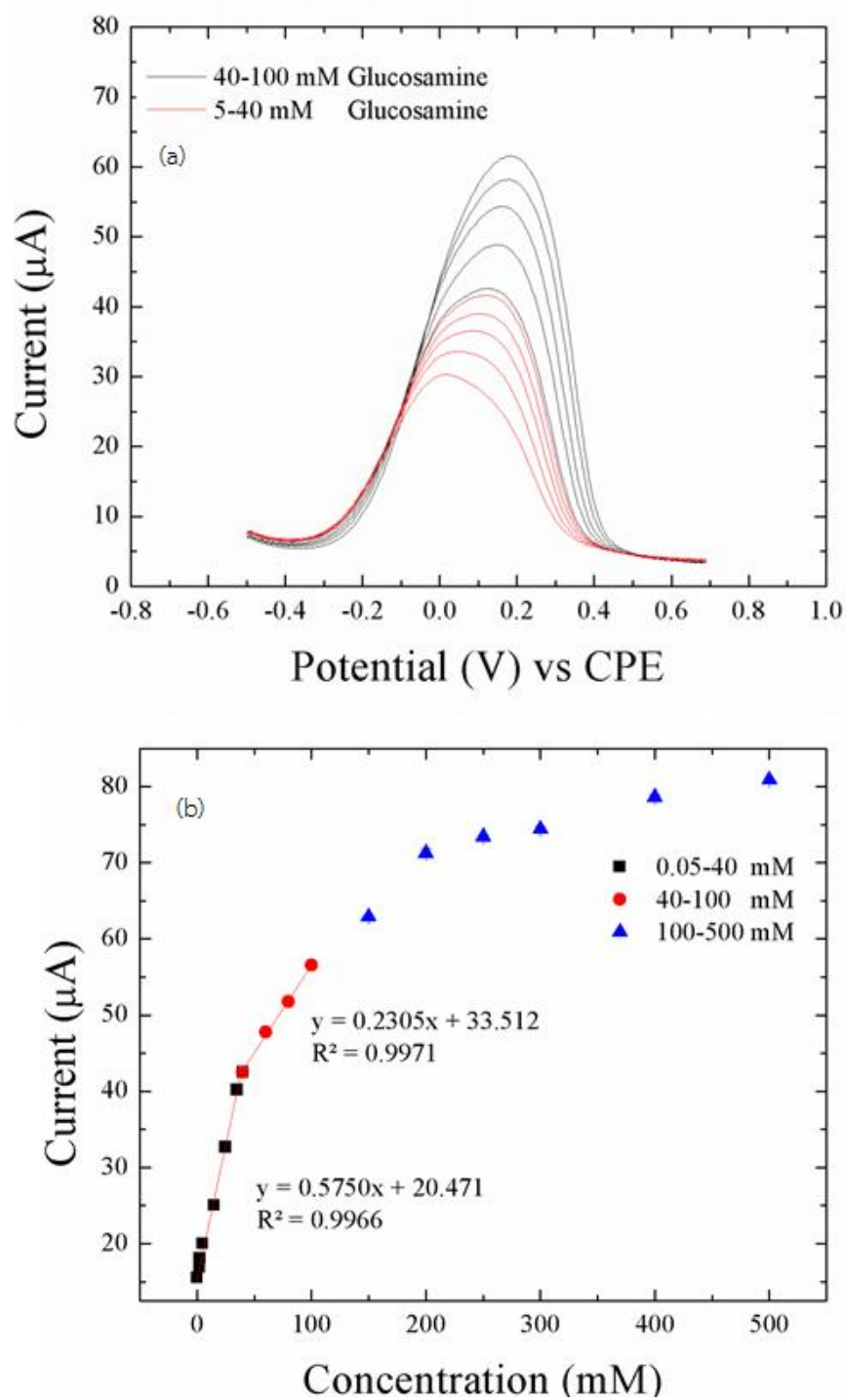


Figure 4.12 (a) Voltammograms of 5 to 100 mM GCM in 0.1 M PBS pH 4.0. (b) A plot of obtained electrochemical signal of standard GCM versus concentration of GCM from 0.05 to 500 mM. The experiments were performed using a scan rate of 100 mV s^{-1} and a potential window from -0.5 to 0.7 V.

From Figure 4.12, the peak currents were slightly shifted when increasing the concentration of GCM. The shifted peaks could be due to polymerization of GCM at low pH, which was a result of the adsorption-controlled process. As illustrated in Figure 4.12 (b), there were two linear curves, which indicated different phenomena occurred at the electrode surface. The first linear range (0.05 – 40 mM), which is a low concentration range, with R^2 equal to 0.9966 was considered as due to the diffusion-controlled process. The second linear range found at higher concentrations of 40 to 100 mM with R^2 equal to 0.9971 was due to the adsorption-controlled process.

From Figure 4.12 (a), there was peak shifting. The position of GCM peak should be the same for a diffusion-controlled process even using different conditions, such as scan rates and concentrations of analyte. In this work, the peak was shifted towards higher potentials when using higher concentrations. This could be due to the mass transfer being an adsorption-controlled process. Because at higher concentrations, there were more analyte attached to the electrode surface, which affected the oxidation kinetics of the analyte. However, this reason may not be strong enough to prove that there were two mass transfer processes. Therefore, the Randle-Sevcik relationship, a well-known relationship for determination of mass transfer processes for reversible and quasi-reversible CVs, was used. This Randles-Sevcik relationship supported that at low concentrations of GCM, a diffusion-controlled process played a crucial role as a linear relationship between square root of scan rate and peak current was obtained (Figure 4.10). Furthermore, using a high concentration of 100 mM GCM, an adsorption-controlled process was considered as an important role for mass transfer process. This was confirmed from a linear plot between scan rate and peak current (Figure 4.11(b)). In addition, an adsorption-controlled process in which the analyte was adsorbed on the electrode surface

could disturb oxidation process of the diffused analyte from the bulk solution. This could cause slow reaction. Therefore, these reasons confirmed two linear ranges obtained from this system.

4.3.2 Limit of Detection and Limit of Quantitation

Limit of detection (LOD) and limit of quantitation (LOQ) were calculated from the first linear equation. LOD and LOQ were obtained from 3 times and 10 times of S/N ratio, respectively. Experimental measurements were thereafter performed to confirm the calculated values. LOD and LOQ were found to be 2.8 and 9.4 μM , respectively, which are the same values as the calculated ones.

4.3.2 Interference Study for Batch Measurements

Generally, GCM can be obtained from chitosan through a hydrolysis process. The reduction of chitosan yields *N*-acetyl-glucosamine and GCM as products, and less than 1 % of chitosan is left from the reaction. Therefore, *N*-acetyl-glucosamine could be the interference for quantitative determination of GCM. A mechanism for detection of GCM using the proposed sensor is demonstrated in Figure 4.13. The amino group of GCM interacts with the gold surface according to the hard-soft acid-base theory (HSAB). However, *N*-acetyl-glucosamine also has an amino group, which could interfere the detection performance of the sensor for detecting GCM. Nevertheless, electron delocalization at the acetyl conformation of *N*-acetyl-glucosamine resulted in weaker interaction between the amino group and gold surface.

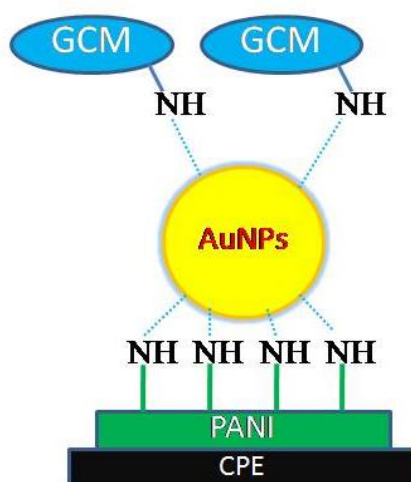


Figure 4.13 Schematic showing the interaction between GCM and AuNPs modified on a CPE.

Therefore, *N*-acetyl-glucosamine, as interference, was studied in this work. Accordingly, *N*-acetyl-glucosamine was mixed with 5 mM GCM at different concentration ratios of 1:10, 2:10, 3:10 and 4:10. The mixtures were subsequently measured using the developed sensor to determine the amount of GCM. Results are shown in Table 4.6.

Table 4.6 Interference study of *N*-acetyl-glucosamine added into a GCM standard solution at different ratios.

Ratio	Averaged Current (μA)	SD	%RSD	%Increasing of Current	t-value	t-critical
1:10	23.74	0.378	1.60	1.02	0.34	2.13
2:10	24.18	0.761	1.72	2.89	1.72	2.13
3:10	24.22	0.535	1.55	3.06	1.55	2.13
4:10	26.59	0.571	2.15	13.10	9.95	2.13

Results show that the ratios between *N*-acetyl-glucosamine:GCM of 1:10, 2:10 and 3:10 were not significantly different in electrochemical signal, but the 4:10 ratio showed 13% increasing of electrochemical signal from the GCM signal. Therefore, the obtained electrochemical signal from the interference was relatively low and could not interfere the detection of GCM. In addition, the student t-test was employed to determine whether there were significant differences between the currents obtained from GCM and those of the mixtures. Using a 95% confidence interval with 0.05 of an alpha value, t-values were calculated to be 0.34, 1.72, 1.55 and 9.95 for 1:10, 2:20, 3:10 and 4:10 ratios, respectively. Compared to a t-critical value of 2.13 ($n = 5$), the currents of 1:10, 2:10 and 3:10 ratios were insignificantly different from that of obtained from 5 mM GCM. However, the ratio of 4:10 was considered as a significant difference because the t-value was higher than the t-critical value. Thus, the highest concentration ratio of *N*-acetyl-glucosamine that would not interfere the GCM detection was at the ratio of 3:10 (w/w).

4.3.3 Inter-day and Intra-day Precisions of Batch Measurements

Intra-day and inter-day measurements were employed to examine the system precision. Inter-day precision was monitored within a month to observe the robustness and electrode's life time.

4.3.3.1 Intra-day Measurements

Intra-day measurements were carried out using 40, 60, 80 and 100 mM GCM using the optimized conditions and measured 10 times for each concentration. Current was then plotted as a function of the number of experiments, as shown in Figure 4.14.

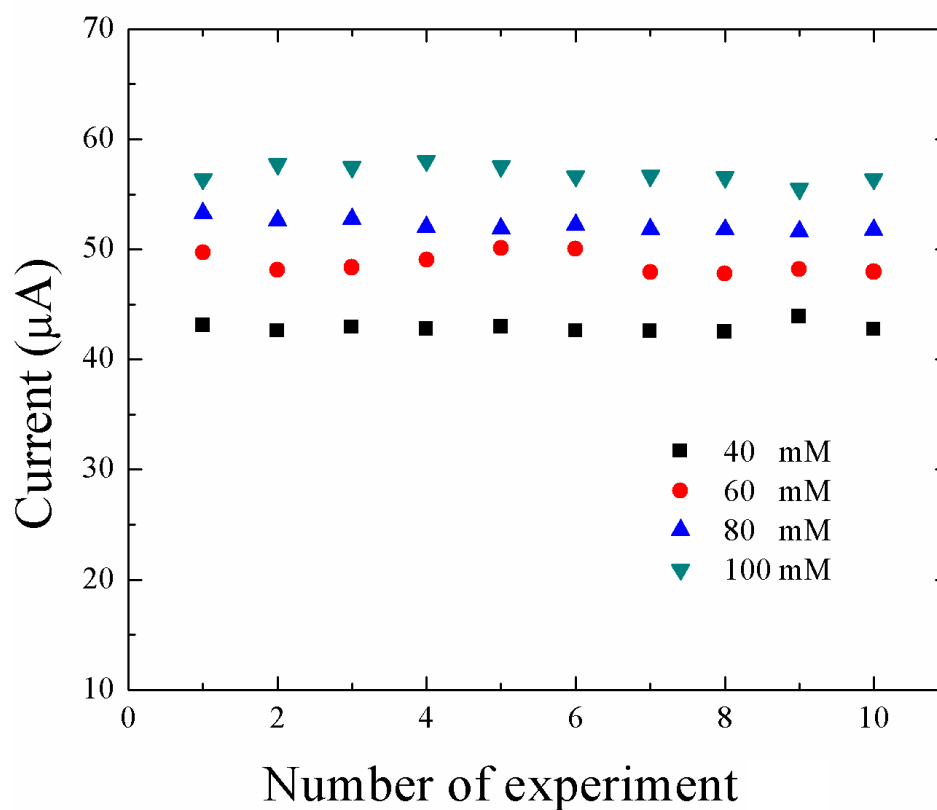


Figure 4.14 Intra-day measurements of 40, 60, 80 and 100 mM GCM using the optimum conditions, as shown in Figure 4.12. GCM solutions were prepared in 0.1 M PBS pH 4.0. Each concentration was measured for 10 times (n =10).

To consider precision, each concentration in Figure 4.14 was averaged and calculated for SD and %RSD. The values of %RSD were found to be lower than 2%. This precision was acceptable according to the Association of Official Agricultural Chemists (AOAC) [59], which suggests that %RSD for measurements of analytes in dietary supplements and botanicals should be less than 8% for the analyte concentration range of 0.01% (w/w).

4.3.3.2 Inter-day Measurements

For inter-day measurements, 5 days in a month with an interval of 7 days were chosen. A concentration series of 40, 60, 80 and 100 mM GCM were measured for comparison. For each concentration, 5 replicates were performed using linear sweep voltammetry. Figure 4.15 illustrates plots of inter-day measurements.

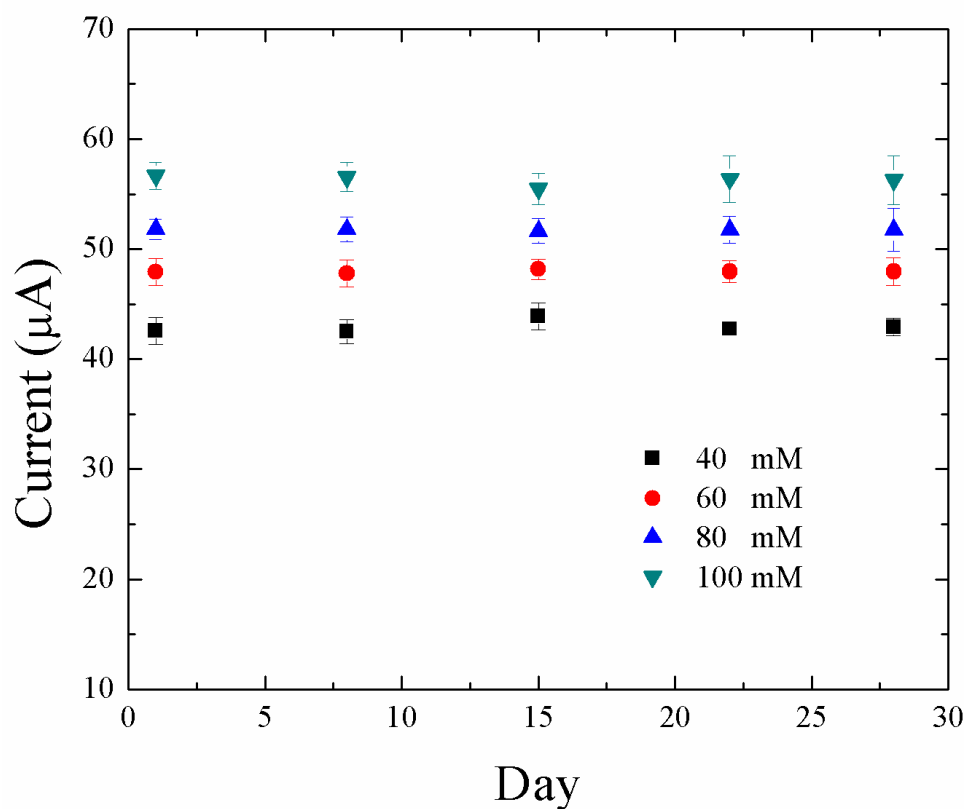


Figure 4.15 Inter-day measurements of 40, 60, 80 and 100 mM GCM using the optimum conditions. The measurements were performed for 5 days in a month with an interval of 7 days.

%RSD of current signal was calculated from each concentration and found to be less than 2, which was acceptable according to the AOAC guideline. Therefore, this GCM sensor together with the optimized conditions provided an easy approach for detection of GCM with highly acceptable inter-day precision.



4.4 Real Sample Analysis for Batch Measurements

To apply the proposed approach for real sample measurements, supplementary products were prepared to have a GCM concentration of 20 mM in 0.1 M PBS pH 4. Supplementary products were obtained from a local pharmacy which included Defence Pharmaceutical Factory, Glocosa, and Millimed. For each sample, obtained signals from experiments were averaged from 10 measurements to determine the concentration of GCM in samples. Results are shown in Table 4.7.

Table 4.7 Real sample measurements using the proposed method. All samples were prepared in 0.1 M PBS pH 4.

Sample	Prepared Concentration (mM)	Labeled Concentration (mg mL ⁻¹)	Measured Concentration (mg mL ⁻¹)	%Error	%RSD
A	20	1500	1508	0.58	0.7
B	20	1500	1504	0.29	1.79
C	20	1500	1502	0.15	1.99

T-values for each sample were calculated to be 1.83, 0.32 and 0.17 for sample A, B and C, respectively. Compared with a t-critical value of 2.77, at a 95% confidence level, these obtained t-values indicated that the measured concentrations of GCM were insignificantly different from the labeled amounts by using t-test with. In addition, the averaged signal showed that high accuracy of the method was obtained with percentage error of less than 2% when compared to the labeled amounts.

4.5 Droplet-based Microfluidics

Droplet-based microfluidics was employed in this work not only for high-throughput experiments, but also for solving the adsorption of analyte on the electrode surface that occurred in the batch system. To perform electrochemical measurements using the droplet system, chronoamperometry was applied in this work. An applied potential was fixed to measure electrochemical current signal versus time. When generated droplets went through the microchannel, they were elongated at the confined channel where the electrode bands were located. It was found that electrochemical signal exhibited the highest current at the beginning of the droplet signal and then decreased exponentially to the steady-state, which followed the Cottrell equation [60]. An example of current signal obtained from droplets containing 5 mM GCM is shown in Figure 4.16.

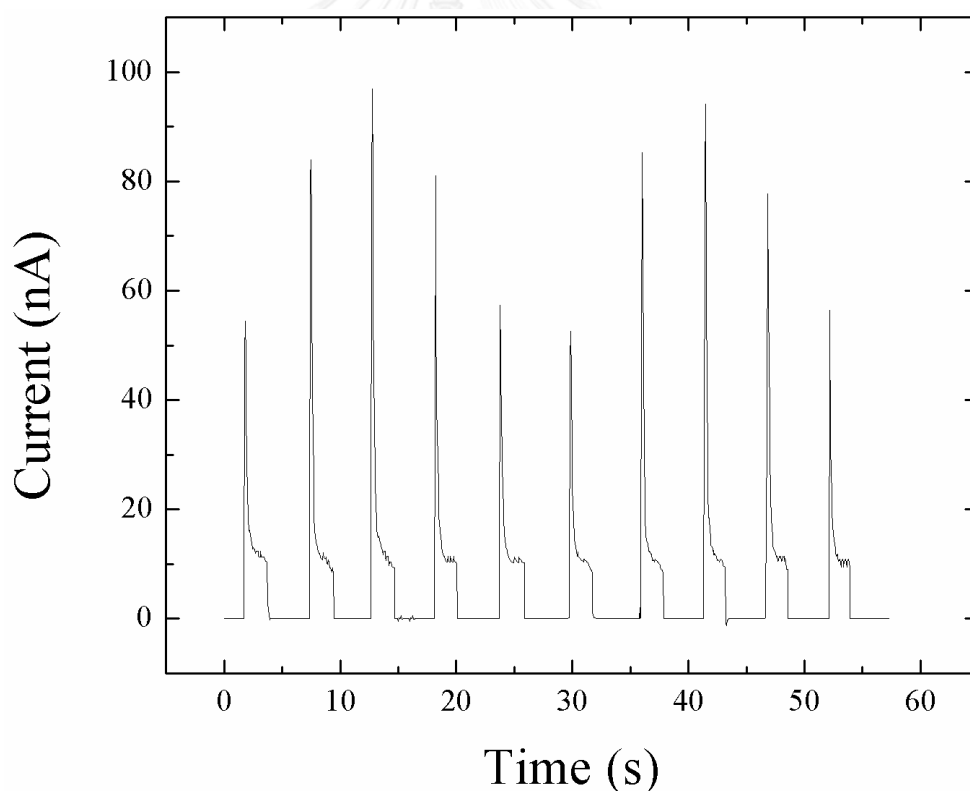


Figure 4.16 A chronoamperogram of droplets containing 5 mM GCM in 0.1 M PBS pH 4. The experiment was performed using an applied potential of 100 mV and droplets were generated using flow rates of 1.4 and 0.6 $\mu\text{L min}^{-1}$ for oil and aqueous solutions, respectively.

Generally, for chronoamperometry, electrochemical current is measured at the steady-state of signal. However, Crooks and co-worker [15] reported that amperometric measurements in droplets at the semi-steady-state resulted in similar signal when compared with the steady-state. In addition, measuring current at the semi-steady state gave reliable results with high accuracy and reproducibility. Therefore, in this work amperometric signal was measured at the end of droplet peaks which was the semi-steady state, as seen in Figure 4.17.

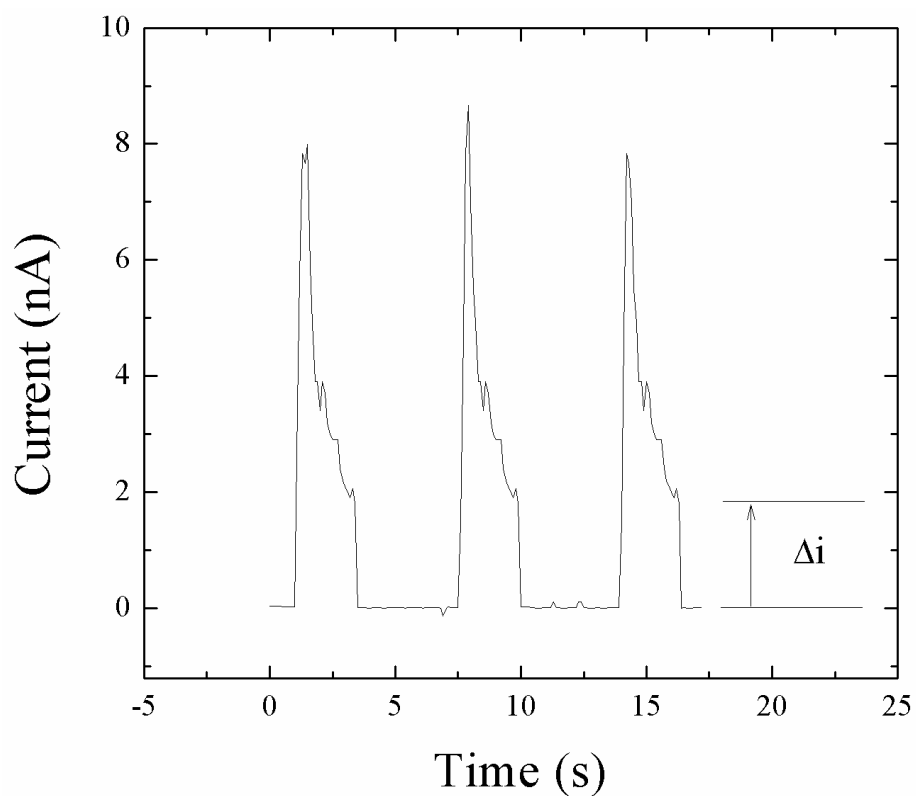


Figure 4.17 Droplet readout of 2 mM GCM. Current (Δi) was measured at the end of droplet peak. The experiment was performed using the conditions as shown in Figure 4.16.

Figure 4.17 demonstrates how to measure electrochemical signal from an amperogram. Δi is the current difference between oil (background) and GCM signals. For oil signal, current was assumed to be 0 nA because oil is not an electro-active species. On the other hand, current signal was obtained from the aqueous solution which exponentially decreased according to the Cottrell equation, as shown in Equation 2.3.



4.5.1 Optimization of Droplet System

4.5.1.1 Flow Rate

For droplet-based microfluidic systems, two parameters (water fraction and total flow rate) were optimized. Water fraction (W_f) indicates the ratio of aqueous phase in the droplet system. There are two parameters related to W_f , which are oil and aqueous flow rates. W_f controls the size of droplet in which the higher W_f , results in the greater droplet size.

Even though W_f is unit-free and independent of channel size, it is related to total flow rate, as shown in Equation 2.1. Accordingly, changing one of these parameters (W_f and total flow rate) and keeping the other parameter fixed was preferred. In addition, to obtain stable droplet generation, W_f is normally maintained to be not higher than 0.5. When the W_f is higher than 0.5, droplet formation is not stable. For example, when W_f is equal to 1.0, laminar flow occurs in the microchannel instead of droplets. In contrary, insufficient water fraction provided very small volume of aqueous droplet in microchannel. The very small water droplet is not stable for flowing along in microchannel. Moreover, total flow rate was also considered because it affects electrochemical signal directly, owing to the used velocity which it could reduce acquisition time in a droplet. In addition, flow rate does not has the effect on droplet size because the droplet size is only related to W_f . Therefore, in this work W_f was fixed at 0.3, 0.4 and 0.5 whilst total flow rate was changed from 1.0 to 3.0 $\mu\text{L min}^{-1}$.

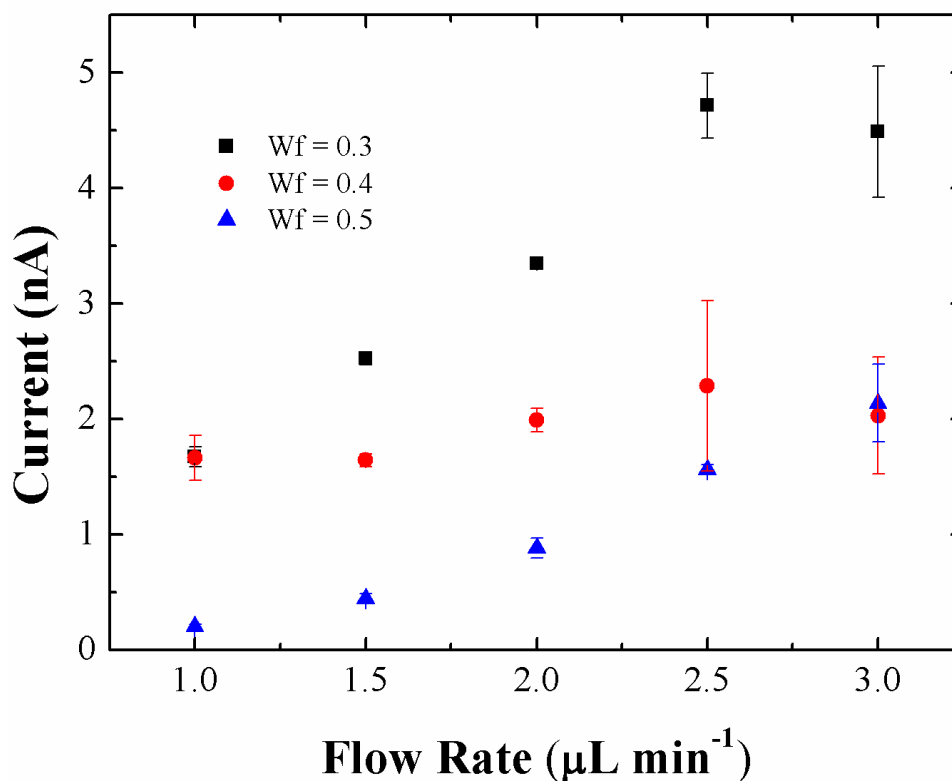


Figure 4.18 Effects of W_f and total flow rate on chronoamperometric measurements of 2.5 mM GCM in droplets. Chronoamperometric measurements in droplets were performed using an applied potential of 100 mV.

Figure 4.18 shows that the lower the W_f , the higher the electrochemical signal. This is due to the exponential decay of electrochemical signal of chronoamperometry with time. It was found that using the longer droplet (higher W_f) provided the lower electrochemical signal. Therefore, W_f of 0.3 was chosen in this work. In addition, stability of droplets in the system was also considered. It was found that if the total flow rate was too high, the obtained signals of analyte were not stable because only the spiking peak at the beginning of droplet signal were observed. In addition, unstable spiking peak could be owing to the pulsation of

syringe pumps which affected electrochemical currents at nanoscales. The most uniform and stable droplet, as considered from SD values, was obtained at the total flow rate of $2.0 \mu\text{L min}^{-1}$, which corresponded to the flow rates of $1.4 \mu\text{L min}^{-1}$ and $0.6 \mu\text{L min}^{-1}$ for oil and aqueous solutions, respectively.

4.5.1.2 Applied Potential

To figure out the optimum potential for the droplet-based system, a hydrodynamic voltammogram was constructed. Hydrodynamic voltammogram is used to point out which potential provides the highest current of analyte compared to background current. It is a plot of the ratio of signal to background (S/B) versus applied potential. A series of applied potential was considered from the range of 50 to 500 mV to construct a hydrodynamic voltammogram, as illustrated in Figure 4.19.

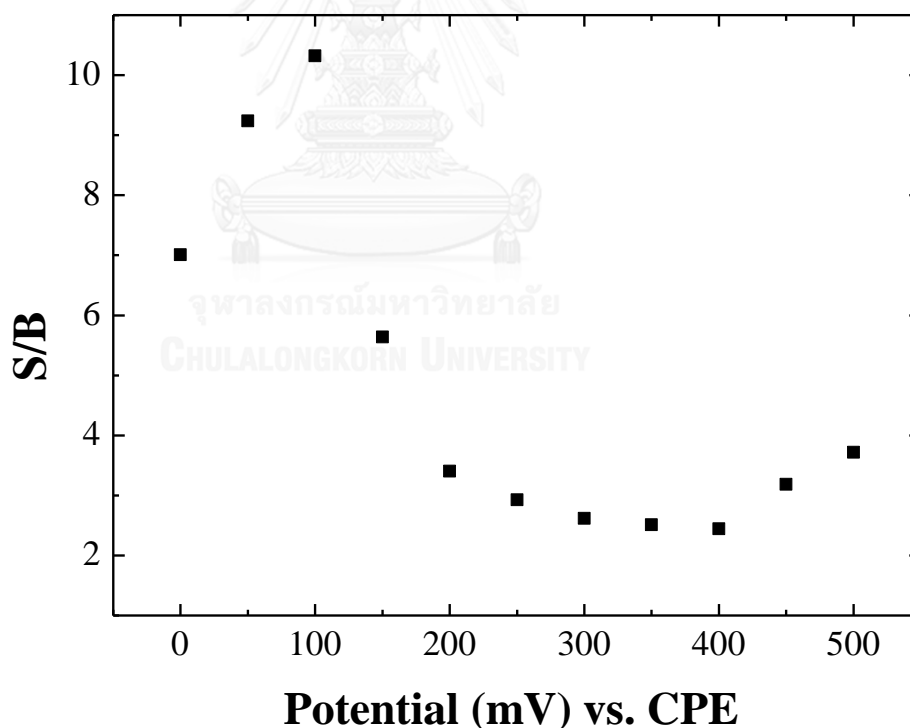


Figure 4.19 A hydrodynamic voltammogram of 2.5 mM GCM determined using the optimized conditions; flow rates of 1.4 and $0.6 \mu\text{L min}^{-1}$ for oil and aqueous solutions, respectively and W_f equal to 0.3.

As shown in Figure 4.19, the S/B signal increased when increasing the applied potential from 0 to 100 mV. Using of higher potentials which means that higher numbers of electrons were added in the system. Thus, the higher the potential, the higher the electrochemical signal. However, it was found that using applied potentials greater than 100 mV; S/B signals were diminished. It is because the oxidation current of GCM decreased when high potentials were applied as, according to the CV of GCM in Figure 4.8. Therefore, an applied potential of 100 mV was chosen for the droplet system because it provided the highest S/B.

4.5.2 Analytical Performance

Similar to batch measurements, the analytical performance, including LOD, LOQ and linearity of the droplet-based system for determination of GCM were also determined. A concentration series of GCM from 0.5 to 30 mM was prepared in 0.1 M PBS pH 4 and measured for current using the optimized conditions. Figure 4.20 (a) shows amperograms of droplets containing GCM at different concentrations. Subsequently, a calibration curve (Figure 4.20 (b)) was constructed using the obtained electrochemical currents from the amperograms in Figure 4.20 (a). A linear range, LOD and LOQ were considered from the constructed calibration curve. LOD and LOQ were calculated using 3 and 10 times of S/N, respectively.

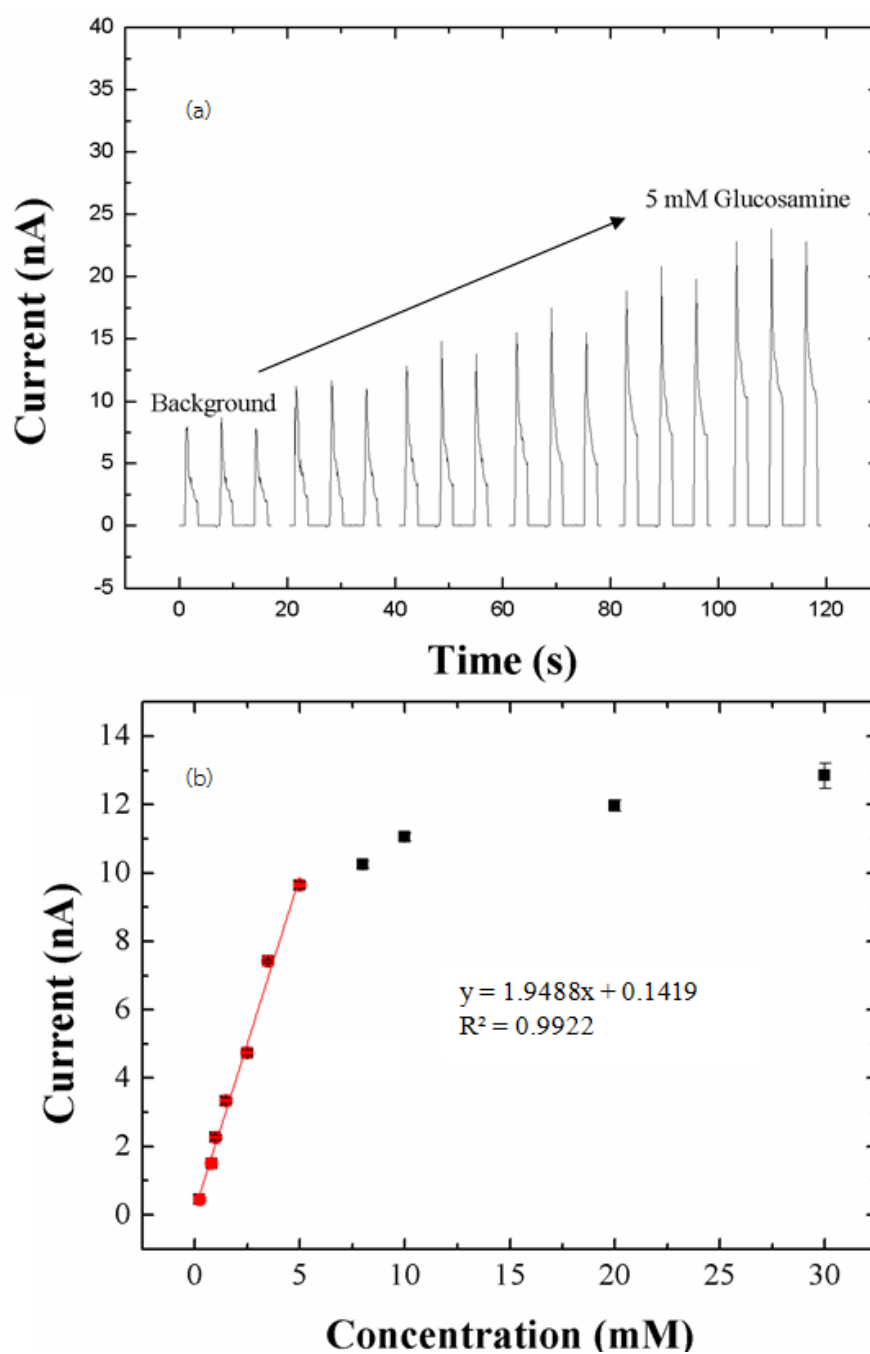


Figure 4.20 (a) Chronoamperometric readout of droplets containing a concentration series of GCM from 0 to 5 mM. The measurements were carried out using a total flow rate of $2.0 \mu\text{L min}^{-1}$ and $W_f = 0.3$ to generate droplets containing GCM. The applied potential was 100 mV vs. CPE. (b) A plot of current versus GCM concentration shows a linear range from 0.45 to 5 mM.

From Figure 4.20, a linear range was found to be in the range of 0.45 to 5 mM with $R^2 = 0.9922$. LOD and LOQ were calculated to be 0.45 and 1.45, respectively.

4.5.3 Interference Study

To study the effect of *N*-acetylglucosamine as an interference for determination of GCM using the droplet system, *N*-acetylglucosamine was mixed with 5.0 mM GCM at the same ratios as used in the batch measurements, which were 1:10, 2:10, 3:10, 4:10 and 5:10 (*N*-acetyl-glucosamine:GCM). Figure 4.21 demonstrates a bar chart which compared current signal obtained from 5 mM GCM and the mixtures.

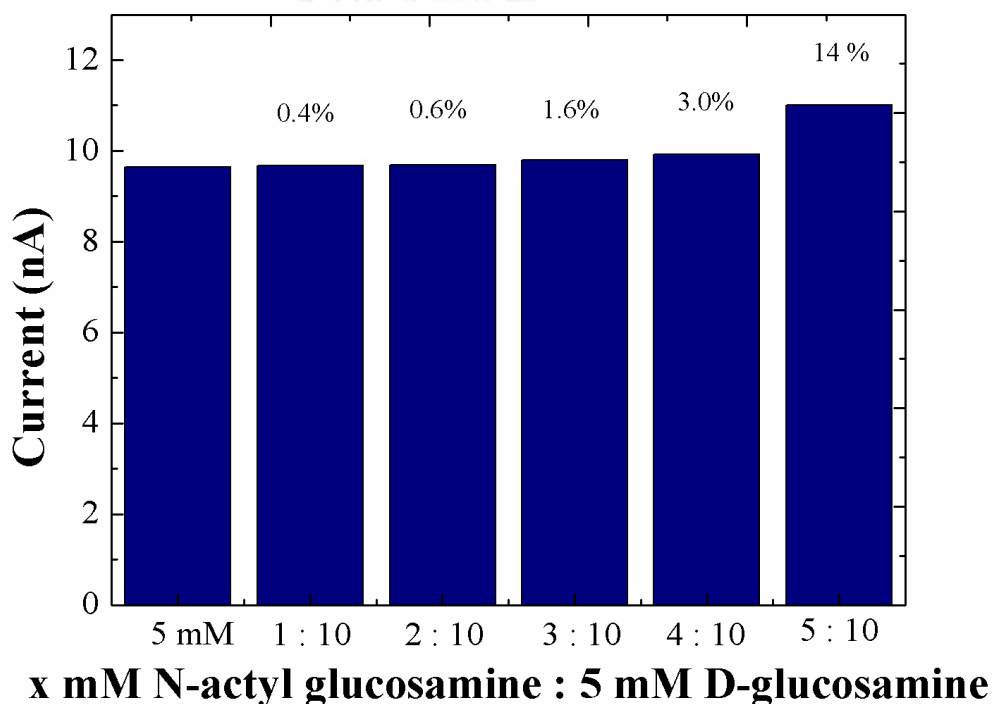


Figure 4.21 A bar chart shows a comparison between current signal obtained from 5.0 mM GCM and that from the mixtures of 5 mM GCM and *N*-acetylglucosamine at different ratios. Percentage different of each ratio were demonstrated above its bar. Experimental conditions were the same as shown in Figure 4.20.

It was found that currents obtained from the ratios of 1:10, 2:10, 3:10 and 4:10 were slightly different from the current of 5 mM GCM. However, at the ratio of 5:10 (*N*-acetyl-glucosamine: GCM) the current was enhanced about 14%. Therefore, the obtained electrochemical signal from the interference was relatively low and could not interfere the detection of GCM. In addition, the student t-test was employed to determine whether there were significant differences between the currents obtained from GCM and those of the mixtures. Using a 95% confidence interval with 0.05 of an alpha value, t-values were calculated to be 0.49, 0.31, 0.47, 1.2 and 8.8 for 1:10, 2:20, 3:10, 4:10 and 5:10 ratios, respectively. Compared to a t-critical value of 2.77 ($n = 5$), the currents of 1:10, 2:10, 3:10 and 4:10 ratios were insignificantly different from that of obtained from 5 mM GCM. However, the ratio of 5:10 was considered as a significant difference because the t-value was higher than the t-critical value. Thus, the highest concentration ratio of *N*-acetyl-glucosamine that would not interfere the GCM detection was at the ratio of 4:10 (w/w).

4.5.4 Precision

4.5.4.1 Intra-day Measurements

Intra-day measurements were performed using 1.5, 2.5 and 3.5 mM GCM prepared in 0.1 M PBS pH 4.0. Current signal from droplets containing GCM was measured from 50 droplets ($n = 50$) for each GCM concentration. As demonstrated in Figure 4.22, electrochemical currents were plotted as a function of the number of droplets.

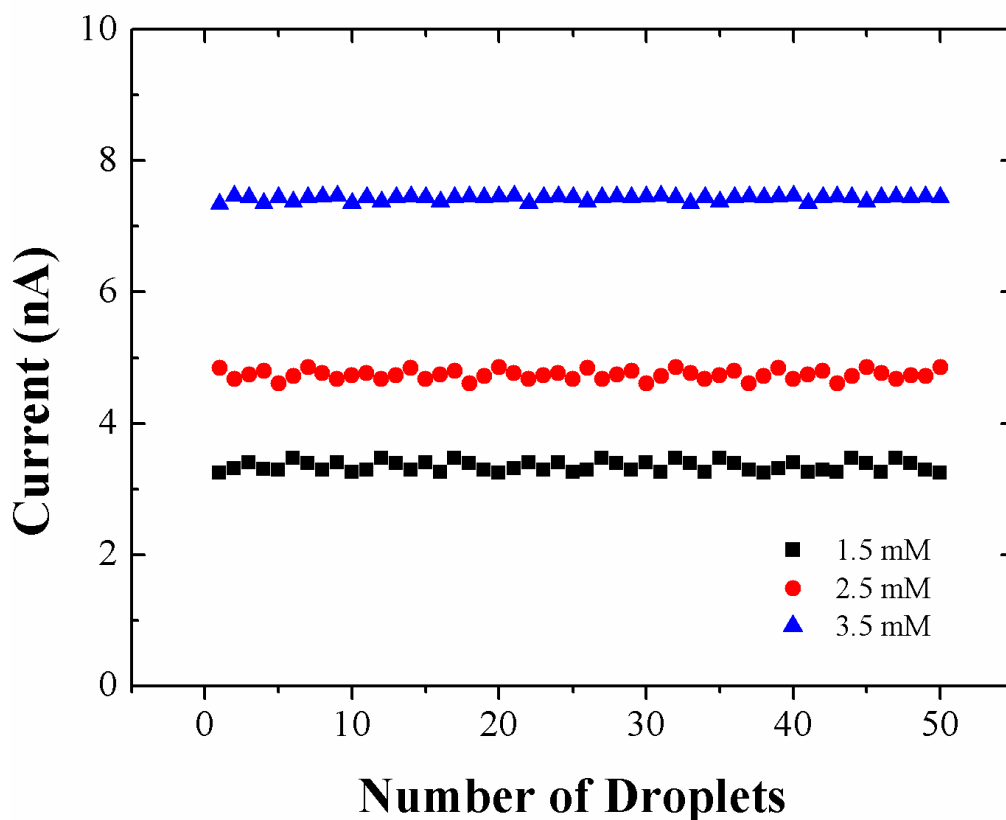


Figure 4.22 Intra-day measurements of 50 droplets containing 1.5, 2.5, and 3.5 mM GCM. Experimental conditions were the same as shown in Figure 4.20.

From Figure 4.22, %RSD of the current signals was less than 3%, which is acceptable precision according to the AOAC, which set %RSD to be lower than 8% for an analyte concentration of 0.01% (w/w). This indicates high intra-day precision of the developed droplet-based microfluidic system for determination of GCM.

4.5.4.2 Inter-day Measurements

For inter-day precision, measurements of 3.5 mM GCM in droplets were performed for 3 days ($n = 3$) within a week. In addition, current signal was monitored from 10 droplets for each day and plotted as a function of the number of droplets, as shown in Figure 4.23.

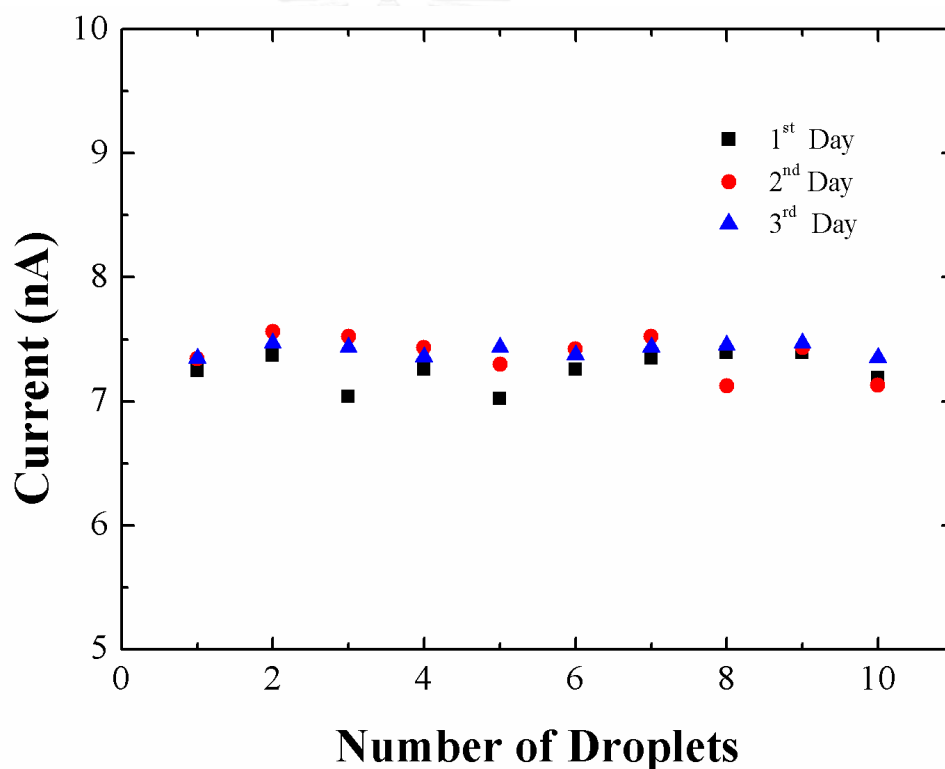
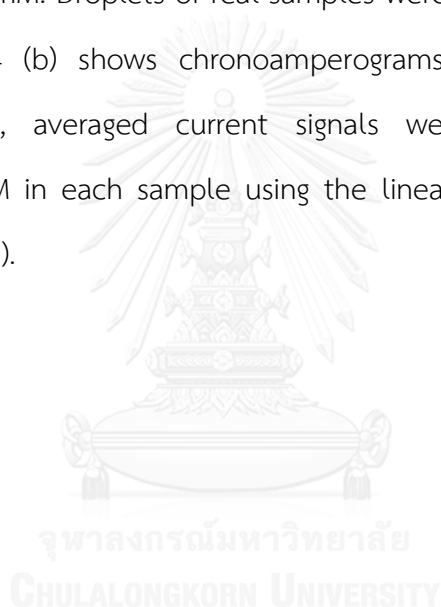


Figure 4.23 Inter-day measurements of 3.5 mM GCM in droplets for 3 days ($n=3$). All experiments were carried out using the conditions as shown in Figure 4.20.

For inter-day precision, %RSD of the currents measured from 3 days were found to be less than 5%. Using the student t-test, the currents obtained among three days for inter-day experiments were not statistically different at a 95% confidence level ($t\text{-value} = 0.43 < t\text{-critical} = 2.11$). These indicate high repeatability of the droplet system for intra-day and inter-day measurements of GCM.

4.5.6 Real Sample Analysis

All dietary supplements were prepared in 0.1 M PBS pH 4.0 at a concentration of 3.5 mM. Droplets of real samples were generated and measured for currents. Figure 4.24 (b) shows chronoamperograms of droplets containing all samples. After that, averaged current signals were used to calculate the concentration of GCM in each sample using the linear equation of the calibration curve in Figure 4.24 (a).



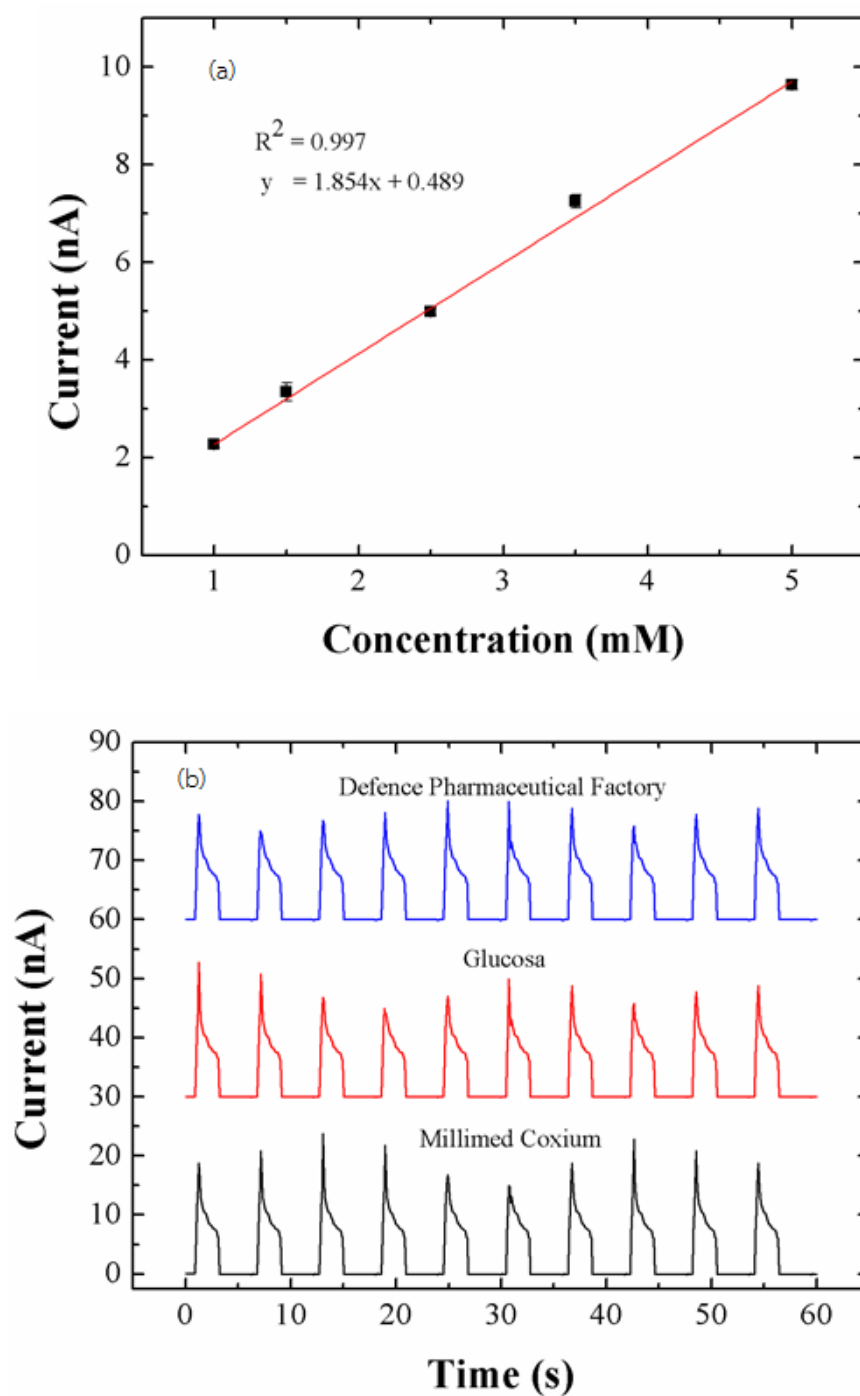


Figure 4.24 (a) A calibration curve of GCM obtained from the droplet measurements. (b) Chronoamperograms from the measurements of GCM in real samples (Defence Pharmaceutical Factory, Glucosa and Millimed) using the droplet system. All experiments were carried out using the conditions as shown in Figure 4.20.

The amounts of GCM in the samples determined using the droplet system are shown in Table 4.8. Results show that the percentage error between the measured concentrations and the labeled amounts were found to be less than 2%. In addition, to validate the results obtained from the microfluidic method, t-test was applied using a 95% confidence level. As illustrated in Table 4.8, t-values were less than t-critical values, which indicated insignificant difference between the measured and labeled amounts of GCM in the real samples.

Table 4.8 Measurements of GCM in supplementary products using the droplet system.

Sample	Prepared Concentration (mM)	Labeled Concentration (mg mL ⁻¹)	Measured Concentration (mg mL ⁻¹)	%Error	%RSD
A	3.5	1500	1516	1.07	2.08
B	3.5	1500	1499	0.07	0.71
C	3.5	1500	1510	0.67	1.68

Moreover, to validate the droplet system for determination of GCM in supplement products, capillary electrophoresis (CE) was employed to determine the amount of GCM in the supplementary products. For CE experiments, GCM in the samples was dissolved in 100 mM borate buffer and left overnight to allow GCM to form complex with borate as much as possible. Figure 4.25 (a) shows electropherograms of 1 to 10 mM GCM standard solutions obtained from CE measurements. After that, a calibration curve was constructed using corrected peak area versus concentration, as illustrated in Figure 4.25 (b).

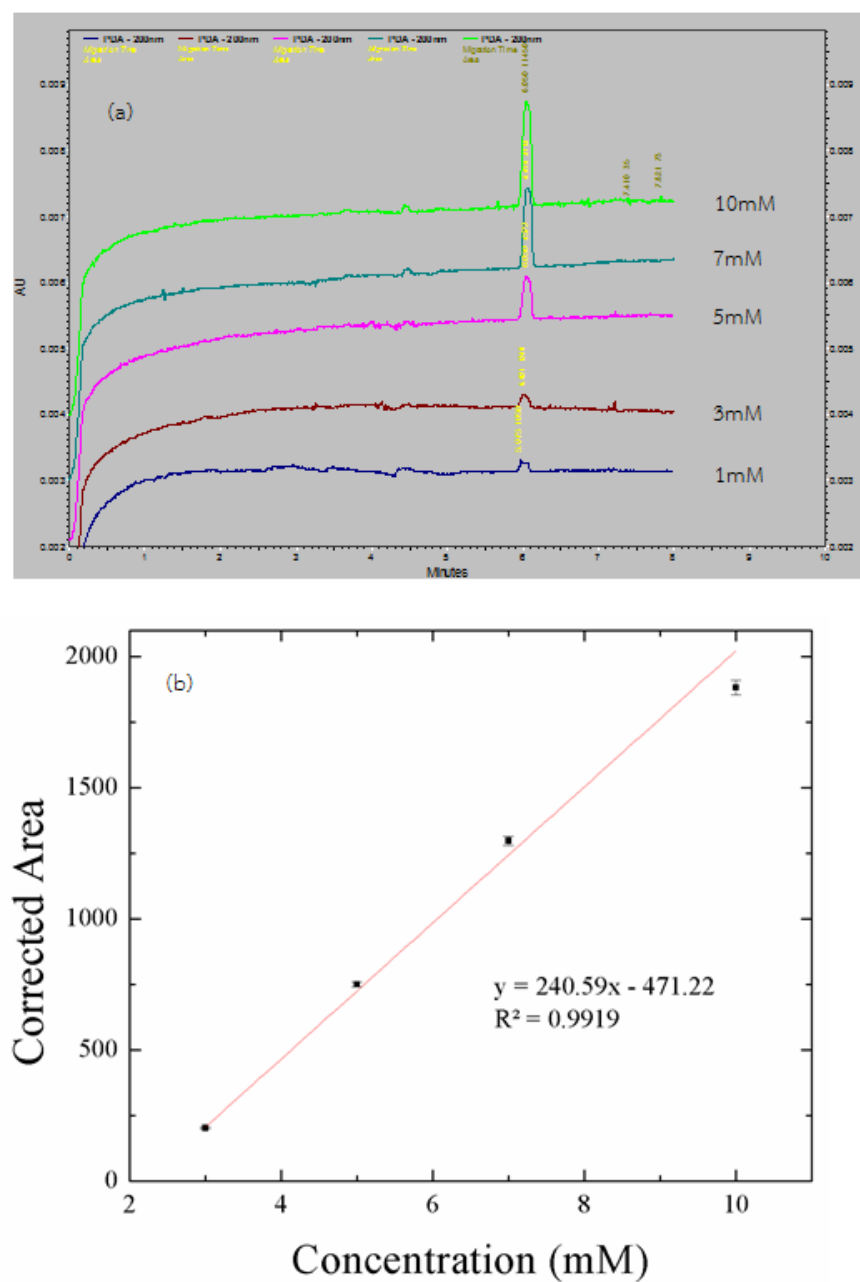


Figure 4.25 (a) Electropherograms of GCM standard solutions prepared in 100 mM borate buffer at a concentration series of 1 to 10 mM. (b) A calibration curve plotted between corrected areas of GCM and concentration. CE conditions: background electrolyte as 100 mM Borate adjust to pH 9 with 0.1 M NaOH, 75 μm ID x 60.2 cm (50 cm of the detector) uncoated fused-silica capillary; temperature 25 $^{\circ}\text{C}$; voltage 30 kV; UV detection at 200 nm, and 0.5 psi sample injection for 10 s.

To determine the amounts of GCM in the real samples, all samples were prepared at a concentration of 8 mM in 100 mM borate buffer, left overnight and then measured using the CE method. Corrected areas of all samples were investigated and converted to concentrations using the equation of the calibration curve. CE results are presented in Table 4.9.

Table 4.9 Comparison of the amounts of GCM in samples determined using batch, droplet and CE systems. A, B and C represent brands of Defence Pharmaceutical Factory, Glucosa, and Millimed, respectively.

Sample	Labeled (mg mL ⁻¹)	Batch (mg mL ⁻¹)	Droplet (mg mL ⁻¹)	CE (mg mL ⁻¹)
A	1,500	1,508	1,516	1,516
B	1,500	1,504	1,499	1,512
C	1,500	1,502	1,510	1,505

The Student t-test was employed to compare results obtained from the two methods (CE and droplet). It was found that the amounts of GCM in the real samples determined using both methods were insignificantly different at a 95% confidence interval because t-value of A, B and C were 0.25, 0.79, and 0.45, respectively, which lower than t-critical, 2.91, for all real samples (n=3). These confirmed high accuracy and reliability of the droplet system for determination of GCM.

CHAPTER 5

CONCLUSIONS

Herein, an electrochemical sensor using CPEs modified with PANI and AuNPs for determination of glucosamine in supplementary products. In this work, central composite design was used as a method for optimization of the amounts of AuNPs and PANI for electrode modification and pH of the working solution. To do CCD experiments, a well-like microfluidic device with a 0.8 cm punched hole was used for batch experiments. Results from the CCD experiments, which were obtained from linear sweep voltammograms showed that the optimum amounts of AuNPs and PANI were 0.3 and 3 mg L⁻¹, respectively and pH of the working solution was pH 4.0. Using the optimum conditions for determination of glucosamine, two linear ranges were obtained in the ranges of 0.05-40 mM and 40-100 mM, respectively. Limits of detection and quantitation were calculated from the first calibration curve to be 2.8 and 9.4 μM, respectively. High precision of batch measurements was achieved with %RSD lower than 2%. In addition, the labeled amounts of pharmaceutical products were compared with experimental data. Using t-test, it was found that the amount of glucosamine obtained from the developed method is insignificantly different from the labeled amounts.

Furthermore, a droplet-based microfluidic system was coupled with the proposed electrochemical sensor. The analysis of glucosamine was performed in a high-throughput manner with a sample throughput of at least 60 samples h⁻¹. In addition, the adsorption of the analyte on the electrode surface was prevented due to compartmentalization in droplets. To perform droplet-based microfluidic experiments, droplets were generated using a T-junction microfluidic platform in which oil and aqueous solution flow rates were 1.4 and 0.6 μL min⁻¹, respectively, with a water fraction equal to 0.3. In addition, chronoamperometric measurements were used for the droplet system with an applied potential of 100 mV. Linearity of the droplet system for determination of glucosamine was found to be in the range of 0.5–5 mM with LOD and LOQ of 0.45 and 1.45 mM, respectively. High intra-day and

inter-day (evaluated among 3 days) precisions for the detection of 50 droplets containing glucosamine were obtained with %RSD less than 3%. The system was successfully used to determine the amounts of glucosamine in supplementary products with percentage error and relative standard deviation less than 3%. In addition, the amounts of glucosamine measured using the droplet system were in good agreement with those obtained from a traditional CE method. These indicate high accuracy and precision of the proposed system for determination of glucosamine in supplementary products.



REFERENCES

- [1] Van Manen, M.D., Nace, J., and Mont, M.A. Management of Primary Knee Osteoarthritis and Indications for Total Knee Arthroplasty for General Practitioners. The Journal of the American Osteopathic Association 112(11) (2012): 709-715.
- [2] Salazar, J., Bello, L., Chávez, M., Añez, R., Rojas, J., and Bermúdez, V. Glucosamine for Osteoarthritis: Biological Effects, Clinical Efficacy, and Safety on Glucose Metabolism. Arthritis (2014): 432-463.
- [3] Pashkova, E., Pirogov, A., Bendryshev, A., Ivanaynen, E., and Shpigun, O. Determination of underivatized glucosamine in human plasma by high-performance liquid chromatography with electrochemical detection: Application to pharmacokinetic study. Journal of Pharmaceutical and Biomedical Analysis 50(4) (2009): 671-674.
- [4] Cheng, R., et al. Optical Turn-On Sensor Based on Graphene Oxide for Selective Detection of d-Glucosamine. Analytical Chemistry 84(13) (2012): 5641-5644.
- [5] Tran, T.M., Alan, Y., and Glass, T.E. A highly selective fluorescent sensor for glucosamine. Chemical Communications 51(37) (2015): 7915-7918.
- [6] Mora, M.I. and Marioli, J.M. HONEY CARBOHYDRATE ANALYSIS BY HPLC, WITH ELECTROCHEMICAL DETECTION, USING A NI-CR ALLOY ELECTRODE. Journal of Liquid Chromatography & Related Technologies 24(5) (2001): 711-720.
- [7] Cataldi, T.R.I., Campa, C., and De Benedetto, G.E. Carbohydrate analysis by high-performance anion-exchange chromatography with pulsed amperometric detection: The potential is still growing. Fresenius Journal of Analytical Chemistry 368(8) (2000): 739-758.
- [8] Tominaga, M., Nagashima, M., and Taniguchi, I. Controlled-potential electrosynthesis of glucosaminic acid from glucosamine at a gold electrode. Electrochemistry Communications 9(5) (2007): 911-914.

- [9] Dhand, C., Das, M., Datta, M., and Malhotra, B.D. Recent advances in polyaniline based biosensors. Biosensors & Bioelectronics 26(6) (2011): 2811-2821.
- [10] Yang, Y.J. and Huang, H.J. A polyaniline-modified electrode-based FIA system for sub-ppb-level chromium(VI) analysis. Analytical Chemistry 73(6) (2001): 1377-1381.
- [11] Suea-Ngam, A., Rattanarat, P., Chailapakul, O., and Srisa-Art, M. Electrochemical droplet-based microfluidics using chip-based carbon paste electrodes for high-throughput analysis in pharmaceutical applications. Analytica Chimica Acta 883 (2015): 45-54.
- [12] Tseng, R.J., Huang, J.X., Ouyang, J., Kaner, R.B., and Yang, Y. Polyaniline nanofiber/gold nanoparticle nonvolatile memory. Nano Letters 5(6) (2005): 1077-1080.
- [13] Duffy, D.C., McDonald, J.C., Schueller, O.J.A., and Whitesides, G.M. Rapid prototyping of microfluidic systems in poly(dimethylsiloxane). Analytical Chemistry 70(23) (1998): 4974-4984.
- [14] Song, H., Tice, J.D., and Ismagilov, R.F. A Microfluidic System for Controlling Reaction Networks in Time. Angewandte Chemie International Edition 42(7) (2003): 768-772.
- [15] Liu, H. and Crooks, R.M. Highly reproducible chronoamperometric analysis in microdroplets. Lab on a Chip 13(7) (2013): 1364-1370.
- [16] Luo, C., et al. Picoliter-volume aqueous droplets in oil: Electrochemical detection and yeast cell electroporation. ELECTROPHORESIS 27(10) (2006): 1977-1983.
- [17] Liu, S.J., et al. The electrochemical detection of droplets in microfluidic devices. Lab on a Chip 8(11) (2008): 1937-1942.
- [18] Han, Z.Y., Li, W.T., Huang, Y.Y., and Zheng, B. Measuring Rapid Enzymatic Kinetics by Electrochemical Method in Droplet-Based Microfluidic Devices with Pneumatic Valves. Analytical Chemistry 81(14) (2009): 5840-5845.
- [19] Whitesides, G.M. The origins and the future of microfluidics. Nature 442(7101) (2006): 368-373.

- [20] Doi, H., Takahara, T., Minamoto, T., Matsushashi, S., Uchii, K., and Yamanaka, H. Droplet Digital Polymerase Chain Reaction (PCR) Outperforms Real-Time PCR in the Detection of Environmental DNA from an Invasive Fish Species. Environmental Science & Technology 49(9) (2015): 5601-5608.
- [21] Song, H., Chen, D.L., and Ismagilov, R.F. Reactions in droplets in microfluidic channels. Angewandte Chemie-International Edition 45(44) (2006): 7336-7356.
- [22] Niu, X.Z., Gielen, F., Edel, J.B., and deMello, A.J. A microdroplet dilutor for high-throughput screening. Nature Chemistry 3(6) (2011): 437-442.
- [23] Srisa-Art, M. Microdroplet reactors for high-throughput chemistry and biology. PhD Thesis, Department of Chemistry, Faculty of Science, Imperial Collage, London, 2010.
- [24] Liang L. Wu, W.X., Mark Bachman, Guann-Pynn Li. Passive Generation of Droplets in Mini and Microchannels. in ASME 5th International Conference on Nanochannels, Microchannels, and Minichannels pp. 619-623. Puebla, Mexico,, 2007.
- [25] Tice, J.D., Song, H., Lyon, A.D., and Ismagilov, R.F. Formation of droplets and mixing in multiphase microfluidics at low values of the Reynolds and the capillary numbers. Langmuir 19(22) (2003): 9127-9133.
- [26] deMello, A.J. Control and detection of chemical reactions in microfluidic systems. Nature 442(7101) (2006): 394-402.
- [27] Bringer, M.R., Gerdt, C.J., Song, H., Tice, J.D., and Ismagilov, R.F. Microfluidic systems for chemical kinetics that rely on chaotic mixing in droplets. Philosophical Transactions of the Royal Society of London Series a- Mathematical Physical and Engineering Sciences 362(1818) (2004): 1087-1104.
- [28] Xia, Y.N. and Whitesides, G.M. Soft lithography. Annual Review of Materials Science 28 (1998): 153-184.
- [29] McDonald, J.C., et al. Fabrication of microfluidic systems in poly(dimethylsiloxane). ELECTROPHORESIS 21(1) (2000): 27-40.
- [30] Bard, A.J.F., L.R. Electrochemical methods: Fundamentals and Applications, ed. edition, n. New York: John Wiley & Sons, 2001.

- [31] Pang, S.C., Anderson, M.A., and Chapman, T.W. Novel electrode materials for thin-film ultracapacitors: Comparison of electrochemical properties of sol-gel-derived and electrodeposited manganese dioxide. Journal of the Electrochemical Society 147(2) (2000): 444-450.
- [32] Fisher, A. Linear Sweep and Cyclic Voltametry: The Principles [Online]. 2016. Available from: www.ceb.cam.ac.uk [19 June 2016]
- [33] Atila, A. and Yilmaz, B. Determination of Bosentan in Pharmaceutical Preparations by Linear Sweep, Square Wave and Differential Pulse Voltammetry Methods. Iranian Journal of Pharmaceutical Research : IJPR 14(2) (2015): 443-451.
- [34] Apilux, A., Dungchai, W., Siangproh, W., Praphairaksit, N., Henry, C.S., and Chailapakul, O. Lab-on-Paper with Dual Electrochemical/Colorimetric Detection for Simultaneous Determination of Gold and Iron. Analytical Chemistry 82(5) (2010): 1727-1732.
- [35] Mareev, S.A., et al. Chronopotentiometric Response of an Electrically Heterogeneous Permselective Surface: 3D Modeling of Transition Time and Experiment. The Journal of Physical Chemistry C 120(24) (2016): 13113-13119.
- [36] Kelloner, R.M., J.M.; Otto, M.; Valcarcel, M.; Widmer, H.M. Analytical Chemistry: A Modern Approach to Analytical Science. 2nd ed. New York: John Wiley & Sons, 2004.
- [37] Loch, A. Chronoamperometry/chronocoulometry [Online]. 2016. Available from: www.basinc.com [19 June 2016]
- [38] Sameenoi, Y., et al. Microfluidic Electrochemical Sensor for On-Line Monitoring of Aerosol Oxidative Activity. Journal of the American Chemical Society 134(25) (2012): 10562-10568.
- [39] Hrapovic, S., Liu, Y.L., Male, K.B., and Luong, J.H.T. Electrochemical biosensing platforms using platinum nanoparticles and carbon nanotubes. Analytical Chemistry 76(4) (2004): 1083-1088.
- [40] Guo, S.J. and Wang, E.K. Synthesis and electrochemical applications of gold nanoparticles. Analytica Chimica Acta 598(2) (2007): 181-192.

- [41] Reed, M.A., Zhou, C., Muller, C.J., Burgin, T.P., and Tour, J.M. Conductance of a molecular junction. Science 278(5336) (1997): 252-254.
- [42] Yang, M., et al. Electrochemical determination of arsenic(III) with ultra-high anti-interference performance using Au-Cu bimetallic nanoparticles. Sensors and Actuators B-Chemical 231 (2016): 70-78.
- [43] Kanyong, P., Rawlinson, S., and Davis, J. Fabrication and electrochemical characterization of polydopamine redox polymer modified screen-printed carbon electrode for the detection of guanine. Sensors and Actuators B-Chemical 233 (2016): 528-534.
- [44] Liu, G., Yang, X., Li, Y., Yang, Z., Hong, W., and Liu, J. Continuous Flow Controlled Synthesis of Gold Nanoparticles Using Pulsed Mixing Microfluidic System. Advances in Materials Science and Engineering 2015 (2015): 11.
- [45] LaCourse, D.C.J.a.W.R. Liquid Chromatography with Pulsed Electrochemical Detection at Gold and Platinum Electrodes. Analytical Chemistry 92(10) (1990): 589A-597A.
- [46] Zhang, M., Qing, G., Xiong, C., Cui, R., Pang, D.-W., and Sun, T. Dual-Responsive Gold Nanoparticles for Colorimetric Recognition and Testing of Carbohydrates with a Dispersion-Dominated Chromogenic Process. Advanced Materials 25(5) (2013): 749-754.
- [47] Kurniawan, F., Tsakova, V., and Mirsky, V.M. Gold nanoparticles in nonenzymatic electrochemical detection of sugars. Electroanalysis 18(19-20) (2006): 1937-1942.
- [48] Balint, R., Cassidy, N.J., and Cartmell, S.H. Conductive polymers: Towards a smart biomaterial for tissue engineering. Acta Biomaterialia 10(6) (2014): 2341-2353.
- [49] Dhand C, D.N., Mishra S, Solanki PR, Mayandi V, Beuerman RW, Ramakrishna S, Lakshminarayanan R, Malhotra BD. Polyaniline-based biosensors. Nanobiosensors in Disease Diagnosis 4 (2015): 25-46.
- [50] Baker, C.O., et al. Size Control of Gold Nanoparticles Grown on Polyaniline Nanofibers for Bistable Memory Devices. Acs Nano 5(5) (2011): 3469-3474.

- [51] Brereton, R.G. Chemometrics: Data Analysis for the Laboratory and Chemical Plant. U.K.: Wiley: Chichester, 2003.
- [52] Brereton, R.G. Applied Chemometrics for Scientists. U.K.: Wiley: Chichester, 2007.
- [53] Amdoun, R., et al. Optimization of the Culture Medium Composition to Improve the Production of Hyoscyamine in Elicited *Datura stramonium* L. Hairy Roots Using the Response Surface Methodology (RSM). International Journal of Molecular Sciences 11(11) (2010): 4726-4740.
- [54] Bardpho, C., Rattanarat, P., Siangproh, W., and Chailapakul, O. Ultra-high performance liquid chromatographic determination of antioxidants in teas using inkjet-printed graphene-polyaniline electrode. Talanta 148 (2016): 673-679.
- [55] Sameenoi, Y., et al. Poly(dimethylsiloxane) cross-linked carbon paste electrodes for microfluidic electrochemical sensing. Analyst 136(15) (2011): 3177-3184.
- [56] Volpi, N. Capillary electrophoresis determination of glucosamine in nutraceutical formulations after labeling with anthranilic acid and UV detection. Journal of Pharmaceutical and Biomedical Analysis 49(3) (2009): 868-871.
- [57] Grzelczak, M., Vermant, J., Furst, E.M., and Liz-Marzán, L.M. Directed Self-Assembly of Nanoparticles. ACS Nano 4(7) (2010): 3591-3605.
- [58] Colm T. O'Mahony, R.A.F., Tandra Goshal, Justin D. Holmes and Michael A. Morris The Thermodynamics of Defect Formation in Self-Assembled Systems. in Moreno-Piraján, J.C. (ed.). U.K.: InTech, 2011.
- [59] Chemists, A.o.O.A. Guidelines for Dietary Supplements and Botanicals. AOAC OFFICIAL METHODS OF ANALYSIS Appendix K (2013): 1-32.
- [60] Wang, Y., et al. Electrocatalytic oxidation and detection of N-acetylcysteine based on magnetite/reduced graphene oxide composite-modified glassy carbon electrode. Electrochimica Acta 111 (2013): 31-40.



APPENDIX

จุฬาลงกรณ์มหาวิทยาลัย
CHULALONGKORN UNIVERSITY

VITA

Mr. Akkapol Suea-ngam was born on Tuesday 8th October 1991 in Bangkok, Thailand. In 2010, he graduated a high school level from a Science division from Suankularb Wittayalai School, Bangkok, Thailand. After that, he studied for the Bachelor's degree of Science in Chemistry, Chulalongkorn University and complete in 2014. In addition, he graduated Master Degree of Science at Chulalongkorn University and complete in 2016. His address after graduation is 97 Phetkasem road, soi Phetkasem 53, Bangkae, Bangkok, Thailand.

